NASA/TM—2021–20210010031

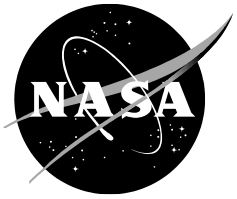

Design and Development of Nano-electro Fuel Batteries and Rim-driven Motors for Electrified Aircraft Applications

Kurt V. Papathakis
Armstrong Flight Research Center
Edwards, California 93523

June 2021

NASA STI Program ... in Profile

Since its founding, NASA has been dedicated to the advancement of aeronautics and space science. The NASA scientific and technical information (STI) program plays a key part in helping NASA maintain this important role.

The NASA STI program operates under the auspices of the Agency Chief Information Officer. It collects, organizes, provides for archiving, and disseminates NASA's STI. The NASA STI program provides access to the NTRS Registered and its public interface, the NASA Technical Reports Server, thus providing one of the largest collections of aeronautical and space science STI in the world. Results are published in both non-NASA channels and by NASA in the NASA STI Report Series, which includes the following report types:

- TECHNICAL PUBLICATION. Reports of completed research or a major significant phase of research that present the results of NASA Programs and include extensive data or theoretical analysis. Includes compilations of significant scientific and technical data and information deemed to be of continuing reference value. NASA counterpart of peer-reviewed formal professional papers but has less stringent limitations on manuscript length and extent of graphic presentations.

- TECHNICAL MEMORANDUM. Scientific and technical findings that are preliminary or of specialized interest, e.g., quick release reports, working papers, and bibliographies that contain minimal annotation. Does not contain extensive analysis.

- CONTRACTOR REPORT. Scientific and technical findings by NASA-sponsored contractors and grantees.

- CONFERENCE PUBLICATION. Collected papers from scientific and technical conferences, symposia, seminars, or other meetings sponsored or co-sponsored by NASA.

- SPECIAL PUBLICATION. Scientific, technical, or historical information from NASA programs, projects, and missions, often concerned with subjects having substantial public interest.

- TECHNICAL TRANSLATION. English-language translations of foreign scientific and technical material pertinent to NASA's mission.

Specialized services also include organizing and publishing research results, distributing specialized research announcements and feeds, providing information desk and personal search support, and enabling data exchange services.

For more information about the NASA STI program, see the following:

- Access the NASA STI program home page at http://www.sti.nasa.gov

- E-mail your question to help@sti.nasa.gov

- Phone the NASA STI Information Desk at 757-864-9658

- Write to:
  NASA STI Information Desk
  Mail Stop 148
  NASA Langley Research Center
  Hampton, VA 23681-2199

NASA/TM—2021–20210010031

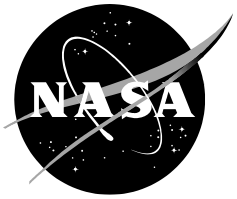

Design and Development of Nano-electro Fuel Batteries and Rim-driven Motors for Electrified Aircraft Applications

Kurt V. Papathakis
Armstrong Flight Research Center
Edwards, California 93523

National Aeronautics and
Space Administration

Armstrong Flight Research Center
Edwards, California 93523-0273

June 2021

Acknowledgments

National Aeronautics and Space Administration (NASA): Pat Loyselle (Glenn Research Center, Cleveland, Ohio, co-Principal Investigator); Robert McSwain (Langley Research Center, Hampton, Virginia, co-Principal Investigator); Starr Ginn, Jason Lechniak, Abby Waddell, and Joseph Morello (Armstrong Flight Research Center, Edwards, California); Jeffrey Chin, and Bri Demattia (Glenn Research Center, Cleveland, Ohio); and Siena Whiteside, Chris Stelter, and Nik Zawodny (Langley Research Center, Hampton, Virginia).

Empirical Systems Aerospace, Inc.: Andrew R. Gibson (President & CEO), Eric Naess (Aerospace Engineer)
(contract)

Influit Energy, LLC: John Katsoudas (Founder & CEO), Elena Timofeeva (Founder, COO & Director of R&D), Carlo Segre (Founder & CTO)
(contract)

The Boeing Company: Rich Ouellette (formerly), Don Drouin (formerly)
(Space Act Agreement Annex #23831)

Engineered Precision, Inc.: Jeff Uhrig (President), Bobby Bialczak (Senior Research Scientist)

This report is available in electronic form at

http://

Table of Contents

Abstract

The National Aeronautics and Space Administration Convergent Aeronautics Solutions project seeks to determine feasibility of emerging technologies in aeronautics. The Aqueous, QUick-Charging Battery Integration For Electric flight Research study pursued the feasibility of nano-electro fuel and rim-driven motor technologies integrated together for aircraft implementation. Development of the NEF technology was in partnership with Influit Energy, LLC (Chicago, Illinois). A rim-driven motor, designed by the project team, sized to represent one of 24 motors in the propulsion system of the tandem electric super-short takeoff and landing aircraft is discussed. The development of this electric super-short takeoff and landing concept was in partnership with The Boeing Company (Chicago, Illinois). The integrated system design of the nano-electro fuel and rim-driven motor technologies within the wing section was in partnership with Empirical Systems Aerospace, Inc. (ESAero) (San Luis Obispo, California). The feasibility benchmark for the nano-electro fuel battery was to attain 100 mA/cm^2 within two years, a 50-fold increase over the demonstrated cell performance before the Convergent Aeronautics Solutions Aqueous, QUick-Charging Battery Integration For Electric flight Research activity. The team achieved 85 mA/cm^2 in the nano-electro fuel flow cell at the end of the two years. The Aqueous, QUick-Charging Battery Integration For Electric flight Research project team determined the technology to be both inflammable and nonexplosive (unless multiple, simultaneous system failures occur) which would provide a safer alternative to conventional lithium-ion based battery systems.

Nomenclature

3-D	three-dimensional
A	ampere
AFRC	Armstrong Flight Research Center
ASAB	Aeronautics Systems Analysis Branch
AQUIFER	Aqueous, QUick-charging battery Integration For Electric flight Research
A_0	free stream capture area
A_0/A_{cap}	throat capture area and ratio
BARC	Broadband Acoustic Rotor Codes
BCS	Battery Control System
BFL	balanced field length
BPF	blade passage frequency
CAS	Convergent Aeronautics Solutions
CC	coated cathode
CDL	CDUCT-LaRC
CF	carbon fiber
CFR	Code of Federal Regulations
C_p	coefficient of pressure
C_T	coefficient of thrust
CTOL	conventional takeoff and landing
C/cm^2	coulomb per centimeter squared
D	diameter
DAC	Design / Analysis Cycle
DAQ	data acquisition
DN	bearing factor
DOF	degrees of freedom
EC	electrochemical capacitor

EMI	electromagnetic interference
ESAero	Empirical Systems Aerospace, Inc.
eSSTOL	electric super-short takeoff and landing
FAA	alkaline stable anion-exchange membrane (for electrodialysis applications)
FAS	homogeneous anion and cation exchange membrane (for electrodialysis and reversed electrodialysis)
FB	flow battery
GEN	generation
GHO	Great Horned Owl
HR	hazard report
ID	inner diameter
IDFF	interdigitated flow fields
IDFF-R	interdigitated flow fields ramped
kn	knot
kPa	kilopascal
kW	kilowatt
kWh	kilowatt-hour
KCl	potassium chloride
KOH	potassium hydroxide
kg/L	kilogram per liter (equal to g/cm^3)
lb	pound
lbf	pound-force
LaRC	Langley Research Center
Li-ion	lithium-ion
LSAWT	Low Speed Aeroacoustic Wind Tunnel]
m	modes
mA	milli-Ampere
mAh	milli-Ampere hour
mho	reciprocal of an ohm
MCR	Mission Concept Review
Mod	modification
mA/cm^2	milli-Ampere per square centimeter
nmi	nautical miles
N	Newton
NACA	National Advisory Committee for Aeronautics
NASA	National Aeronautics and Space Administration
Na_2S	sodium sulfide
NEF	nano-electro fuel
NiCd	nickel-cadmium
NSGA	non-dominated sorting genetic algorithm
OD	outer diameter
OML	outer mold line
OH	hydroxyl
OpenVSP	Open Vehicle Sketch Pad
PAS	Propeller Analysis System
PCI	Peripheral Component Interconnect
PERF-INT	performance requirement, integration
PXI	PCI eXtensions for Instrumentation
RCC	Rotating Current Collector
RDF	rim-driven fan
RDM	rim-driven motor

RFB	redox (reduction-oxidation) flow battery
S	serpentine
SiC	silicon carbide
SLSD	sea level standard day
SOFC	solid oxide fuel cell
SPL	sound pressure level
SSTOL	super-short takeoff and landing
STOL	short takeoff and landing
TE	trailing edge
TOGW	takeoff gross weight
TPM	technical performance metric
TRL	technology readiness level
VDC	volts direct current
Vmag	velocity magnitude
VTOL	vertical takeoff and landing
v/nD	advance ratio
W	watt
W/inch	watts per inch
W/kg	watts per kilogram
Wh/kg	watt-hour per kilogram
Wh/L	energy density
ZEST	Zero-Emissions Super-short Takeoff and landing

Technology Description

The National Aeronautics and Space Administration (NASA) Convergent Aeronautics Solutions (CAS) project investigates technology feasibility for new, disruptive technologies. The Aqueous, QUick-charging battery Integration For Electric flight Research (AQUIFER) project investigated nano-electro fuel (NEF) and rim-driven motor (RDM) technologies integrated together in a wing section (Wing Demonstrator). The system goal was to reduce and/or eliminate in-flight fire and explosion hazards associated with the conventional battery system; improve the acoustic signature of the electric motors; and co-locate these technologies to reduce cable lengths and electromagnetic interference (EMI) concerns. The specific technology targets were to achieve 100 mA/cm^2 in a NEF flow battery cell; demonstrate no fire or explosion hazards; and integrate the technology with an RDM into a Wing Demonstrator.

The planned technology improvements for both NEF and RDM were captured as progressing from technology readiness level (TRL) 4 to TRL 6 (see the chart, “NASA Technology Readiness Level,” following section, “Technology Application and Future Work Considerations”). The two-year project was chosen during the NASA CAS selection process and officially began in October of 2018 and finished in September of 2020.

The NEF concept takes a traditional flow battery where the anode and cathode materials are fluids which are pumped across a membrane to create an electric current and suspends specially coated nanoparticles to drastically improve the energy carrying capacity of the fluid, as shown in the top middle portion of figure 1.

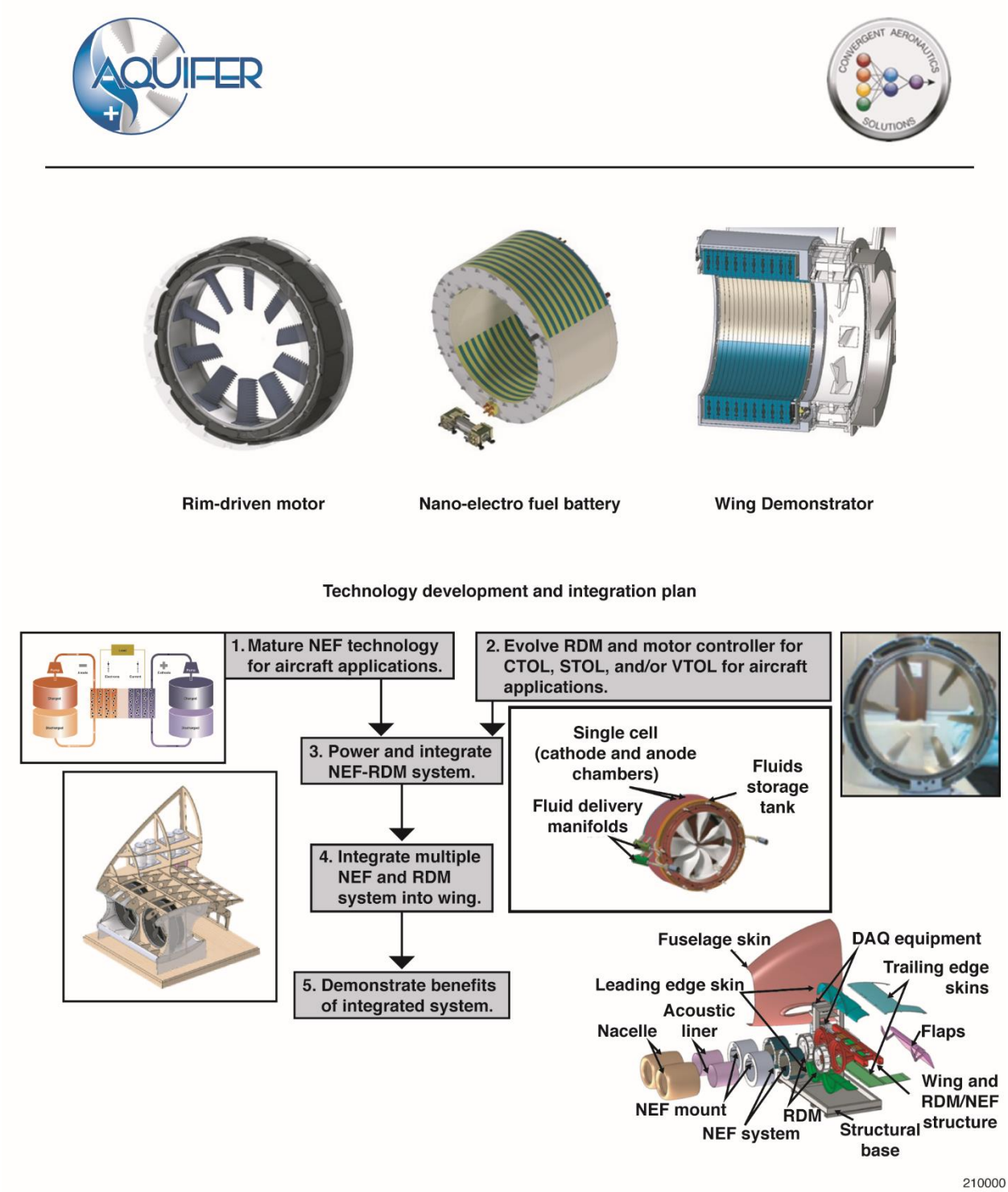

Figure 1. The Aqueous, QUick-charging battery Integration For Electric flight Research technology summary: rim-driven motor (top-left); nano-electro fuel battery (top-center); motor plus battery integration within the Wing Demonstrator (top-right); and the technology development and integration plan (bottom).

A significant benefit of a fluid battery concept is the ability to exchange the fluid during refueling instead of charging. This concept enables the ability to pump the fluid in and out of the

system during ground refueling and charging the fluid off-aircraft at a designated charging station. Battery cycle life is currently unknown, but no perceivable degradation has occurred during charge/discharge cycle testing for the dozens of cycles completed to date.

The RDM concept is an electric motor without a hub and driven from the outer circumference, shown in the top-left portion of figure 1. This configuration places the rotor fan blade tips toward the center of the duct, reducing the tip speed Mach number, thereby reducing the sound pressure level (SPL) produced by the fan blade tips. Reduction or complete removal of the hub can reduce drag, noise, and improve motor integration factors. A proof-of-concept design methodology using this technology is presented as a case study. NASA and The Boeing Company (Chicago, Illinois) uses an all-electric Zero-Emissions Super-short Takeoff and landing (ZEST) aircraft as a case study for this design.

The AQUIFER is integrating the NEF and RDM technologies together into a flight-scale Wing Demonstrator in order to understand integration challenges with these new technologies and is shown in the top-right portion of figure 1. NASA has partnered with Influit Energy (Chicago, Illinois) for NEF development; Engineered Precision, Inc. (Costa Mesa, California) for RDM development; Empirical Systems Aerospace, Inc. (ESAero) (San Luis Obispo, California) for Wing Demonstrator integration and testing; and The Boeing Company for future aircraft design considerations and potential air-bearing research.

The AQUIFER technology development and implementation plan is shown in the bottom of figure 1. A synopsis of the technology feasibility assessment is shown in table 1 and shows the NASA CAS targets for the end of September 2020 as well as the results and discussions from the feasibility assessment.

Table 1. Feasibility assessment results (synopsis).

Technology	CAS target*	Results	Feasibility assessment
NEF	• Inflammable / Nonexplosive • 100 mA/cm^2 • TRL four to six	• Inflammable / Nonexplosive • 85 mA/cm^2 ** • 200 mA/cm^2 ***	NEF development has steadily improved throughout project, starting at 1 mA/cm^2 at 3.6 VDC and matured to 85 mA/cm^2 at 3.6 VDC for three minutes.
RDM	• 9000 RPM at □90 percent efficiency • Improved acoustics signature from standard electric-ducted fan • TRL four to six	• Designed to target values (with air bearings) • Medium/High confidence in acoustics improvements for RDM	RDM with conventional bearings is not feasible, but with air bearings, design appears valid and acoustics testing would be required to provide evidence of improved acoustics signature.

Wing Demonstrator	• Integrated NEF-powered / RDM wing section	• Development ended before hardware fabrication • No apparent technological barriers with Wing Demonstrator specifically	Integration design, hazard analysis, operational perspective, and operability all appear feasible. Wing Demo fabrication, testing, and delivery were cut once CAS management chose to end AQUIFER execution.

*Target technology performance based on original project ending (September 30, 2020).
**85 mA/cm^2 achieved in NEF flow cell (Sep. 2020), CAS target was 100 mA/cm^2
***200 mA/cm^2 achieved in NEF Rotating Current Collector (RCC) cell (Jul. 2020)

Nano-electro Fuel (NEF) Technology

The NEF hardware represents the first generation (GEN 1) of the NEF chemistry which includes nanoparticle fluid anolyte and catholyte and is shown in figure 2. The GEN 2 of the NEF chemistry replaces the nanoparticle fluid anolyte with an air or gaseous oxygen O_2 anode. Beyond GEN 2, the “Vision System” represents the final technology level for the NEF. Performance values are used as the basis for the cooperative effort with The Boeing Company for their ZEST aircraft design.

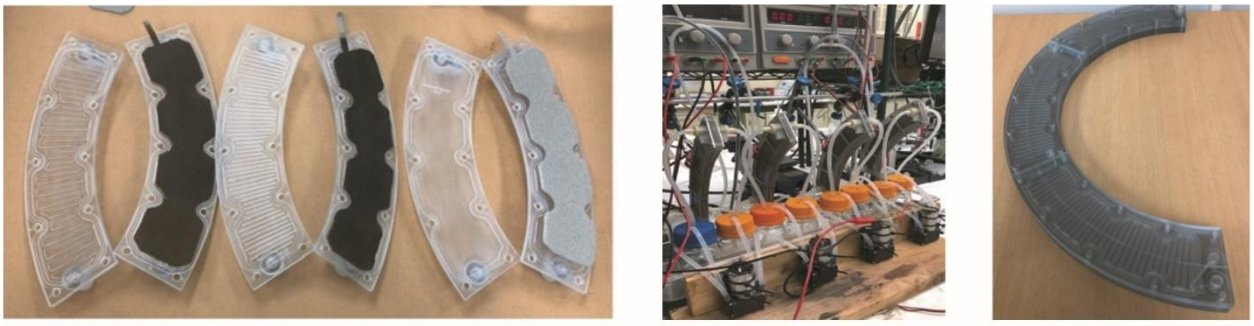

Figure 2. (left) The nano-electro fuel GEN 1 annular cells; (middle) cell testing; and (right) half-annular stack fully connected.

The development of nanofluids for the transport and storage of energy in a solid-liquid composite material versus solid electrodes in conventional batteries has been ongoing for several years. Potential use cases for nanofluid energy storage exist wherever energy is transported and utilized in a liquid format (i.e., petrochemical use in converting chemical bonds into mechanical work) or where applications using fixed-format energy storage would benefit from a wholly new design space (i.e., electric transportation applications).

The AQUIFER project partnered with Influit Energy to provide a unique, novel rechargeable nanotechnology-based NEF flow battery designed to eliminate fire/explosion hazards and decouple power and energy of the battery design while maintaining competitive energy density performance. The NEFs are low-viscosity suspensions of nanoscale battery materials (cathode and anode) in water-based electrolytes. The nanoscale size of the active materials enables stable suspensions; rapid charge/discharge kinetics; and high loading of solid electrode materials resulting in a flow battery competitive with lithium-ion (Li-ion) batteries (approximately 130 Wh/kg and 350 Wh/L at system level) and an operating temperature range of -40 °C to +80 °C. The transformational aspect of NEF technology is the merging of two well-established battery formats: (1) solid battery chemistries with high energy density; and (2) the

pumpable format of redox flow batteries. One important aspect to producing the NEF technology is the process of preparing and dispersing nanoscale electrode materials in aqueous electrolyte at high solid loading. This process enables high system-level energy density in low-viscosity liquids, positioning rechargeable NEF batteries as an alternative to gasoline/fossil fuels.

The pumpability of NEF energy storage will enable rapid refueling and vertically-integrated energy storage ecosystems, enabling energy needs for both stationary operations, transportation, and the shift toward renewable energy. The viscosity of the fluid must not be too high as to prevent pumpability or force pump-power requirements to become a substantial power draw on the system.

Unlike Li-ion batteries or fossil fuels, high energy density NEF liquids offer inflammable, inherently safer energy storage solutions for remote locations or installations where high voltage infrastructure is unavailable. Additionally, the use of Earth-abundant elements in NEF formulations enables low cost (one-half the cost of Li-ion) geographical and geopolitical advantages versus mining and procuring lithium from Asia.

The NEF technology will also enable greater efficiency and longer “per charge” operations. The flow battery format enables the separation of power and energy storage capacity with the flexible design features, intrinsic to flow batteries. This format feature enables novel approaches to the electrification of both civilian and military transportation and devices, and specifically allows aerospace advances toward the following: distributed power delivery; reduced EMI with stack and motor colocation; optimization of aerodynamics; and rapid vehicle/plane/ship refueling options (not available with conventional battery packs). High thermal conductivity of nanosuspensions is an additional feature of NEF technology that can be explored in the future, potentially allowing combined electrical energy storage and thermal management functions in new vehicle designs.

The NEF battery technology is a transformational advancement of redox flow battery concepts where energy is stored and released through a reversible electrochemical reaction between two electrolytes. The cathodic and anodic electrolytes are stored externally to the battery and circulated through the reactor as required, providing separation between power ratings and energy storage capacity and is shown in figure 3.

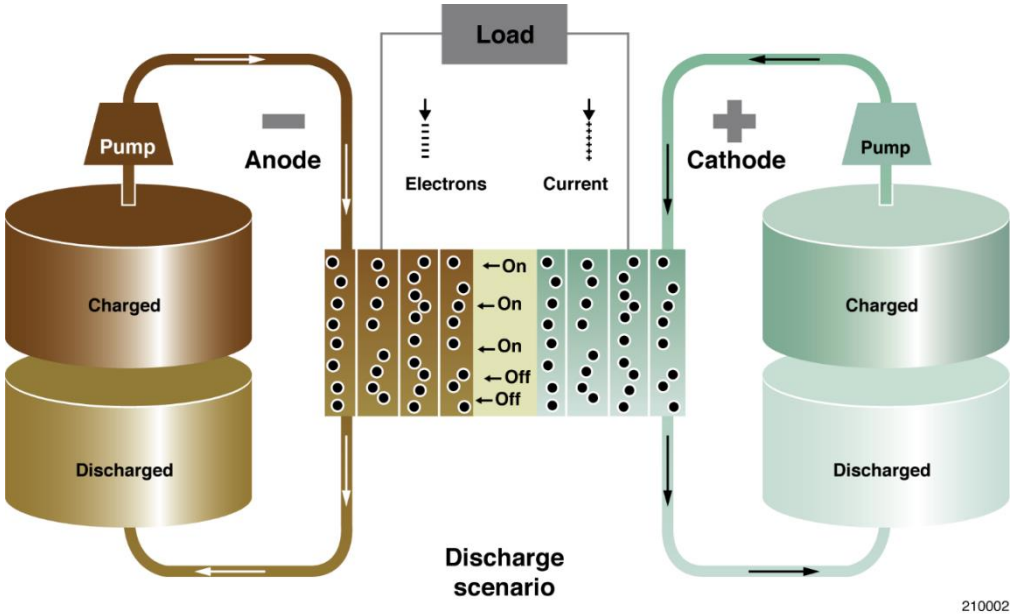

Figure 3. The nano-electro fuel architecture concept: GEN 1 has fluid anolyte and catholyte; GEN 2 has an air or O2 anode and fluid catholyte.

The main limitation of electrolyte-based flow batteries is the low-energy densities (40-80 Wh/L) as a result of the limited solubility of redox salts. Instead of redox salts, NEF technology uses stable dispersions of solid cathode and anode nanomaterials in aqueous electrolyte as the rechargeable battery fuel. Nanoparticle suspensions have significantly higher stability than micron-sized suspensions as a result of relative balance of Brownian motion and gravity. At a manageable viscosity increase, the NEF fuel can be prepared with as high as 60-volume percentage solid loading in electrolytes and up to 80-volume percentage (>70-percent weight percentage) in a self-suspended solventless format. Keeping viscosity low is key to keeping pumping requirements and other parasitic losses low. Viscosity can be controlled by appropriate surface modification of the redox nanoparticles. Unsupported nanoparticles in suspensions provide an additional advantage to intercalation-based redox chemistry. The volume expansion during intercalation/deintercalation does not affect the integrity of the electrode, unlike electrode materials attached to the current collectors that suffer permanent loss of capacity. Concurrently, if nanoparticles are smaller than the self-healing threshold for a given material, the defects resulting from volume changes in the nanoparticles can self-repair; thus, minimizing the loss of capacity and providing an extended battery life cycle.

The AQUIFER concept employs Influit Energy unique flow cell designs that are optimized for use with nanosuspension electrodes. The cell design does not require the addition of carbon nanotubes or other conductive fillers into the cathode and anode dispersions; suspended nanoparticles effectively charge/discharge as they are pumped through the corresponding cathode/anode cell chambers with the current collector. This design approach allows the dramatic increase in the volumetric energy density of NEF GEN 1 (up to 354 Wh/L) and is shown in the right side of figure 4. Additionally, avenues toward realizing the enormous potential of clean energy for environmental, social, and economic sustainability can be recognized.

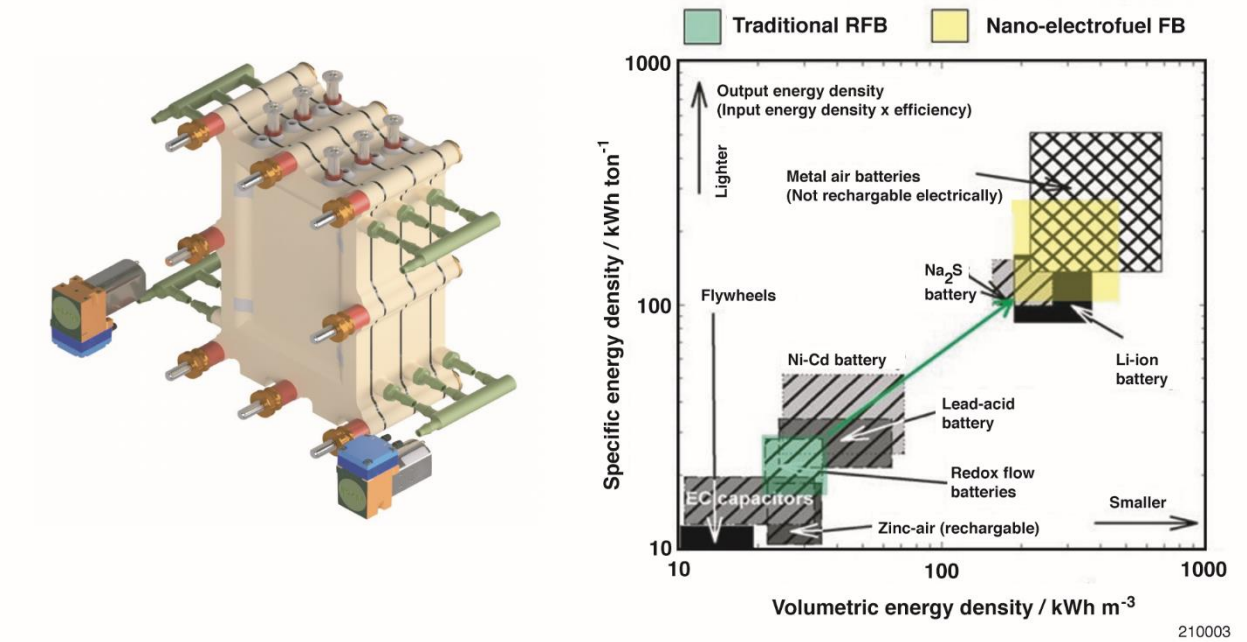

Figure 4. (left) Conceptual design of the nan-electro fuel flow battery cells; (right) comparison of energy density in different types of batteries, demonstrating the potential of the nan-electro fuel technology as compared to traditional redox flow batteries.

Electrical energy is stored in redox nanoparticles included in the NEFs. In battery discharge mode, NEFs undergo a spontaneous electrochemical reaction with cathodic nanofluid being reduced and anodic nanofluid being oxidized. The difference between electrochemical

potentials for cathodic and anodic redox reactions defines the cell potential. Under steady-state rest conditions, the cathodic and anodic NEFs are stored in two separate reservoirs (or half-cell bodies); separated by an ion-conducting electron insulating membrane. Excluding diffusion across the membrane and corrosion reactions, which take effect over long durations, NEFs cannot be discharged without a closed circuit. The spontaneous electrochemical reaction of the battery discharge only occurs when there is a path for electrons to flow from the first half-cell body to the second half-cell body (closed circuit). Once the circuit is closed, the electrons start flowing from anode current collector to cathode current collector through the circuit. The ions are flowing through the ion-conductive membrane for compensation of charge created at the cathode. When the cathodic and anodic NEFs flow through an electrochemical cell at closed circuit electron movement from anodic to cathodic, material commences and an electrical current is generated. The energy of the electrons that leave the anode is higher than the energy of electrons delivered at the cathode; therefore, work is done. In battery charging mode the flow of cathodic and anodic fluids is reversed, and corresponding redox reactions are reversed under the application of an external energy source.

The nano-electro fuel may be stored in charged or discharged form, separate from the electrochemical device. This design feature provides improved flexibility in design concepts and operational considerations.

An advantage of using nanoparticle suspensions as active energy-storing electrolytes instead of electroactive salt solutions, is that both ion-exchange and porous membranes could be used for cell membranes. As long as the pore size is smaller than the size of the nanoparticles, no cross-over and mixing between cathodic and anodic nanoparticles will occur. Ion and base electrolyte species can freely travel through the membrane to compensate for charge transfer and can improve reaction kinetics and reduce the cell impedance.

The advantage to separating the power stack from NEF storage tanks is the reduction of inactive packing materials from approximately 65-weight percent in solid-state batteries down to 35-weight percent in NEF flow batteries and is shown in figure 5.

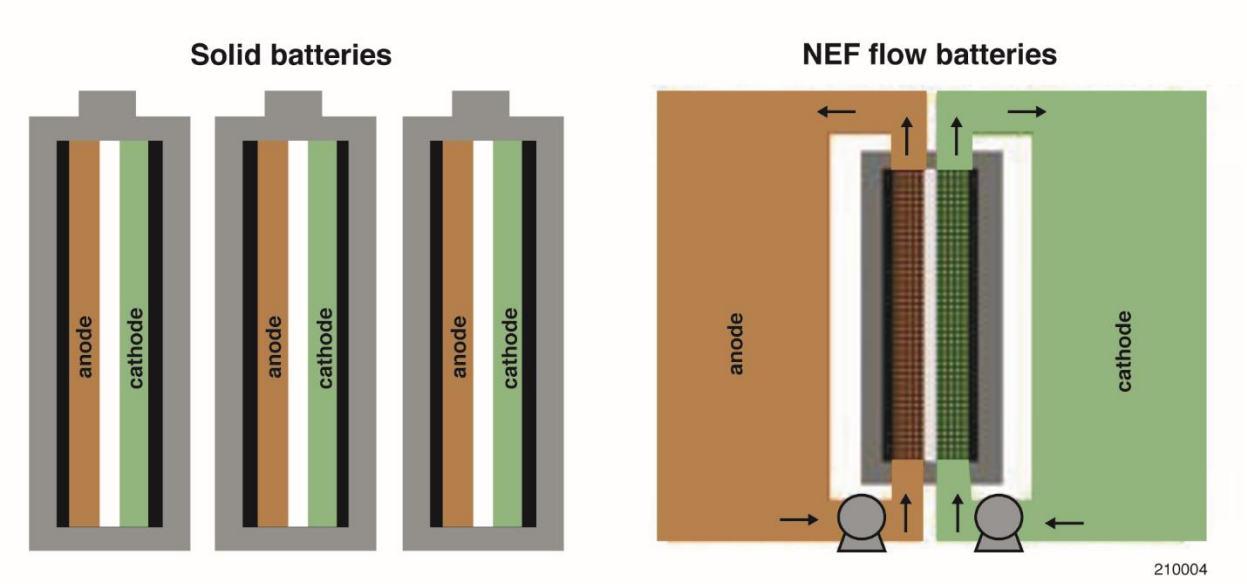

Figure 5. (left) Illustration of conventional solid batteries; (right) the nano-electro fuel flow batteries. Solid batteries scale linearly with system size (55-70 weight percent of packing material) while the nan-electro fuel systems provide a higher energy density in larger systems because of the separation of reactants and reduction in packing material (15-35 weight percent packing).

Although the NEF approach appears to be applicable to any battery chemistry implemented in solid format - including high energy density Li-ion battery materials - current development focuses on aqueous electrolytes for both economic and technical reasons. Li-ion battery materials and organic electrolytes are an order of magnitude and more expensive than aqueous analogs; even with the higher cell voltage, the result is a higher cost per kWh. From a technical perspective NEF with Li-ion chemistries in organic electrolytes, although possible, face additional challenges such as: slow reaction kinetics, solid-electrolyte interface (SEI) layer formation, and electrolyte sensitivity to air and moisture; therefore, there is an environmental and manufacturing appeal to the development of aqueous NEF batteries.

Prior to the AQUIFER project, Influit Energy conducted screening of potential candidate anode and cathode materials for aqueous NEF electrodes and chose to initially focus on the use of ferric oxide (Fe_2O_3) as anode and gamma manganese dioxide (γ-MnO_2) as cathode candidates because of their high energy storage capacity, availability, natural abundance, and low costs. The techno-economic performance model shows significant potential of the chosen materials toward competitive energy density (Wh/kg) and cost in U.S. dollars per kWh. The concept of the ability of NEF electrodes to charge and discharge over multiple cycles at approximately 80-percent efficiency has currently been demonstrated at low solid concentrations (5- and 10-weight percentage). Suspensions, however, with high nanoparticle loadings (greater than 70-weight percentage) and low viscosities have been achieved in alkaline electrolytes. These two properties – good electrochemistry and low viscosity at high particle loadings – are the pre-requisites for realizing high energy density NEF batteries. The approach to achieving these properties (developed by Influit Energy researchers) is based on engineering of surface properties of nanomaterials that enable both electrochemical activity and colloidal stability of suspensions. The AQUIFER effort utilized already tested surface modifications of cathode and anode nanoparticles and focused on demonstration of the full toroidal flow cell with cathode and anode NEF, shown in figure 6.

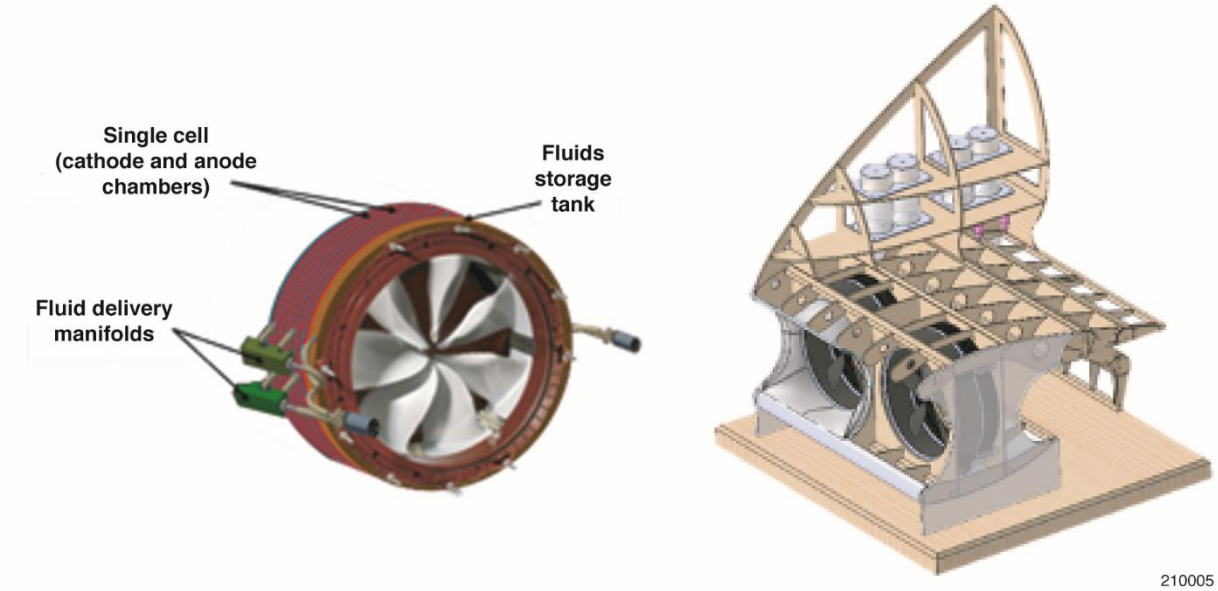

Figure 6. (left) 12-VDC and 8.3-A radial motor stack, and (right) integrated Wing Demonstrator with advanced rim motor and conceptual nan-electro fuel system.

The initial technology development roadmap within the AQUIFER project consisted of seven tasks, as seen in table 2.

Table 2. The NEF development tasks.

Task		Description
1	Membrane optimization	Preliminary results were obtained with Nafion™ NR212 membrane, which is proton conducting membrane and has a fundamental performance limitation for alkaline chemistries. Specifically, there are essentially no protons that exist in alkaline media, thus ion transport on charge results in transfer of water molecules across the membrane. Water molecules transferred from cathode chamber to anode chamber will result in electrolyte level disbalance and the thickening and eventual drying out of cathode nanofluid, as a result cells stop working. One of the first tasks, therefore, was to identify an anion conducting membrane, which would accommodate the transport of hydroxyl $(OH)^-$ groups on charge, addressing the electrolyte drag problem.
2	Nanofluid optimization for single-flow cell tests	Nanofluid optimization which included particle concentration, additives, and electrolyte variations was scheduled to follow the membrane optimization.
3	Cell flow field optimization for annular cell design and validation	Other flow battery chemistries have demonstrated flow field within the cells, critical for the current density and discharge efficiency because the flow field determines the rate of collisions between redox active species in the solution and the current collector. Task three was dedicated to the design and testing of different flow field geometries within the annular flow cells.
4	Stack design and validation	To deliver a 12-VDC and 100-W stack to spin the RDM motor, six annular sector cells have to be combined in one continuous ring cell; ten of such ring cells, each delivering 1.2 VDC, have to be combined into a stack to deliver 12 VDC. It was proposed to do a stepwise validation of a stack, first combining sector cells into a 6-VDC stack before assembly and testing of the final deliverable.
5	Development of the Battery Control System and balance of plant	The purpose of this task is to have monitoring and control options for the battery operations.
6	Manufacturing stack and cell components	This task is intended for scaling up the cell production for the large stack deliverables.
7	Nanofluids production	This is an ongoing task throughout the project; initially, to produce sufficient amounts of fluids for individual cell testing and later, producing the nanoparticles and nanofluid for the two prototype stacks. Future work

considerations related to implementation of novel nanofluid electrodes in an electrochemical flow reactor are electrolyte management; prevention of side reactions; and mitigation of osmotic drag of electrolyte across the membrane. These nanofluid problems can result in varying NEF concentration during charge/discharge; cell impedance; incomplete charge and discharge of nanoparticles; and instability of the surface treatment through multiple charge and discharge cycles.

Rim-driven Motor Technology

The RDM concept was derived from previous acoustics and motor design work on the Air Force Research Laboratory (AFRL) Great Horned Owl (GHO) unmanned aerial vehicle project. The legacy RDM concept was ultimately not chosen because of acoustic problems associated with the mechanical bearings; researchers decided that the design would be competitive using an air or magnetic bearing solution. These motors were investigated by the AQUIFER team and were decided to be a logical integration partner with the proposed annular NEF cells because of their potential to reduce noise - another barrier toward electric flight. A 9- and 14-in diameter RDM, developed by the AQUIFER team, is shown in figure 7.

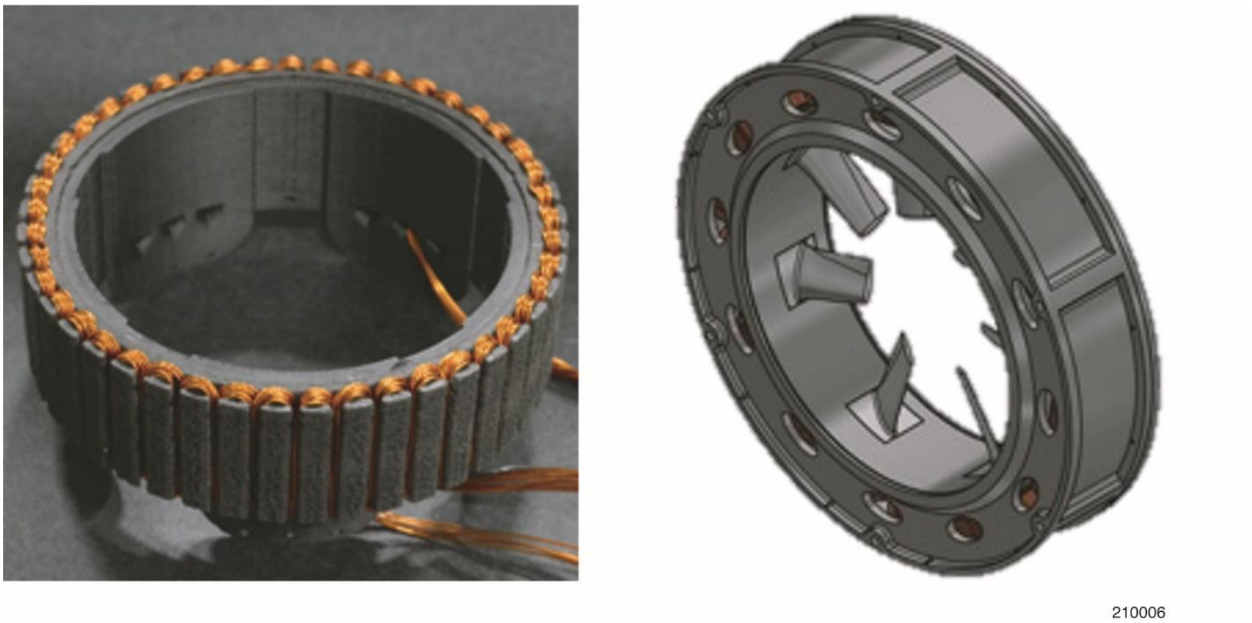

Figure 7. (left) The National Aeronautics and Space Administration in-house three-dimensional (3-D) printed 9-in diameter rim-driven motor prototype; and (right) the Engineered Precision, Inc. 14-in diameter rim-driven motor final design with blades and outer frame.

The RDM generates torque at the outer diameter of the spinning structure, rather than at the hub; the RDM is lighter and more efficient than conventional designs because of its ability to produce higher rotor-tip speeds. At a set power and larger relative radii, the motor provides a large torque advantage (meaning, the current can be reduced; therefore, reducing both mass and increasing efficiency). The unique form factor provides a large surface area for cooling and

allows for many integration benefits when coupled with the co-located NEF stack. The absence of a hub reduces drag, cabling, and eliminates support struts; thus, reduced blade passes of the fan across static structures occurs, resulting in the overall reduction of the acoustic footprint. Concentrating the motor mass around the outside of the duct also allows for tighter structural integration, resulting in shared structural support of the wing, battery, and motor. Potentially, thermal management can be combined between the battery, motor, and duct skin.

The brushless permanent-magnet design is housed within a duct and sized for an annular inner diameter of 14 inches. The distributed nature of the propulsors allows the individual power of each motor to be less than 13 kW. This combination of large area and relatively low torque drives the motor design toward non-traditional solutions. The bladed hoop also places unique structural requirements on the blades, which are subjected to atypical mechanical stresses. The battery is mounted axially aft of the motor with fluid running in a hoop around the duct as well as transversely through the wing, as shown in Figure 8.

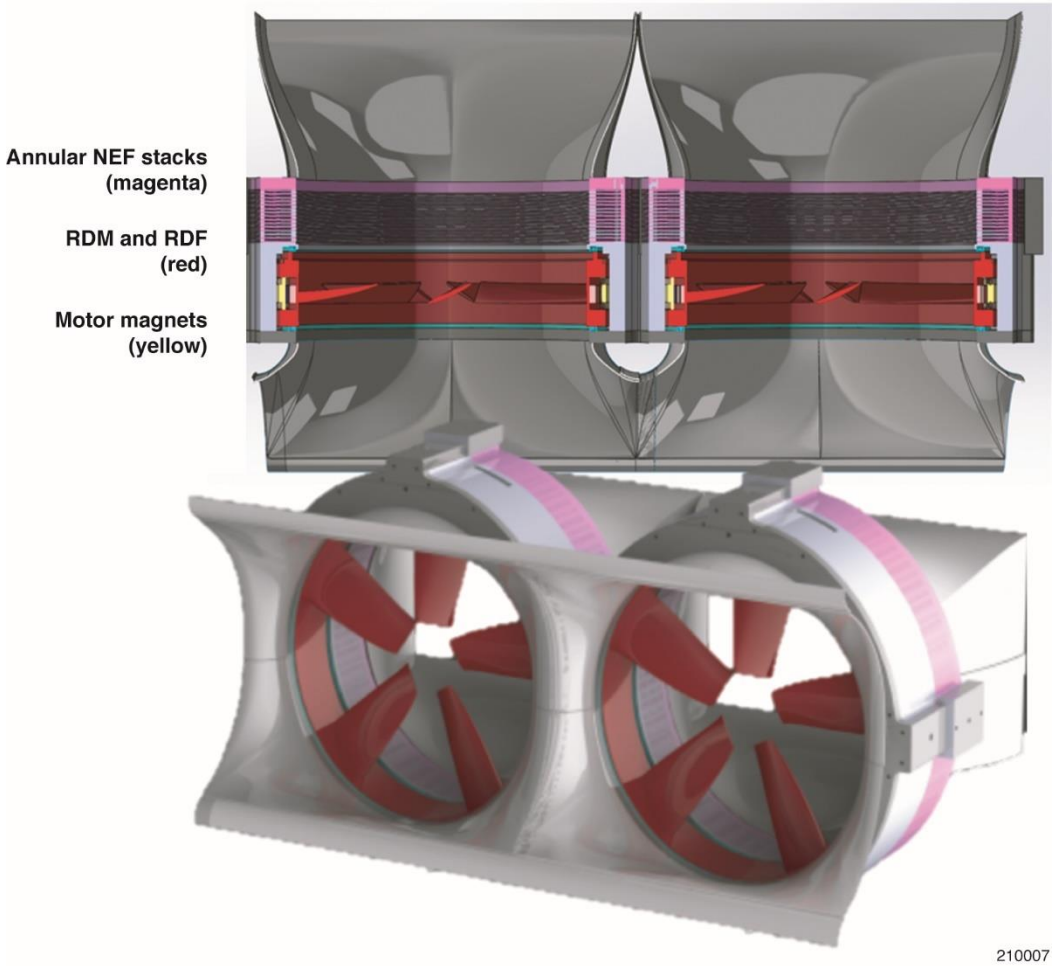

Figure 8. Two rim-driven motors within an integrated structure (similar to the Zero-Emissions Super-short Takeoff and landing aircraft wing concept). Fan blades are bright red; the rotor is light red; magnets are blue; the nano-electro fuel annular battery stacks are purple; the fixed geometry is gray

Rim-driven Motor Design Challenges

There are several technological barriers associated with the RDM concept, as it relates to the AQUIFER concept. There are battery limitations from the NEF, requiring the motor and controller to operate at far below optimal voltage conditions. The bearings are the crux of the technology and are a limiting factor for technology proliferation. Mechanical bearings will not be feasible; therefore, there is a derived requirement for either air-bearing technology or magnetic-levitation bearings.

Battery Challenges

As a result of the currently low TRL of the battery (see the chart, “NASA Technology Readiness Level,” following section, “Technology Application and Future Work Considerations”), the 2020 demonstrator prototypes are being sized to 12 volts direct current (VDC) and 1.5 A. The development is currently focused on improvements to the aqueous solution and adapting the conductive membrane to be integrated into an annular form factor for the propulsor. Radial thickness of the prototypes and power levels will not reflect flight sizes. These limitations drive the thickness requirement for the motor and have minimum power requirements to operate.

Bearing Challenges

Flight-scale bearing system design is out-of-scope of the AQUIFER project, so traditional roller bearings are being implemented beyond their rated capabilities. The project has accepted the limited life, added weight, and added drag associated with this compromise; as a result, an additional requirement on the motors to overcome the increased drag and reject bearing heat is required.

Weight Challenges

Determining the power densities of state-of-the-art motors can vary as a result of different weight accounting. The integrated nature of the RDM make this definition even more difficult to define. The overall weight of each motor will likely need to be greater than 3 kg and oversized for prototyping, installation, and to address safety precautions.

The Wing Demonstrator Design

This section depicts the AQUIFER technology concept; a brief synopsis of the feasibility assessment as it pertains to the three major technology elements (NEF, RDM, and Wing Demonstrator); and key project events. The purpose of the Wing Demonstrator was to take two advanced technologies: (1) the NEF battery system; and (2) an RDM; and demonstrate the integration of these two systems into a Wing Demonstrator based on the NASA/Boeing ZEST concept, shown in figure 9.

Figure 9. The original NASA / Boeing Zero-Emissions Super-short Takeoff and landing concept.

The AQUIFER concept (shown in figure 10) demonstrates the integration of the NEF and RDM technologies into the Wing Demonstrator, retiring or reducing the following electric propulsion concerns: fire/explosion hazards, recharging time, radiated EMI, coupled power and energy, range limitations, and noise concerns. The purpose of the AQUIFER project was to verify or prove those benefits.

Barriers to entry for electrified aircraft propulsion using traditional battery technologies can be summarized as: fire / explosion hazards, recharging time, electromagnetic interference EMI, coupled power and energy, and range.

The decoupling of energy storage from power plants, in the flow battery format, allows for new design flexibility to address the barriers listed above. The associated advantages are:

- The aqueous base fluid is nonexplosive.
- Reduced charging time by exchanging expended NEF fluid for pre-charged fluid.
- Separation of storage tanks from the power stack, allowing the co-location of the stack and motor, reducing the cable runs present in traditional electric vehicle designs.
- Flow batteries power rating and energy storage capacity are decoupled.
- GEN 1 NEF systems with similar energy density to the Li-ion systems with additional plans for developing a much higher energy density system in a GEN 2 chemistry, addressing large-body aircraft and their resultant range problems.

The Wing Demonstrator was used to address the barriers listed above and is shown in Figure 10. The associated chart represents the AQUIFER concept.

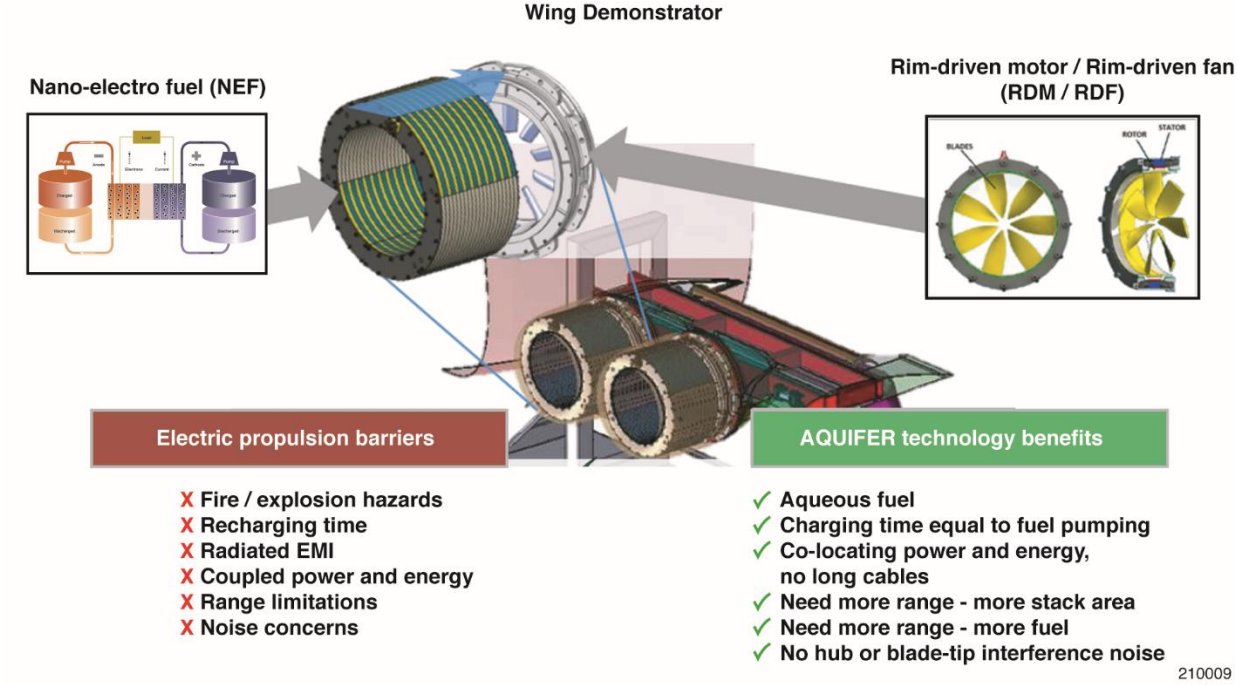

Figure 10. The Aqueous, QUick-charging battery Integration For Electric flight Research concept.

The initial Wing Demonstrator design produced by NASA, shown in figure 11, provided a simple integration of the NEF and RDM systems but added little benefit to lessons learned for the true structural integration because it did not include structural members or any structural analysis.

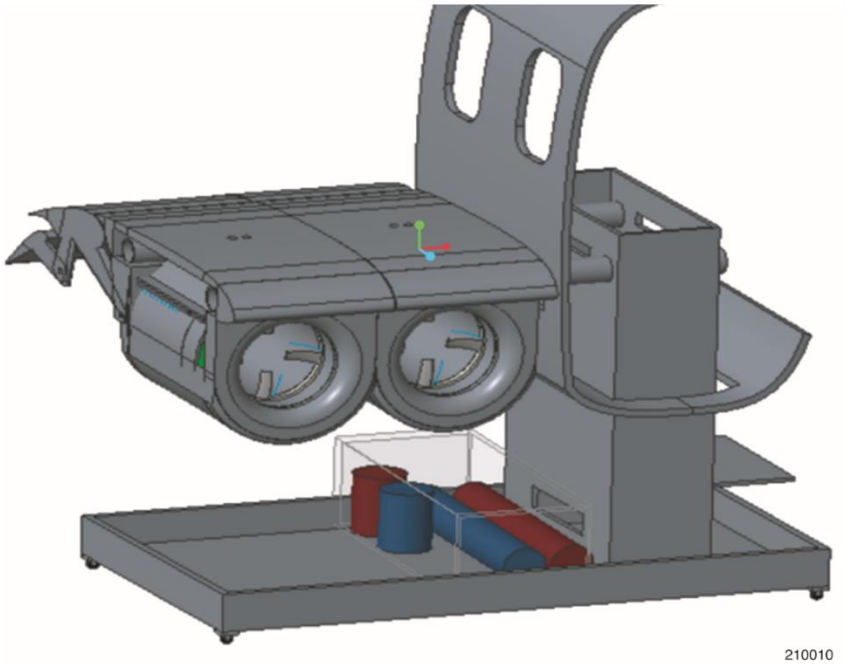

Figure 11. Original Wing Demonstrator design.

The ESAero was contracted to design the Wing Demonstrator system and integrate the NEF and RDM system. This system was to resemble The Boeing Company ZEST design, showing the technology integration in a viable wing design. Initially, the Wing Demonstrator was based

on a design with the NEF and RDM features integrated in a tandem wing, although design changes to the ZEST concept relocated the nacelle to the front of the wing. To best represent the ZEST design, the Wing Demonstrator was modified to align with the updated configuration and is shown in figure 12.

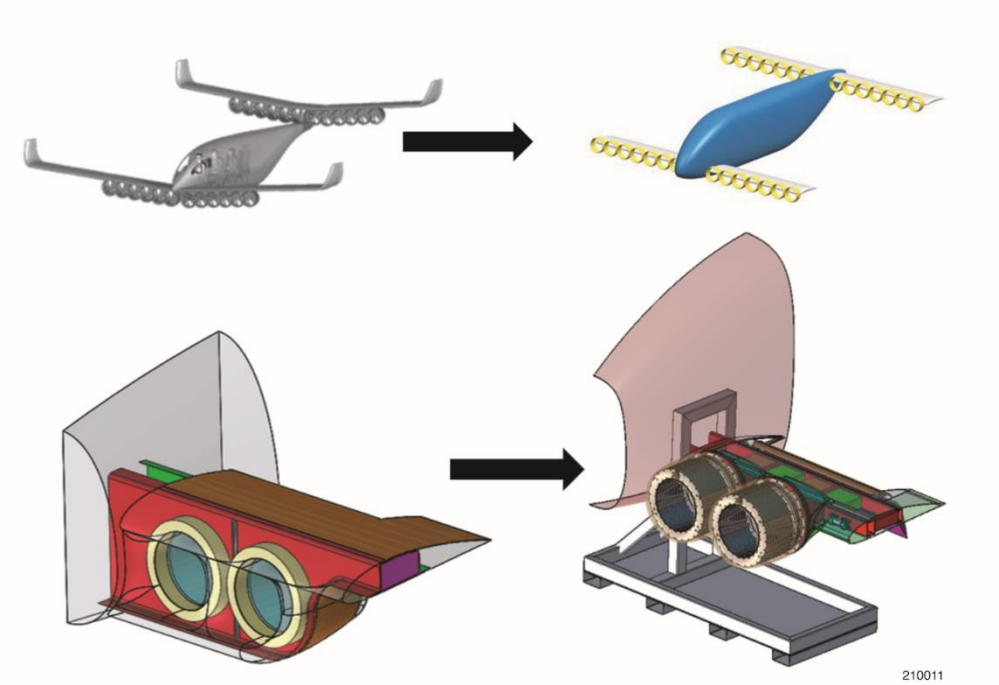

Figure 12. Zero-Emissions Super-short Takeoff and landing design and Wing Demonstrator progression.

The exploded view of the Wing Demonstrator design is shown in figure 13. The design integrated the NEF and RDM technologies into a flight-like wing, complete with lifting surfaces and skin. Because of the power availability from the NEF GEN 1 stack (goal of 100 W), the RDMs would be downrated.

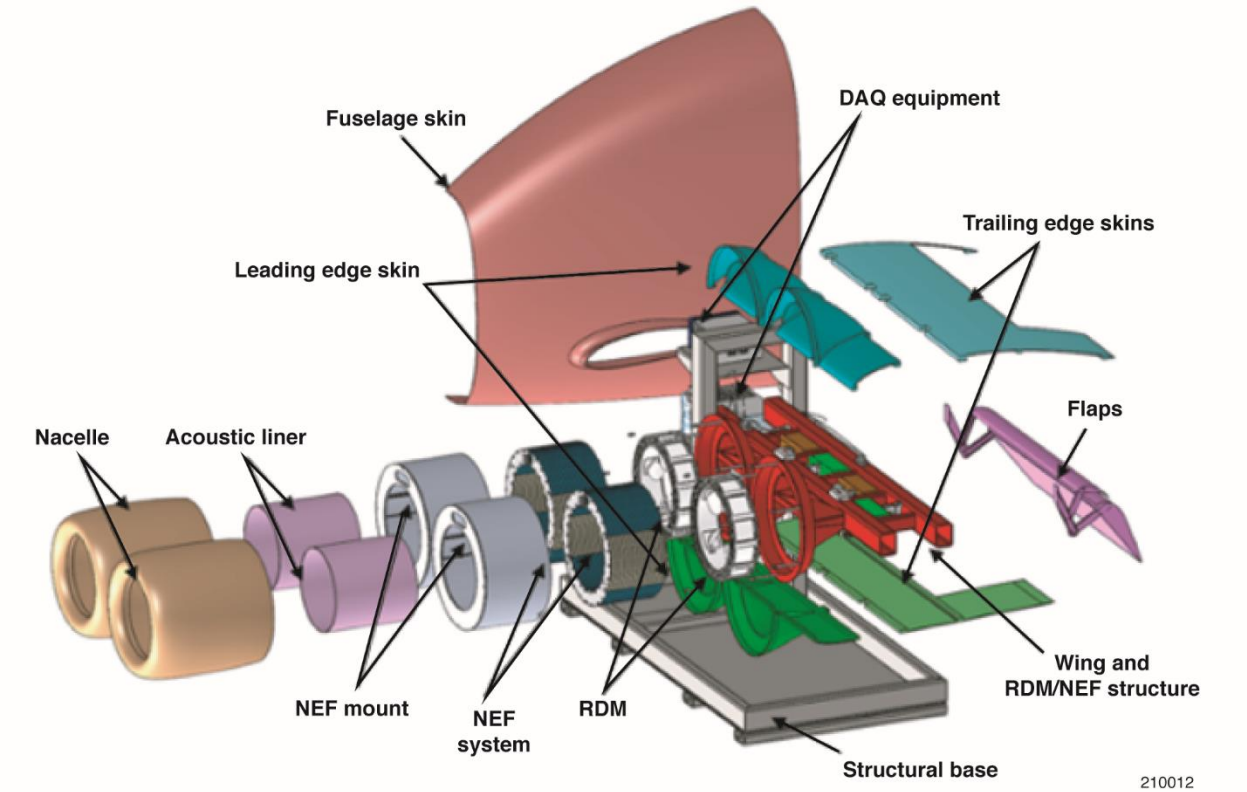

Figure 13. The Aqueous, QUick-charging battery Integration For Electric flight Research Wing Demonstrator, integrating the nano-electro fuel and rim-driven motor technologies into a flight-scale hardware demonstrator.

Potential Aircraft Applications

The AQUIFER project was a collaboration between NASA and The Boeing Company and investigated technology applications and aircraft studies. The following section shows some of the aircraft design and performance analyses and other relevant information related to The Boeing Company ZEST concept and the NASA electric super-short takeoff and landing (eSSTOL) concepts. The ZEST concept has matured from the ZEST 1.0 and preliminary designs (shown as ZEST 0) through ZEST 8.0 A and B variants, shown in figure 14.

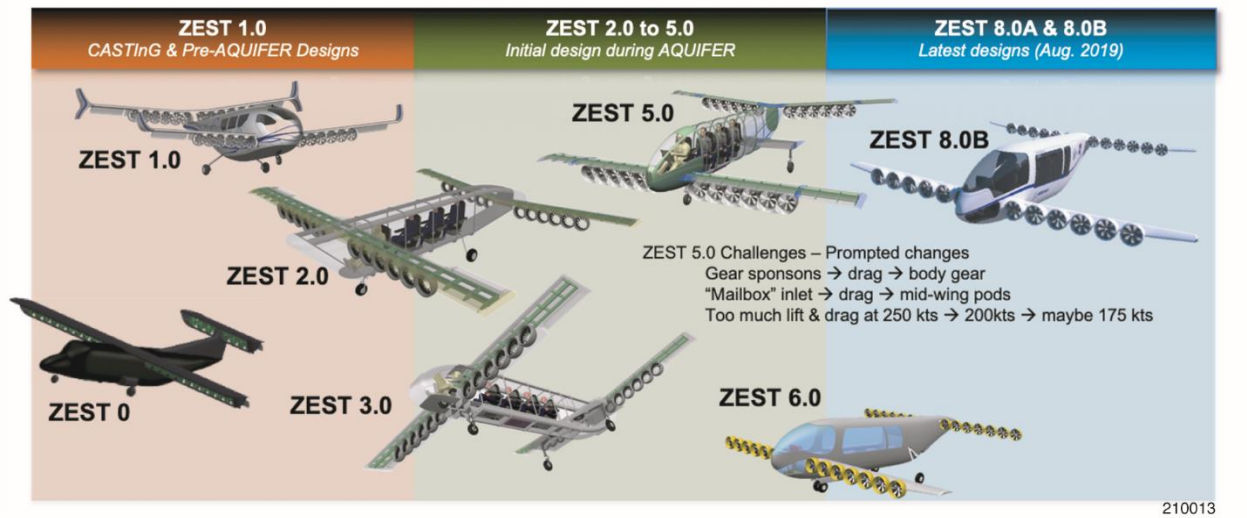

Figure 14. The Boeing Company Zero-Emissions Super-short Takeoff and landing development roadmap.

The aircraft has remained a tandem wing configuration throughout the process, although the number of NEF/RDM pairs; the location of motors relative to the wing; and the size of the motors has changed throughout the development process. Design considerations and lessons learned for the NEF, RDM, and integration technologies (although designed by NASA) were provided to The Boeing Company. The Boeing Company, in turn, continued to update their models and relayed those aircraft design lessons back to the AQUIFER team. The changes in the design of the Wing Demonstrator reflected the back-and-forth relationship between NASA and The Boeing Company. The ZEST 8.0 A and B concepts were the last update to the design before the AQUIFER execution phase was stopped. Figure 15 shows the NEF technology roadmap and technology improvement during the AQUIFER project. Specific energy values for various technologies as reference are as follows: Current NEF specific energy estimate: 10-29 Wh/kg; GEN 1 max specific energy estimate: 81 Wh/kg; the X-57 airplane battery system (installed): 125 Wh/kg; and GEN 2 max theoretical-specific energy: 745 Wh/kg.

Figure 15 shows the NASA X-57 “Maxwell” airplane as a point design. The Twin Otter, Pilatus PC-12 (Pilatus Aircraft Ltd, Stans, Switzerland) and the Cessna Skyhawk (The Cessna Aircraft Company, Wichita, KS) airplane annotations are shown for twin-engine turboprop comparisons.

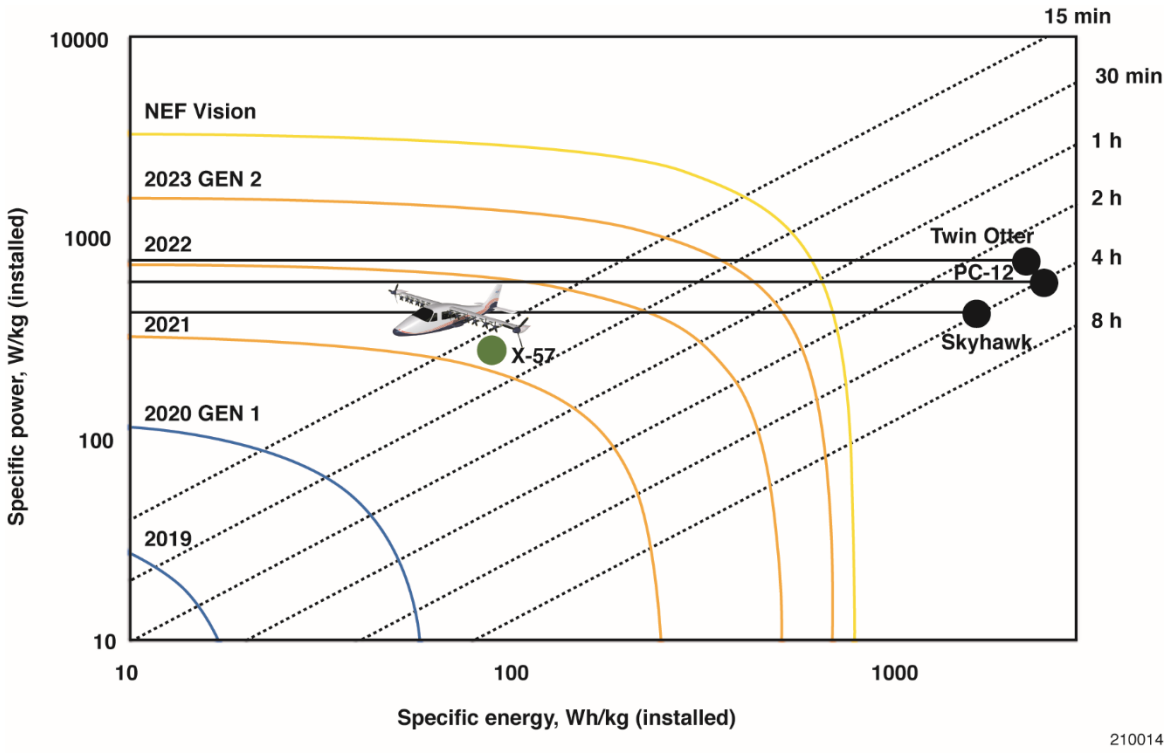

Figure 15. The nano-electro fuel technology development roadmap.

Methodology for Determining Feasibility

The feasibility assessment for the AQUIFER project is broken into primary and secondary feasibility criteria. The primary and secondary feasibility criteria are listed below.

Primary Feasibility Criteria

- Nano-electro fuel fluids produce no spark/fire / explosion ignition, to include mixing anolyte and catholyte.
- A single nano-electric fuel cell can operate at a current density of 100 mA/cm^2.

Secondary Feasibility Criteria

- A rim-driven motor designed to integrate with the nano-electro fuel cells can operate at a power output of 4 kW.
- Nano-electric fuel can power a rim-driven motor.
- An aircraft designed with rim-driven motors can provide acoustic benefits.
- An aircraft designed with ducted fan blades can provide propulsion airframe interaction benefits.
- A nano-electric fuel and rim-driven motor can be integrated into an aircraft wing.

The AQUIFER project relates to two of the NASA Aeronautics Research Mission Directorate Strategic Thrusts: (1) Strategic Thrust 3: ultra-efficient commercial vehicles; and (2) Strategic Thrust 4: transition to low-carbon propulsion. Strategic Thrust 3 and AQUIFER has near- and mid- to long-term applicability. Near term, NEF and RDM technologies provide improvements for fire safety, noise, and losses as a result of electromagnetic interference and provides 100-percent emissions-free aqueous fuel. Mid- to long-term applicability for NEF and RDM

technologies provide improved energy density solutions for battery systems and improved thrust and motor efficiencies.

The AQUIFER project is a feasibility assessment based on the NEF and RDM technology developments coming together into the integrated Wing Demonstrator solution in order to overcome several barriers to electric flight. This project had three unique technology developments, each with their own feasibility criteria. In order to ascertain the feasibility of the three technology developments, the AQUIFER project produced primary and secondary objectives to prioritize the developments. The primary objectives for the full feasibility assessment were to demonstrate NEF technology at 100-mA/cm^2 energy density and demonstrate the integrated NEF/RDM operation. The secondary objectives were to: demonstrate RDMs capable of Super-Short Take Off and Landing (SSTOL) operation; characterize the RDMs and rim-driven fan (RDF) acoustic performance; complete RDF blade design and development; complete the aircraft mock Wing Demonstrator with two NEF-powered RDMs; and complete transition to an aero project (internal or external to NASA). Some of the design concepts and benefits are implied within the nature of the experiment, and some need to be verified.

In order to successfully measure the primary and secondary objectives, technical performance metrics (TPMs) were used to better assess and grade the feasibility of these technologies. The TPMs for the AQUIFER project are provided in table 3.

Table 3. The Aqueous, QUick-charging battery Integration For Electric flight Research project technical performance metrics.

TPM	Related System	Value	Feasibility Assessment
TPM1	RDM	>90 percent efficiency at 9,000 RPM	Feasible
TPM2		10-50 VDC input	Feasible
TPM3		100-4,000 W output	Feasible
TPM4	NEF	No fire hazard	Feasible
TPM5		100 mA/cm^2 per cell	200 mA/cm^2 measured* 85 mA/cm^2 measured
TPM6		100 W output per Stack	Not conducted**

*200 mA/cm^2 was measured in March 2020 during rotating current collector experiment. 85 mA/cm^2 was measured in August 2020 during NEF flow cell experiment.
**Full stack development was not conducted, so TPM was not verified.

The AQUIFER project was proposed as a feasibility assessment for integration of the NEF and RDM technologies. The feasibility assessment was the culmination of the technology development approach, shown previously in the bottom of figure 1. The NEF technology was in development before CAS but required significant current density improvements to compete with current state-of-the-art battery systems. The RDM technology was chosen as it was originally designed - as an improved acoustics electric motor from the AFRL GHO unmanned aerial vehicle project. The AQUIFER team envisioned this motor as being competitive with state-of-the-art ducted fan electric motors while reducing acoustic sources, accomplished by removing stators in the duct and reducing rotor blade tip speed. Both technologies would be matured as part of the AQUIFER approach, culminating in a fully integrated design and contributing to a better understanding of the benefits of the integrated system.

Current density was chosen as the target unit for effectiveness of the NEF system because it represented the current that the system can provide. Since the tank size (the total energy of the system) can be sized independently, the associated specific energy (Wh/kg) will change with the ratio of NEF stack weight to NEF fuel weight. An identical NEF stack system can have different system-specific energy densities depending on the amount of fuel and the specific energy density of the fuel. Table 4 depicts several of the pertinent details of the NEF technology based on the overarching CAS goal of 100 mA/cm^2. The table also shows the NEF development roadmap from GEN 1, GEN 2, and the final technology level of the Vision System in this report. GEN 1 technology has aqueous-based anode and cathodes, using the nanoparticle fuel for both electrolytic fluids. GEN 2 converts the technology in an oxygen (air battery) system, exchanging the nanofluid anode and replacing it with O_2 or air. The Vision System is the culmination of all the current and efficiency improvements fully implemented.

Table 4. The nano-electro fuel feasibility criteria from the Systems Requirements Review.

		GEN 1 Chemistry			GEN 2 Chemistry			
Technology Parameters		**2018**	**2019**	**2020**	**2021**	**2022**	**2023**	**Vision System**
Current Density	mA/cm^2	6	50	100	200	500	1000	1700
Membrane Active Surface	%	85	85	85	85	85	85	85
Cell Voltage	V	1.2	1.2	1.2	1.28	1.28	1.28	1.28
Cell Outer Thickness	cm	2	0.8	0.6	0.5	0.5	0.4	0.2
Stack Average Density	kg/L	1.2	1.2	1.2	1.2	1.2	1.2	1.2
NEF Discharge Efficiency	%	10	30	60	30	60	80	90
Fuel Specific Energy "Fuel-to-Electricity"	Wh/kg	4	29	81	319	639	852	958
Average Fuel Density	kg/L	2.2	3.3	4.0	6.5	6.5	6.5	6.5

Results, Analysis, and Lessons Learned

This section includes the feasibility assessment results for the NEF and RDM technologies pertaining to physical hardware and laboratory results. Analysis for the Wing Demonstrator and aircraft applications designs are discussed.

Nano-electro Fuel Technology Results

The NEF experimentation prior to the CAS project was obtained using rectangular flow cells with an open flow field (no channels). This project focused on conforming the cell design to the annular ring wrapped around the RDM and increasing the performance metrics such as current density and coulombic efficiency of the cells. Thus, all electrochemical tests in this project were conducted in newly designed annular sector cells.

The electrochemical tests were conducted as charge/discharge curves with gradually increasing current density. Higher current densities on charge typically result in high overpotentials and trigger parasitic side reactions such as oxygen and hydrogen evolution, resulting in nanofluids not being charged. It should be noted that gas evolution is only a problem during charging and thermodynamically does not happen during discharge. When needed, the charge/discharge cycling is repeated at higher- or lower-current density.

The NEF design concept underwent changes to incorporate the AQUIFER project concept and included: updating the stack configuration for improved integration with the RDMs; updating to the Battery Control System (BCS) to power the RDMs; and improving material synthesis to increase the current density in order to meet the AQUIFER feasibility metrics.

Stack Configuration - Square Box or Torus Flow Field

- The original NEF stack design was to be an offshoot of the Influit Energy terrestrial NEF battery pack work. Consideration of the technical challenges of pushing the material performances to levels of turning an electric motor were taken into account (the prevailing thought at the time was stick to what worked in the past).
- It was determined that the motor would require approximately 100 W of power.
- Objections by The Boeing Company to the design of the Influit Energy separate "BOXED" stack system led to a radically new system design whereby the stack would not only supply energy to turn the RDM but would also function as an integrated functional ducted component for the thrust delivered by the motor.

Battery Control System

A Battery Control System can be as basic as voltage monitoring and as complex as a multivariable projection of all possible physical processes in a fully operational environment.

The basic functional design of a redox flow battery is very standard, and all designs for a flow cell - capable of functioning with NEFs - stem from four basic functional blocks: (1) tanks; (2) cell stack; (3) pumps; and (4) fuel. Each of these items will be discussed separately in the sections that follow.

(1) Tanks

In an aqueous-based electrolyte, pH can run from acidic to basic. The redox couples used in this CAS project required a basic electrolyte. A wide array of chemically compatible materials is available depending on how the fluid is tested.

Because the tanks of cathode and anode fluid are separated in space, electrodes placed in the anolyte and catholyte measure the fuel voltage directly. A gas relief valve placed in each tank feed bleeds off any gasses evolved from parasitic losses.

(2) Cell stack

The cell stack is where the electrochemical reactions occur. In order to have an energy releasing chemical reaction, an anode nanoparticle needs to collide onto a conductive metal electrode; at the same time, a cathode nanoparticle collides counter onto a metal electrode. The discharged particles (after collision) are pumped out of the reaction chamber and into the storage tanks. The two reaction chambers are separated by an ion conducting membrane, and each electrode lead exits the sealed reaction chambers. If an electrical device is connected to the stack leads, an electron path is created from the cathode to the anode chambers. As the electron performs work, counter ions diffuse across the ion conductive membrane via the potential between the redox couple and charge transfer. Figure 16 shows that in addition to flow, chamber and electrode geometries affect the collision rate of the redox nanoparticles onto the electrodes and hence their output current.

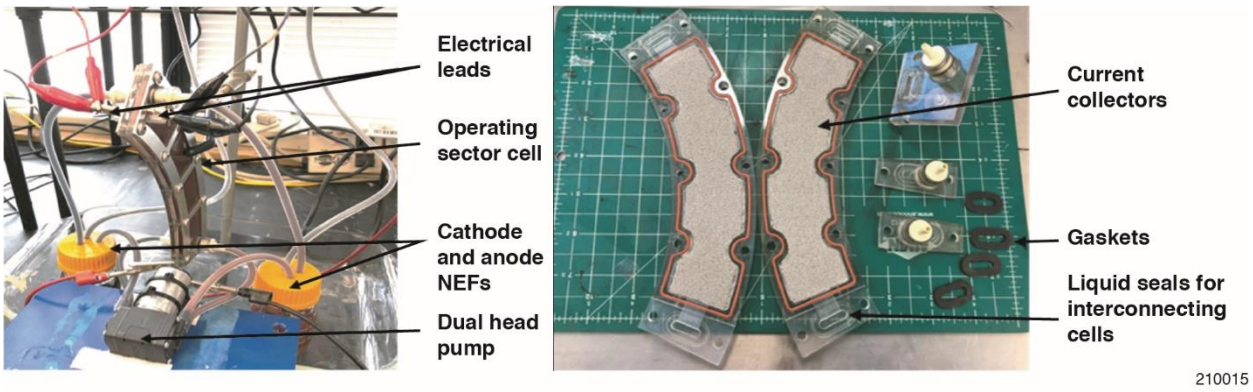

Figure 16. Single annular cell and electrode geometries in testing rig.

(3) Pumps

Because energy is stored in a liquid format, the flow battery design needs to have pumps to convey the liquids into and out of the reaction chamber. Traditional flow batteries are low-energy dense, therefore large pumps are needed to move great volumes of anolyte and catholyte; but as energy density increases, pump size decreases, resulting in less fluid volume required to perform work.

(4) Fuel

The focus for the CAS NEF battery was to hit a material performance of 350 Wh/L at the system level and a current density of 100 mA/cm^2. The anolyte and catholyte redox couple were chosen to avoid the production of hydrogen (H_2) and oxygen (O_2) gas.

Because of the mechanical dependence on coincident nanoparticle electrode collisions, achieving 100 mA/cm^2 not only relies upon the chemical redox reaction but also the tortuous path each nanoparticle takes within the cell; the speed of the ion diffusion across the membrane; and the electrical impedances of the working closed circuit.

The viscosity of the fuel is to be minimized in order to overcome pumping penalties associated with moving charged fluid through a stack and into discharge tanks.

Nano-electro Fuel System Operations

The basic NEF system operation is to power the pumps in order to commence the fluid moving and, thus begin discharge. If wired to latch, energy losses from the pump can be compensated by increasing the volume of stored fluid. Utilizing the voltage potential between anode and cathode tanks uses a proportional-integral-derivative control loop. Maintaining voltage and desired current output can be implemented using pulse-width modulation (PWM) control and a microprocessor.

Test Fixture / Apparatus

There are two critical technology development efforts to building a NEF battery system. The first effort is creating the NEF fluid – synthesizing nanoparticle suspensions; the second is developing the energy extraction system. These efforts result in the eventual union of two independent research tasks and teams.

Material Discussion

The NEF synthesis steps are shown in figure 17. The synthesis processes are shown for both 3- and 50-L batches.

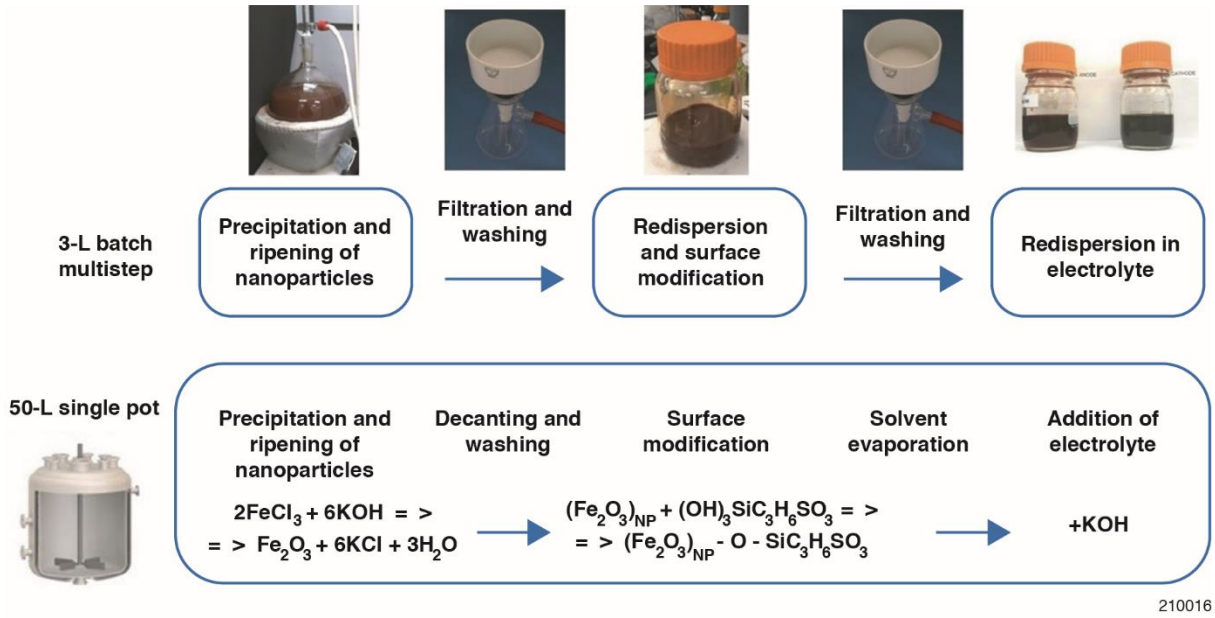

Figure 17. Schematic representation of the current small batch multi-step synthesis versus the proposed single pot scale-up process (nanoparticles remain in the same reactor from precipitation to final nano-electro fuel formulation).

Candidate Material Testing

Each potential candidate suspension is electrochemically tested, first in a coin cell configuration and then in a fluid suspension format. Each fluid suspension format is then benchmarked against coin cell performances and is shown in figure 18.

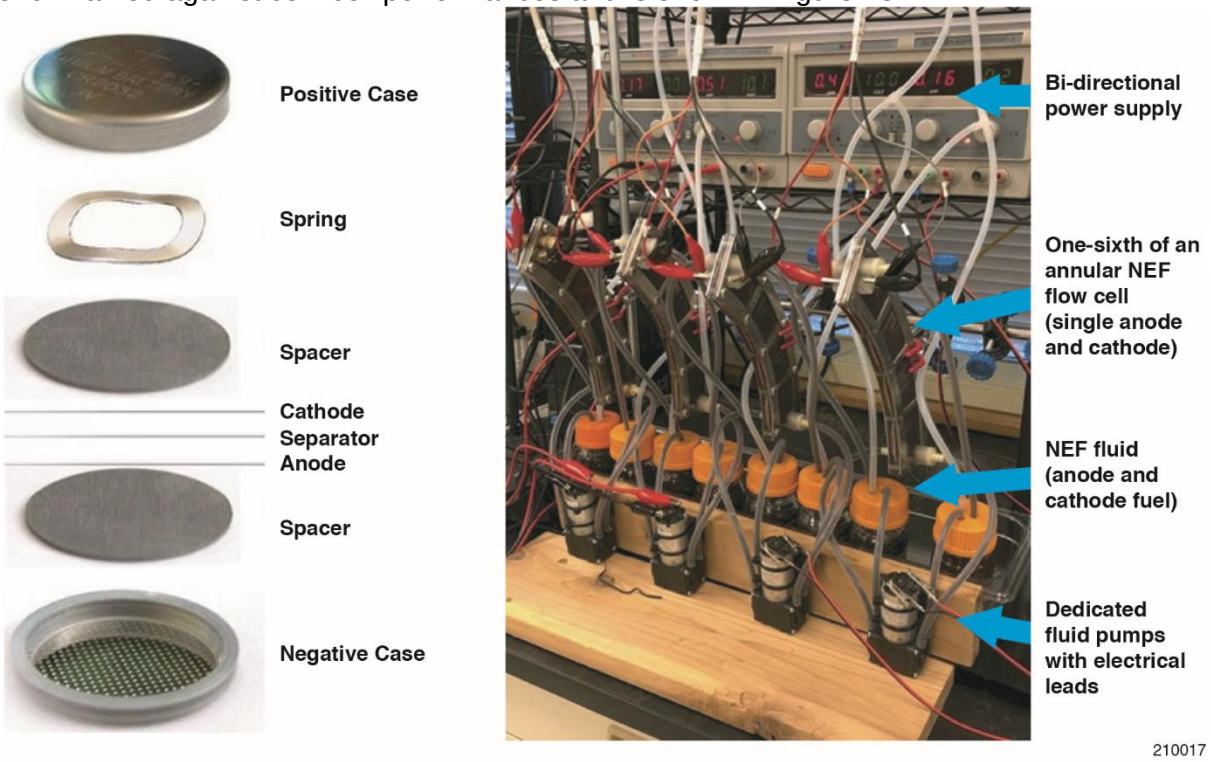

Figure 18. (left) Coin cell construction; and (right) annular flow cell nanofluid testing rig.

A new electrochemical cell design with rotating current collector and small nanofluid volume was conceptualized and designed. The new design was done for two reasons. First, candidate nanofluids needed to be synthesized which is a time consuming and involved process (figure 17); therefore, a means to minimize the testing volumes was implemented to save time and resources. Second, a method needed to be created for determining whether a fluid was performing well while isolating any performance effect of the mechanical cell. This method development was achieved with a new cell design called a rotating current collector (RCC) cell. An RCC test is performed to isolate only the electrochemical behavior of candidate nanofluids; speed up the testing of the nanofluid formulations; and eliminate the effects of the flow field on tested nanofluid performance and is shown in figure 19.

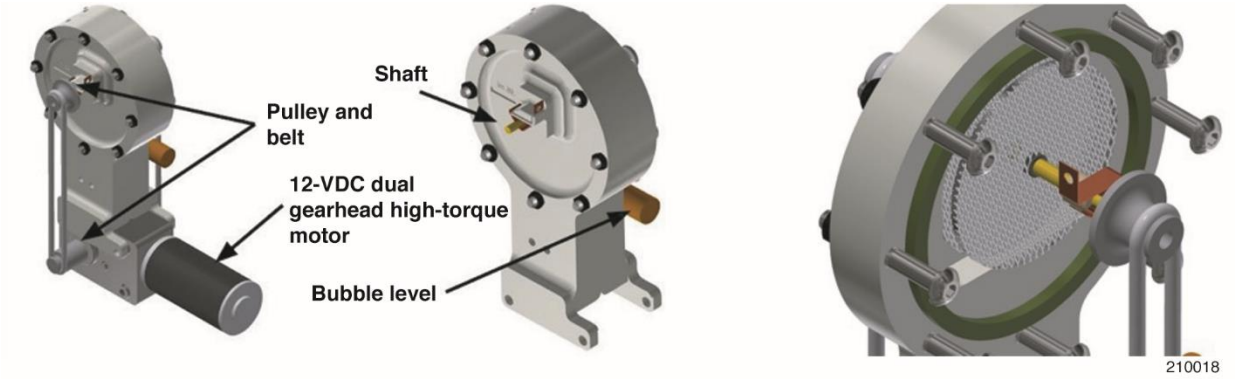

Figure 19. Design of the electrochemical cell with rotating current collectors.

The RCC concept was devised to better understand the effective upper limit for each specific NEF chemistry. By using a motor and centripetal acceleration, the design provides for improved electron transfer and current density. The design is made up of the following features: two external electrical contacts; 5 ml of nanofluid; a nickel (Ni) foam disk rotating current collector; an external high torque DC motor with dual geared outputs, ensuring anode and cathode electrode rotational speeds are matched; and wetted components all chemically inert to potassium hydroxide (KOH) electrolyte. These rotating current collectors are shown during testing in figure 20 and figure 21.

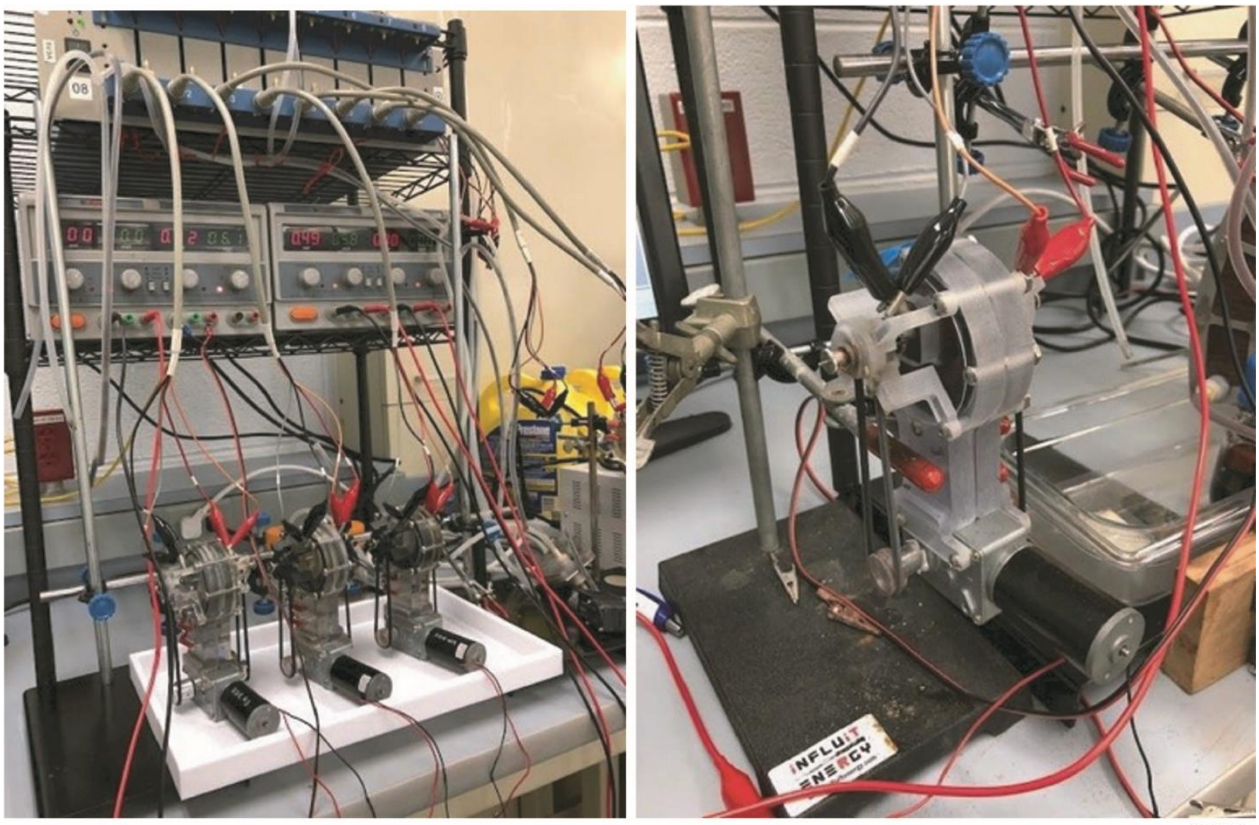

210019

Figure 20. The design and test process for the rotating current collector experiment that would simulate flow through the cells with a minimal amount of fluid.

210020

Figure 21. First prototype of rotating current collector cell.

Convective mass transport in the flow battery electrodes is critical to overall cell performance and operation. Flow field architecture is a key component affecting this mass transport and cell performance and the overall pressure drop and pumping requirement of the cell. Originally, the AQUIFER team used a test cell with an open flow field where fluid was flowing by/through the nickel foam rotating current collector with input at the bottom of the cell and output at the top of the cell. The cells were tested in galvanostatic charge/discharge cycles at different current densities (50-200 mA/cm^2). The tests were conducted under constant pumping power with monitored flow rate and pressure drop within the system. Electrochemical Impedance Spectroscopy (EIS) measurements and analysis were performed before testing and periodically during the cycling to identify changes in cell resistances and monitor the health of the system.

Flow Rate Mapping/Optimization

Performance of a given flow field may strongly depend on operating conditions such as flow rate and temperature; thus, mapping out the performance of a down-selected flow field - as a function of flow rate - leads to further system optimization which includes: higher efficiency; deeper depth of discharge; and acceptable pressure drop. A look into different flow paths resulting in different flow fields is shown in figure 22. The results provide information for the BCS design as well as for balance of plant.

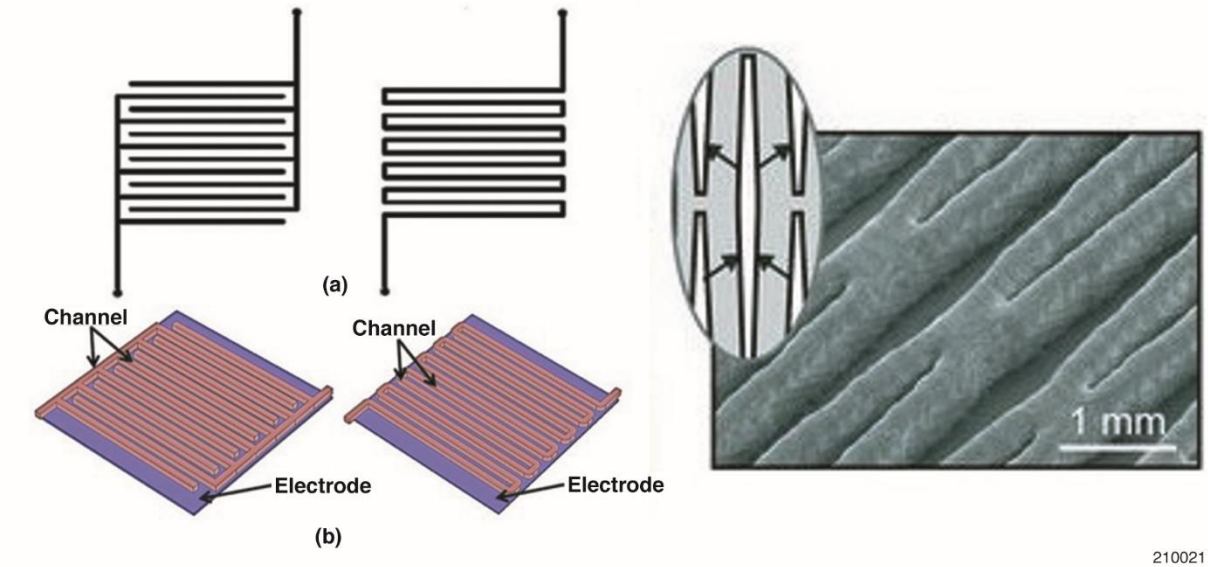

Figure 22. (a) Schematic representation of different flow fields that will be tested: interdigitated flow field; and (b) serpentine flow field; and (right) tapered flow channels with dual pass.

Three new three-dimensional (3-D) flow fields were designed and printed for the single-flow cell tests and included: serpentine paths with ramps; interdigitated flow paths; and interdigitated flow paths with ramps, shown in figures 23 and figures 24.

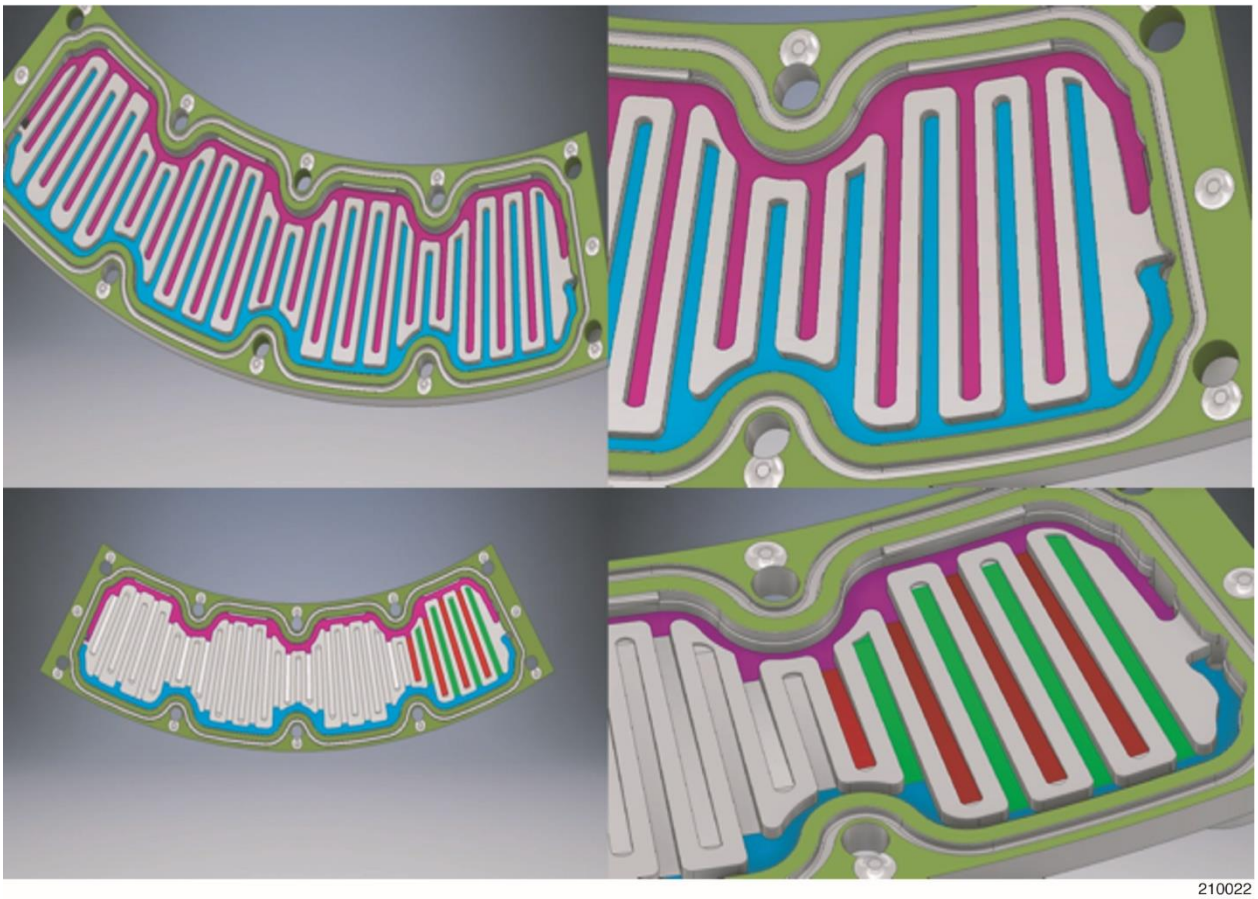

210022

Figure 23. (left- and right-top) Interdigitated cell baseline distance between the branches change depending on the design of the branch; and (left- and right-bottom) interdigitated cell ramp design ramps were made using the triangle theorem, ramps go from each side.

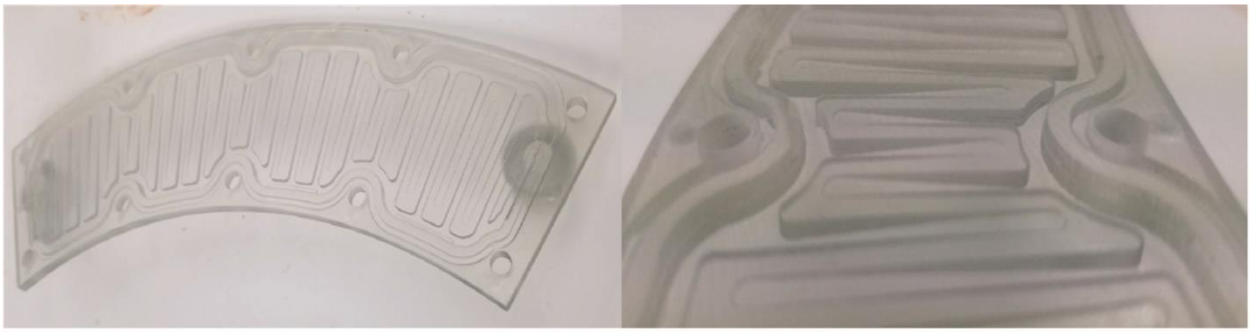

210023

Figure 24. (left) Printed interdigitated ramped flow field; and (right) ramped design forces nanofluid into a higher-pressure zone and higher velocity on underside of Ni foam electrode.

Test of the Prototype Cell Designs

The team developed a thinner cell design for the prototype stack with integrated flow field features and a new manifold fluid delivery system. Manufactured cells were tested and optimized with the final prototype metrics in mind. Cells were tested in galvanostatic charge/discharge mode at different current density with periodic EIS control (i.e. every 10 cycles) to investigate and monitor change in cell impedance and system health. Currently, we

use continuous flow mode for charge and discharge of the fluids. Intermittent modes of operation were envisioned as a latter development.

Membrane down-selection in the first task demonstrated that Nafion™ NR212 (The Chemours Company FC, LLC, Fayetteville, North Carolina) membrane has the highest ionic conductivity within the series (table 5). Later in the project, other deficiencies of this membrane were identified, such as electrolyte drag.

Table 5. Membrane max current at constant potential test.

Membrane	Observations	Max. current at 1.9 VDC	Max. calculated conductivity
Nafion™ NR212 (cationic)	Good mechanical properties, expands in KOH, dries/shrinks quickly in air	5,200 mA	2.74 mho
FAS 50 (anionic)	Good mechanical properties, expands in KOH, dries/shrinks quickly in air	1,100 mA	0.58 mho
FAA 50 (anionic)	Good mechanical properties, expands in KOH, dries/shrinks quickly in air	1,250 mA	0.66 mho
FAA 75 (anionic)	Great mechanical properties, minimum swelling/shrinkage	900 mA	0.47 mho
FAA 75 (anionic)	Poor mechanical properties and high price - failed during the test		—

Testing in the annular sector cells with increasing current densities further revealed a limitation of nickel foam cathode, which at higher overpotentials (higher current densities) would start dissolving in electrolyte. To address this technical barrier, the team developed a coating procedure to prevent direct contact of nickel with electrolyte. Figure 25 shows the gray polymer coated cathodes in the far right of the figure. Initially, we coated electrodes with electronically conductive polypyrrole coating; later, it was revealed that this coating slowly dissolves in potassium hydroxide KOH. Further, we developed a polyaniline coating procedure which has performed well in alkaline electrolyte.

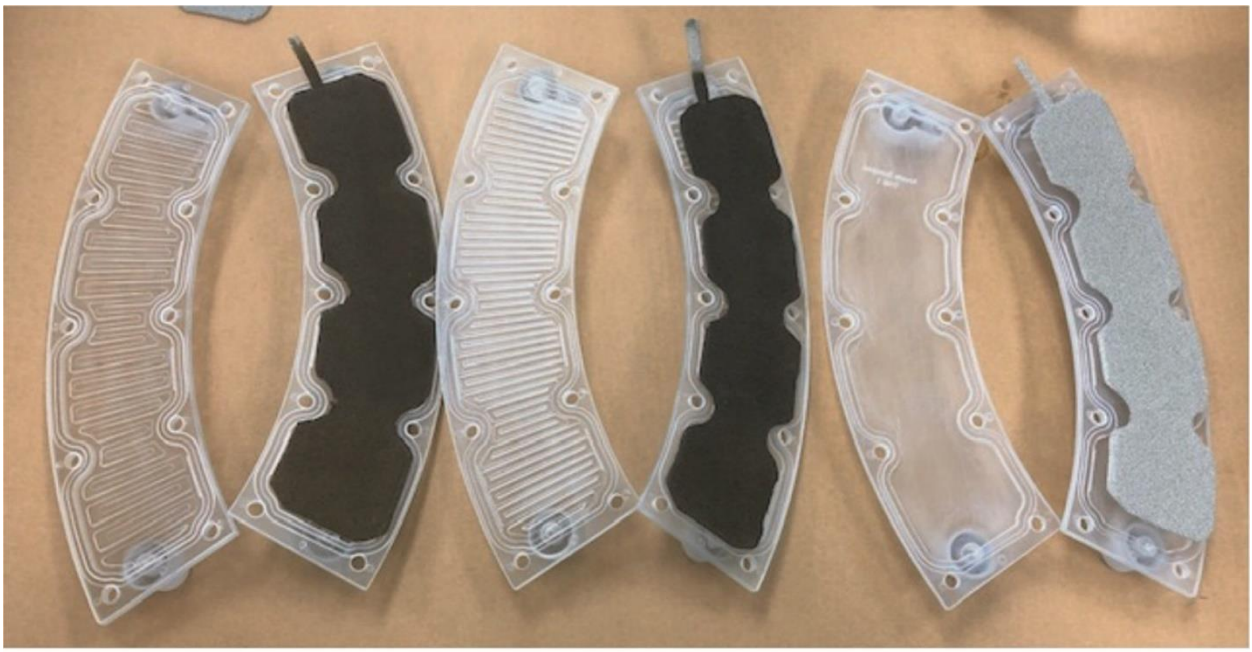

Figure 25, (left) Uncoated porous nickel cells; and (right) polymer coated cell. The three different flow field designs are also shown to: interdigitated, serpentine, and open flow field.

Further testing of the annular sector cells has shown that higher charging currents are possible with coated cathodes and interdigitated flow fields (IDFF). The IDFF and other flow path concepts were investigated to maximize the turbulent mixing of the NEF fuel within the cells while still maintaining minimal increased flow pressure, which would add pumping power requirements; therefore, causing parasitic power loss to the system. The AQUIFER team investigated several flow paths including serpentine and interdigitated flow paths, both concepts are shown in figure 26.

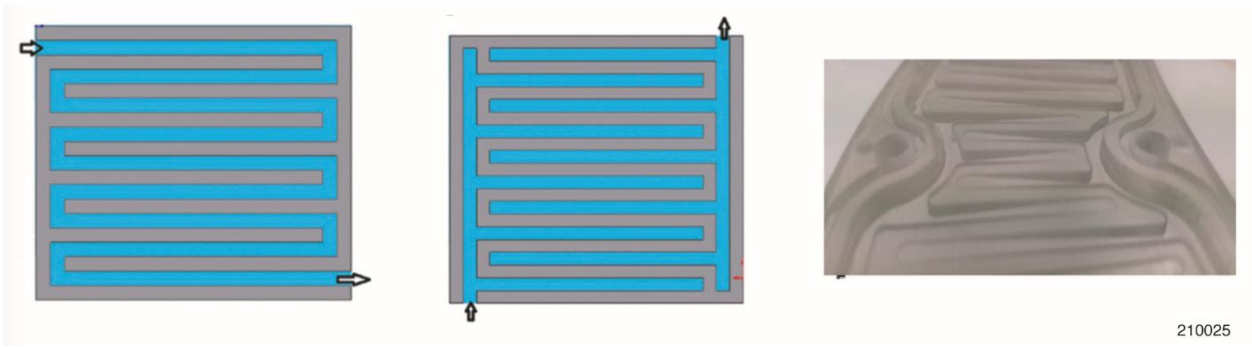

Figure 26. (left) The nano-electro fuel cell flow path considerations: serpentine; (center) interdigitated; and (right) interdigitated with ramps.

Faster flow rate was shown to be beneficial in some instances and can be seen in figure 27.

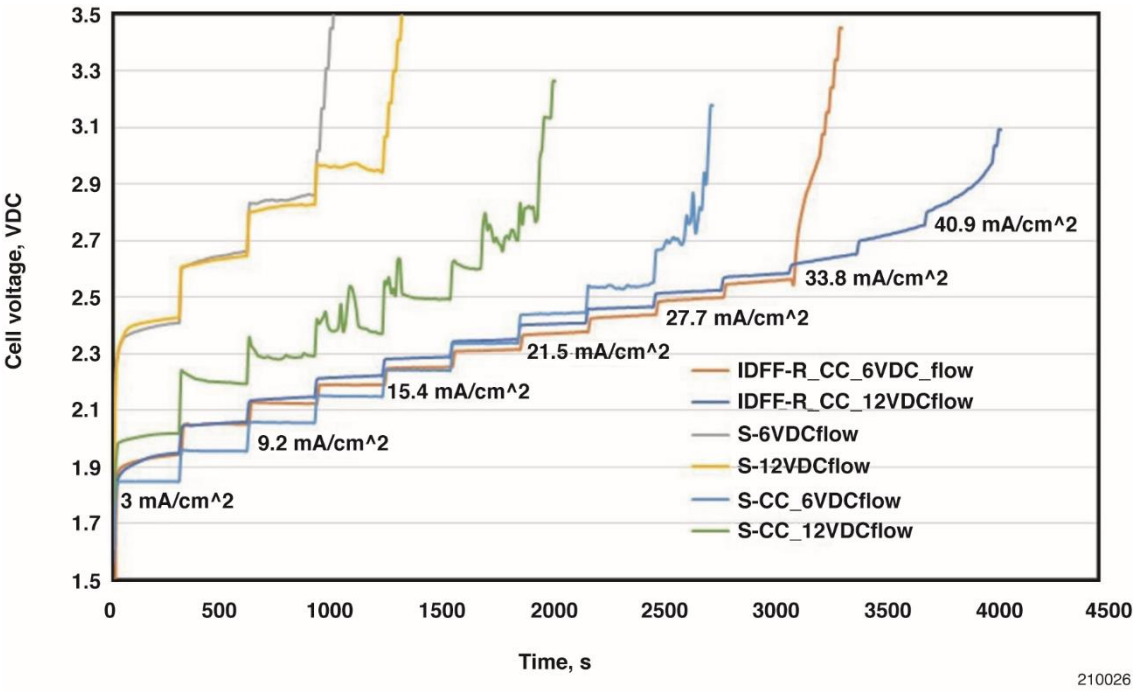

Figure 27. Results on charging current density with a set of cells at different flow rates. Interdigitated flow fields ramped (IDFF-R); serpentine (S); with coated cathode (CC).

The best result was obtained in an annular flow cell with an interdigitated ramped flow field; coated current collector; and Nafion™ NR212 membrane; and allowed for 46-mA/cm^2 maximum charge current and 15.4-mA/cm^2 maximum discharge current and is shown in figure 28.

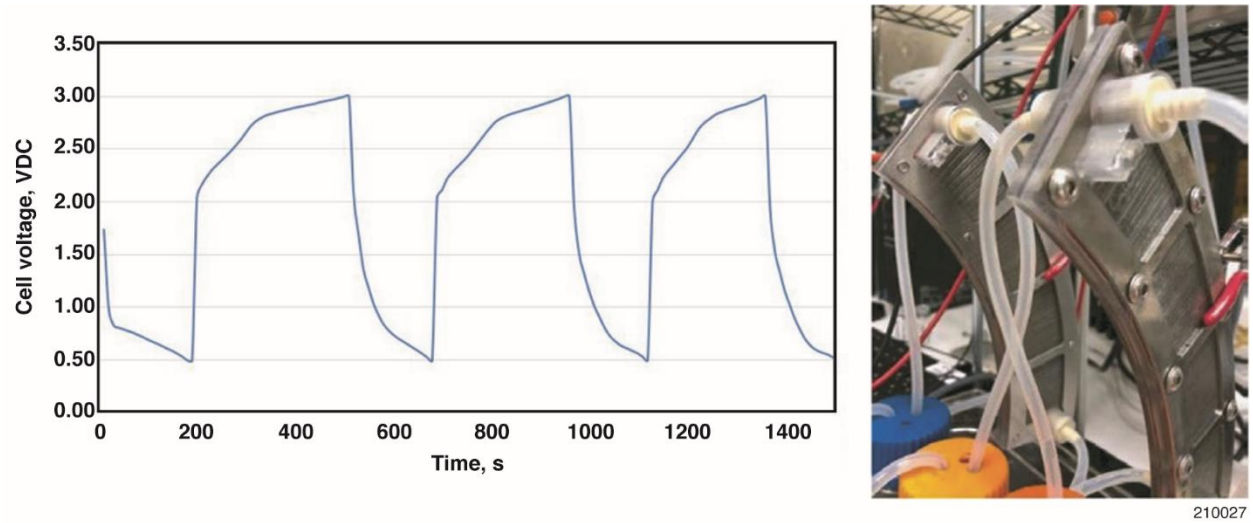

Figure 28. Best cell performance charge/discharge history for an interdigitated ramped flow field, coated current collector, and Nafion™ NR212 membrane. The discharge was performed at 1 A with an average cell voltage of 0.8 VDC to over 200 VDC.

Further, to isolate the flow-dependent behavior from materials-dependent behavior, tests in flow annular cells were switched to the rotating current collector cells described above. This approach also helped minimize the amount of nanofluids needed for each test.

The rotating current collector test also revealed limited capability of the Nafion™ NR212 membrane, creating more of a negative electrolytic drag effect. Electrolyte drag is the

phenomenon where current passed across the membrane also results in the transfer of the electrolyte between the anolyte reservoir to the catholyte reservoir. The RCC test allowed for project improvements towards the performance of the nanofluids using these new cell geometries. The results for the rotating current collector test are shown in table 6. The results show a general degradation of total discharge capacity with increased current density, which is speculated to be caused by currently unmeasured secondary reactions.

Table 6. Length of discharge for given current densities (data for February 2020).

Current density	Discharge time	Total charge density
5 mA/cm^2	2,220 s	11.10 C/cm^2
10 mA/cm^2	1,080 s	10.80 C/cm^2
15 mA/cm^2	725 s	10.88 C/cm^2
25 mA/cm^2	438 s	10.95 C/cm^2
50 mA/cm^2	192 s	9.60 C/cm^2

The AQUIFER team has continued to systematically improve the nanofluid formulations and cathode coating and will revisit membrane down-selection with new and improved cell performances. For the rotating current collector experiment, updated performance data can be seen in figure 29. This data shows the relationship between current density and discharge duration, tested on the RCC. The AQUIFER team succeeded in attaining the 100-mA/cm^2 benchmark, indicated in table 3.

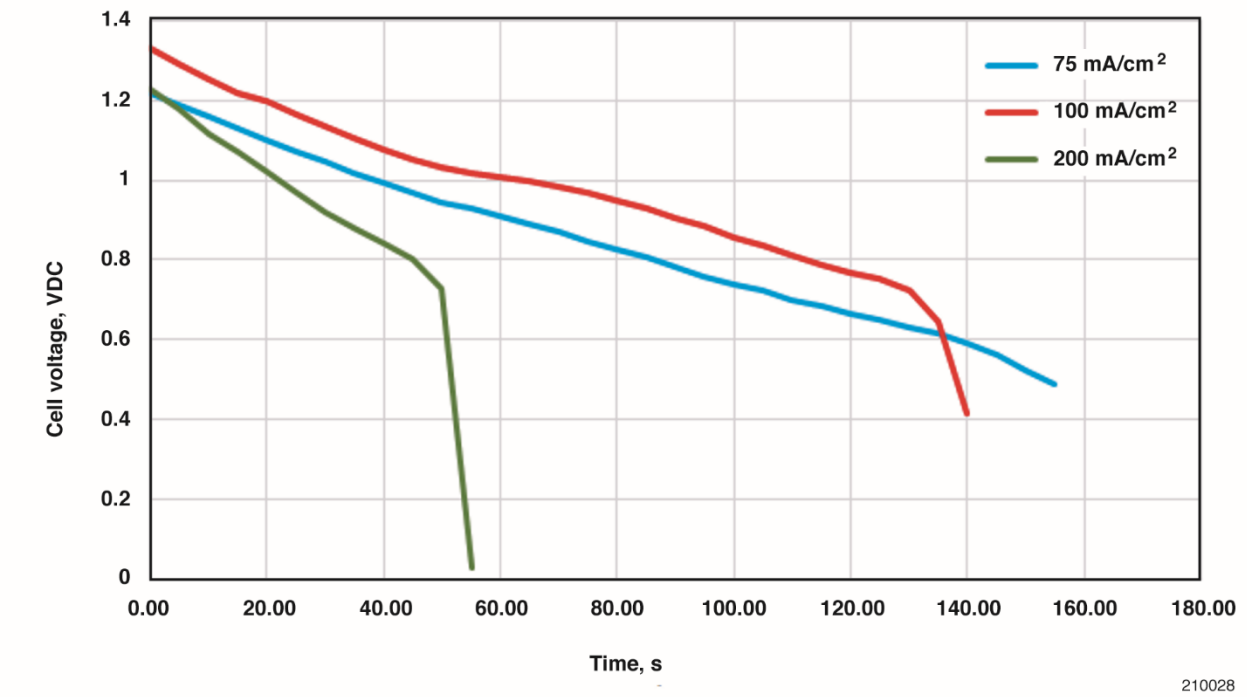

Figure 29. Rotating Current Collector data demonstrating current draw and voltage potential versus discharge time.

To push for higher current densities, the AQUIFER team has chosen to revert to a square-cell concept to improve the design > test > redesign loop. The updated flow cells have 1- and 2-mm IDFF flow channel widths, shown in figure 30. The cells were assembled with updated cell components and tested at different current densities. The surface area of the current collector in these cells is approximately 70 cm^2.

Figure 30. Updated nano-electro fuel flow cells during leak testing (July to August 2020).

The charge and discharge current densities were gradually increased in different tests. The cut-off voltage was adjusted within each test to avoid the parasitic gas evolution reaction. The precision of this adjustment affected the efficiency of charge/discharge cycles.

Table 7 shows the performance of NEF cells. The table shows the comparison and effectiveness of the 1- and 2-mm channels. It appears that a cell with a 2-mm channel shows slightly lower overpotential (difference between charge and discharge voltages), but overpotential increases with the increase in current density. Also, the cell with 2-mm channels showed higher capacity at the same current density. Efficiency of discharge/charge ratio varied from 80 to 95 percent in this series of tests which was related to the accuracy of a chosen cut-off voltage.

Table 7. Current density data for 1- and 2-mm interdigitated flow fields flow channel nano-electro fuel flow cells.

Current draw	1-mm path	2-mm path
3-A draw 43 mA/cm^2	Approximate discharge capacity: 60-mAh discharge capacity Discharge/charge ratio: 86-percent efficiency	Approximate discharge capacity: 65-mAh discharge capacity Discharge/charge ratio: 81-percent discharge efficiency
6-A draw 85 mA/cm^2	Approximate discharge capacity: 29-mAh discharge capacity Discharge/charge ratio: 95-percent discharge efficiency (affected by cut-off voltage)	Approximate discharge capacity: 40-mAh discharge capacity Discharge/charge ratio: 90-percent discharge efficiency (affected by cut-off voltage)

An 85 mA/cm^2 for the NEF cell represents the closest the AQUIFER team got to achieving the 100-mA/cm^2 NEF cell goal presented at Mission Concept Review (MCR).

Nano-electro Fuel Lessons Learned

The fast pace of the project required quick decision and design choices for annular cell designs and consequent electrochemical testing of the 3-D printed cells; the latter resulted in some positive and negative outcomes.

The switch from rectangular to annular cell geometry was time consuming, but limits were pushed on the manufacturing technique, resulting in minimization of the cell thickness (from 2.5 to 0.8 cm) and development of new interconnections and liquid sealing strategies. Identification of corrosion reaction at the cathode current collector allowed the project team to develop a proprietary conductive polymer coating strategy, enabling higher current densities. Experiments with different flow fields within the cell also demonstrated that higher current densities are possible when higher collision rates between nanoparticles and current collectors are favored.

Challenges with nanofluid production required the AQUIFER team to design and devise a rotating current collector experiment. The experiment simulated the flow of the nanofluid without the use of large amounts of fluid for testing; thus, increasing testing throughput while isolating current collector problems from the nanofluid properties.

Gradual fine-tuning of the system allowed the project team to increase the current density from 1 mA/cm^2 at the beginning of the project to 200-mA/cm^2 RCC within 15 months of project start.

The CAS goals for the NEF technology were to demonstrate 100-mA/cm^2 inflammability / non-explosivity on a NEF cell. These goal specifications are listed in table 8.

Table 8. The Aqueous, QUick-charging battery Integration For Electric flight Research nano-electro fuel-specific performance specifications and feasibility assessment.

CAS goal specification	Value	Units	Current spec	Confidence
Current density (discharge) - CAS target	100	mA/cm^2	200* 85	high
Discharge time	180	min	1*	low
Current density (charge)	100	mA/cm^2	>100	high
Surface area per cell (approx.)	>80	cm^2	87.6	high
Annular section	6	cells	Prototype built	high
Stack (1 stack per motor)	60	cells	Prototype designed	high
Current per stack (max)	48	A		medium
Voltage per annular section	1.2	VDC	Demonstrated	high
Stack voltage (max)	12	VDC		high
Stack power (max)	>500	W	GEN 1 – 100 percent	medium
Stack power - CAS target	>100	W	For motor op	high

*200 mA/cm^2 was demonstrated utilizing the rotating current collector test setup and 85 mA/cm^2 for the NEF cell test setup in August 2020, after the execution phase of the project had been ended.

Nano-electro Fuel Troubleshooting

Two major mechanical failure modes have been identified with the NEF cells: (1) the leaking of the nanofluids; and (2) short circuiting of the current collectors.

The leakage was addressed with modification to the cell designs and improved handling procedures, which included thorough leak testing with deionized water prior to introducing cathode and anode nanofluids into the cell. Difficulty procuring the current collectors was also addressed with additional improvements to the cell design and continuity tests during assembly. Other troubleshooting and risk mitigation strategies for identified problems are summarized in table 9.

Table 9. NEF development troubleshooting.

Risk		Mitigation strategy (May 2019)	Status (February 2020)
1	Achieving current density 85 mA/cm^2 in a NEF cell and 200	Will be addressed with three approaches: 1. Flow field geometry	• Flow field geometry and flow rate have shown to have an effect on the

Risk		Mitigation strategy (May 2019)	Status (February 2020)
	mA/cm^2 in an RCC with 100+ mA/cm^2 charging	2. Concentration of nanoparticles 3. Flow rate optimization	charge/discharge current. Cells with interdigitated ramped flow field showed the best performance to date. • Charge current density of 85 mA/cm^2 has been achieved using polymer coated cathode current collector. • Discharge current density of 85 mA/cm^2 has been demonstrated using a polymer coated current collector. • New problem identified and resolved - corrosion of cathode current collector • Helped increasing current density 10x • Mitigation strategy related to concentration of nanoparticles has not been tested to date (2/28/20), but planned for final Influit Energy forensics investigation report (9/30/20) • New mitigation strategy involves introduction of redox active and electrically conductive additives to the electrolyte has been tested but was not shown positive results to date.
2	Increase nanoparticle concentration to 80-weight percentage	Nanoparticle size control will be used to address this risk.	• 70-weight percentage particle concentration is achieved to date

Risk		Mitigation strategy (May 2019)	Status (February 2020)
3	BCS parasitic power is too high	Use external power source, consider full scale system and alternative components	• BCS design in progress - focus on utilization on of low power components
4	Mechanical failure of the 3-D printed cells	Increase wall thickness, consider injection molding manufacturing	• Half full annular cell has been printed and assembled - no problems with mechanical strength in the current cell design
5	Sealing of the cells	Use gaskets instead of O-rings, design modifications	• Seals within the individual sector cells are tested and passed leak test. Inter-cell fluid connections in the full annular cell assembly still have a leak. Mitigation for this challenge is printing complete half ring cathode and anode segments to avoid those seals.
6	Cycling stability	Depending on the cause of degradation (chemical, mechanical, component failure) addressed with the use of stable redox nanoparticles, modification of cell components and designs	To date two problems have been identified and resolved: 1. corrosion of cathode current collector - addressed through coating with conducting polymer. 2. electrodynamic drag of electrolyte from cathode to anode - addressed with a special container that separates anode and cathode fluid by membrane. In the future need to replace Nafion™ NR212 membrane with anionic membranes, which currently have limited commercial availability.

Rim-driven Motor Design and Results

This section discusses the motor requirements and assumption for the novel RDM concept. The motivation for the motor and bearing type, slotless design, and performance are listed below.

Motivation for Radial In-runner

An axial-flux motor design was chosen for the previously performed RDM designs for electric vehicles. This report, alternatively, explores a radial in-runner design geared toward reducing rotor complexity and windage losses at low power. Much like axial flux motors, in-runner motors have the advantage of improved thermal conduction paths from the windings to the outer nacelle and ducting; therefore, having the advantage over out-runner motors. The main drawback of in-runner motors is the added challenge of magnet containment on the rotor, which increases the necessary airgap spacing. Increasing this airgap spacing is a large detriment to motor performance and is especially challenging at high RPMs and large circumferences (ref. 1).

Motivation for Bearing Choice

The following parameter is typically used to determine the proper bearing material lubrication selection. The value is simply the product of the bearing diameter in millimeters, multiplied by the RPM. The most advanced bearing materials and designs have been able to achieve bearing factor (DN) values to upwards of three million; however, these systems only exist in laboratory settings with large lubrication systems. The AQUIFER operates at this upper bound; therefore, non-contact bearings are desired. Table 10 shows the various bearing considerations for the RDM selection. Air bearings typically fall under two categories: aerostatic and aerodynamic. Aerostatic bearings are externally gas pressurized; therefore, the effectiveness of these bearings is greatly reduced at high linear speeds, making the amount of gas necessary at the desired speed and diameter unmanageable. These types of aerodynamic bearings improve at higher speeds but unfortunately have strict loading restrictions and are generally only useful when the machine is in constant operation. Repeated restart and throttling of the fan power and combined loads of the propulsor make this contactless solution incompatible. Magnetically levitated bearings fall into the second category and offer the best solution; however, the complexity and customization of such a design was beyond the capability of this project. An eventual solution will likely involve the use of non-contact bearings. Roller bearings have an upper limit on a design parameter known as the DN value (refs. 2 and 3). See table 10 (refs. 4-6).

Table 10. Rim-driven motor bearing comparison study (refs. 4-6).

Bearing type	Max DN (in millions, approximate)	Power consumption	Restart
Steel roller	1.0	6-8 kW at 12,000 RPM *	Yes
Ceramic roller	3.0	Less than steel, but conflicting data	Yes
Aerostatic	1.0	No data	Yes
Aerodynamic	4.4	9.5 W/inch^2 at 11-lb load	No

Magnetic	4.5	2.1 kW at all speeds *	Yes

*1,000-lb load

To maximize the operational capacity of ball bearings, two pre-loaded angular contact bearings were chosen to react as radial and thrust forces. Ceramic bearings were chosen because they are lighter, highly temperature-resistant, nonmagnetic, and generate less friction than steel bearings.

Bearing drag estimates at this size are typically only provided up to 2,000 RPM, so the trends are extrapolated logarithmically to determine bearing drag up to 9,000 RPM. Operational life is severely limited and because there are associated thermal and noise problems, these bearings cannot be used for a final flight system (ref. 7).

Motivation for a Slotless Design

In order to keep the operating electrical frequency within manageable limits for traditional motor controllers, the pole count on the motor is kept below 24 poles. The low power and strict mass requirements force the stator depth to be extremely thin. The aspect ratio of the teeth would be extremely low at high speeds and would generate unnecessary eddy-current losses. Elimination of the teeth reduces these high-speed iron losses; however, back iron is still required to complete the rotating flux path on a single-rotor design. Magnetic flux must pass through the motor windings in the absence of teeth. For this reason, bundled Litz wire is recommended to reduce the conductor skin effect and minimize eddy current losses within the wire (ref. 7).

Motor Performance Requirements

To make RDMs competitive with a conventional hub design, the power density and efficiency must be comparable to traditional motors. A desired power density of 5 kW/kg was chosen as a performance target for the aircraft in the study. The motor drive (or controller) chosen to drive the RDM should be able to provide maximum power at the respective motor voltage and current. Full power can be determined by either operation at the design point of the motor (e.g. 8 kW) or operation at a reduced point (e.g. 4kW), which is in the interest of preserving the life of the machine. The drive should also be capable of delivering a voltage waveform at the appropriate shape and frequency such that the motor performance is optimized and the desired mechanical speed is achieved. The operation of four-quadrant control may not be necessary, as regeneration in aircraft applications may be impractical and has yet to be determined. Lastly, the drive will be required to accommodate the electrical characteristics of the motor, such as resistance and inductance.

Rim-driven Motor Controller Requirements and Assumptions

The control option for the RDM was envisioned as a dual-purpose controller, controlling both the NEF pump and the RDM input speed. Because the scope of work involved to achieve this option quickly become untenable, the AQUIFER project team chose to identify commercially available options. A specific design requirement was that the controller had to not only be able to control the motor to the power and speed requirements but also control the motor at very low voltage and current - consistent with the Wing Demonstrator requirements.

Final Rim-driven Motor Design Details with Air Bearings

Different configurations of air bearings for both radial and thrust bearings were considered for the final RDM design. Ultimately, air bearings were chosen as there was a viable path to a

prototype within the original project scope and the air bearings solved the three problems with the conventional “thin-section” bearings:

- Thin-section bearings not rated for the speed requirements.
- Unfavorable results in current Finite Element Analysis (FEA) results.
- Mechanical bearings generate undesired tones.

The subcontractor New Way Air Bearings, Inc. (Aston, Pennsylvania) was identified as a partner to create our custom 14-in diameter air bearings. The proposed strategy was to make the motor bearing adaptable: one design having three radial bearings and three thrust bearings; the other design with six apiece. The final design demonstrates the different concepts and is shown in figure 31 and figure 32. While the air bearings do solve some of the technology barriers of the conventional bearings, the weight penalty shown in table 11 demonstrates that the air-bearing solution adds dramatic weight and should be considered a technological intermediate solution, although magnetic bearings present a viable competing design.

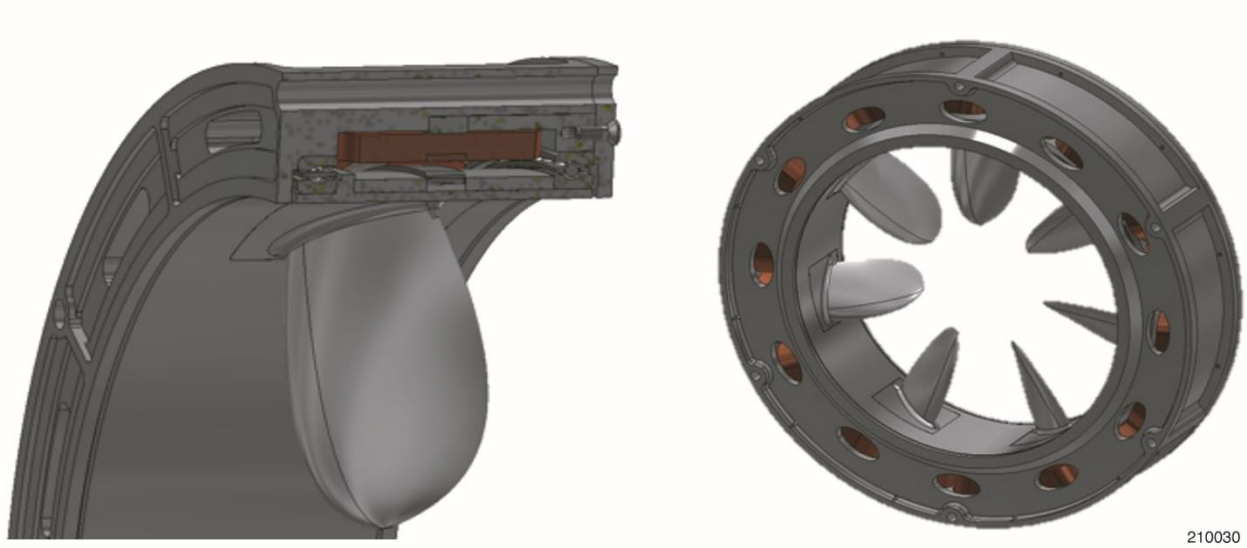

Figure 31. Rim-driven motor final design incorporating the air bearing design (14-in ID and 17-in OD).

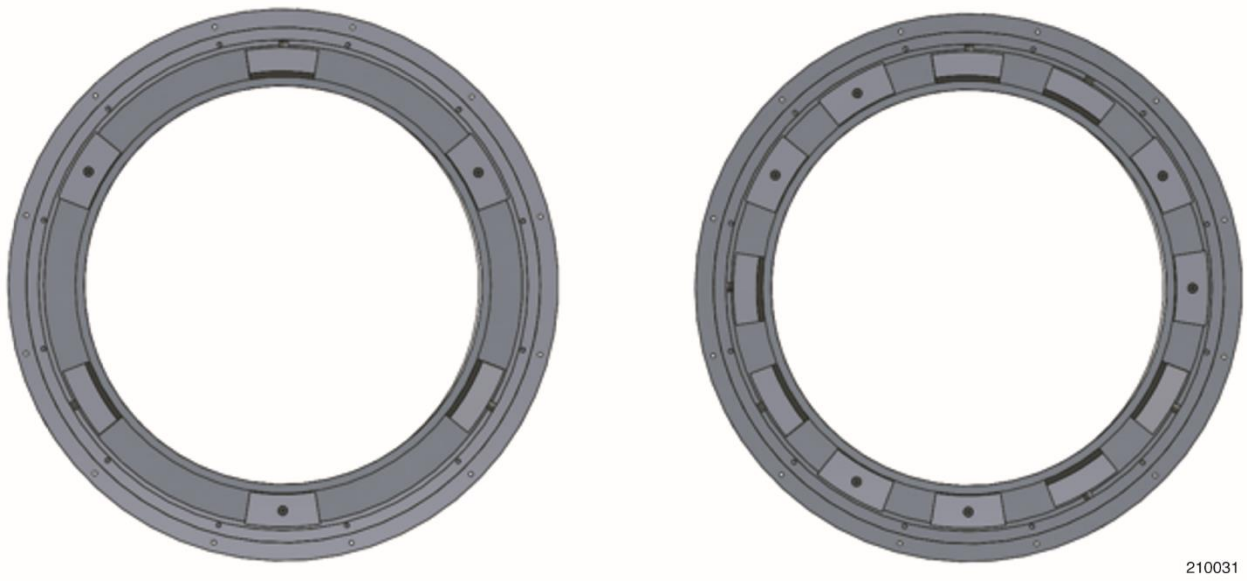

Figure 32. (left) Custom air-bearing solutions (14-in ID and 17-in OD); three radial and three thrust bearings; and (right) six radial and six thrust.

Table 11. Rim-driven motor bearing design weights for thin-section and air bearings.

Rim-driven motor with conventional “thin-section” bearings	Rim-driven motor with air bearings (six radial and six thrust)
30.96 lb	60.43 lb

Rim-driven Motor Design Considerations and Analysis

The 14-in diameter RDM concept was derived from multiple design code iterations and vehicle sizing considerations. The following parameters were chosen to best fit The Boeing Company ZEST concept: thrust, RPM, coefficient of pressure and thrust, blade advance ration, capture area, nozzle definition, mission profiling, and others and are shown in figure 33 and figure 34.

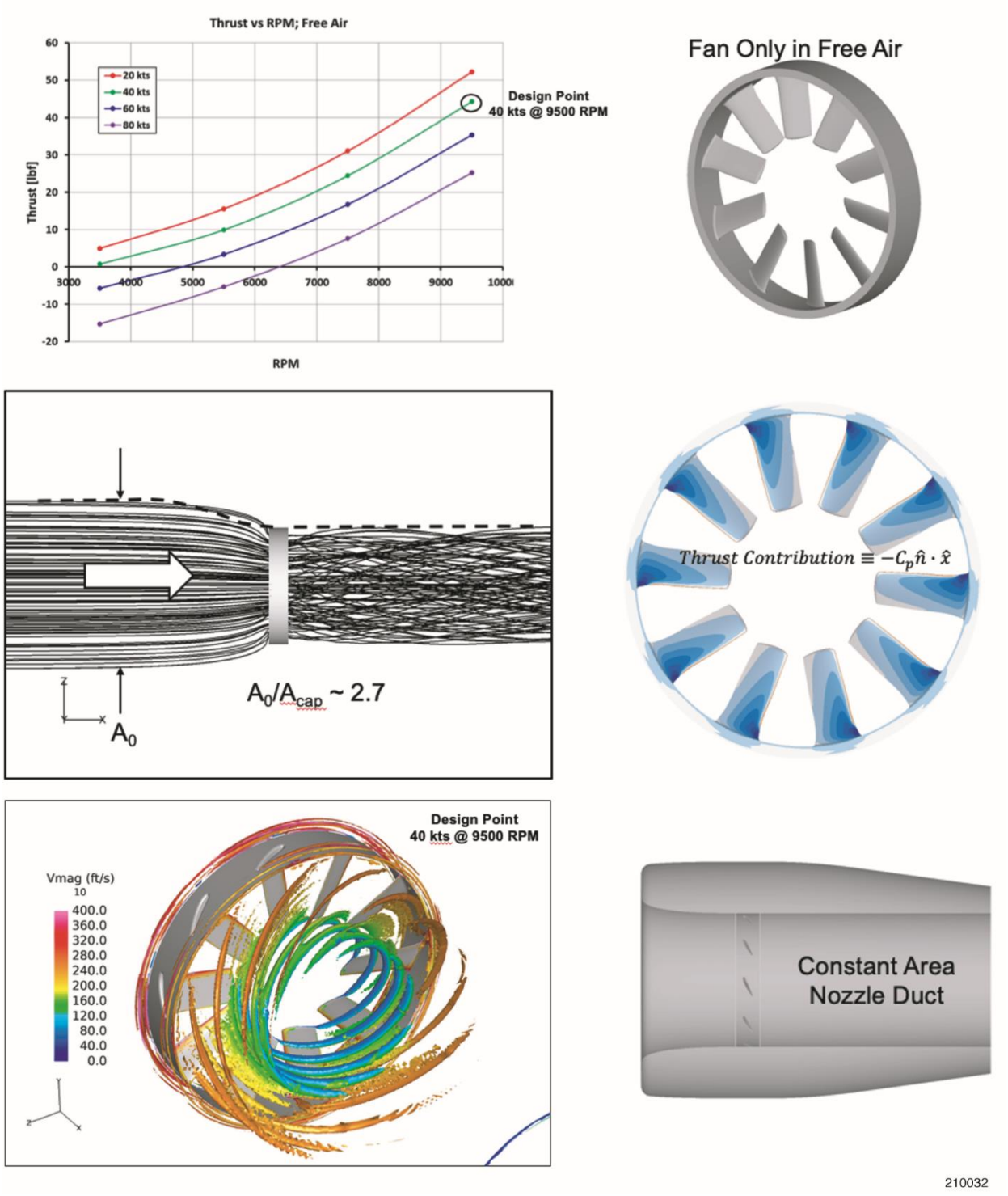

Figure 33. (top-left) Rim-driven fan analysis: fan geometry; (top-right) fan only in free air; (middle-left) side profile duct flow at 40 kn (A0 is free stream capture area and A0/Acap is throat capture area ratio); (middle-right) thrust contribution; (bottom-left) isocontour of “q-criterion” showing tip and root vortices; and (bottom-right) nozzle geometry.

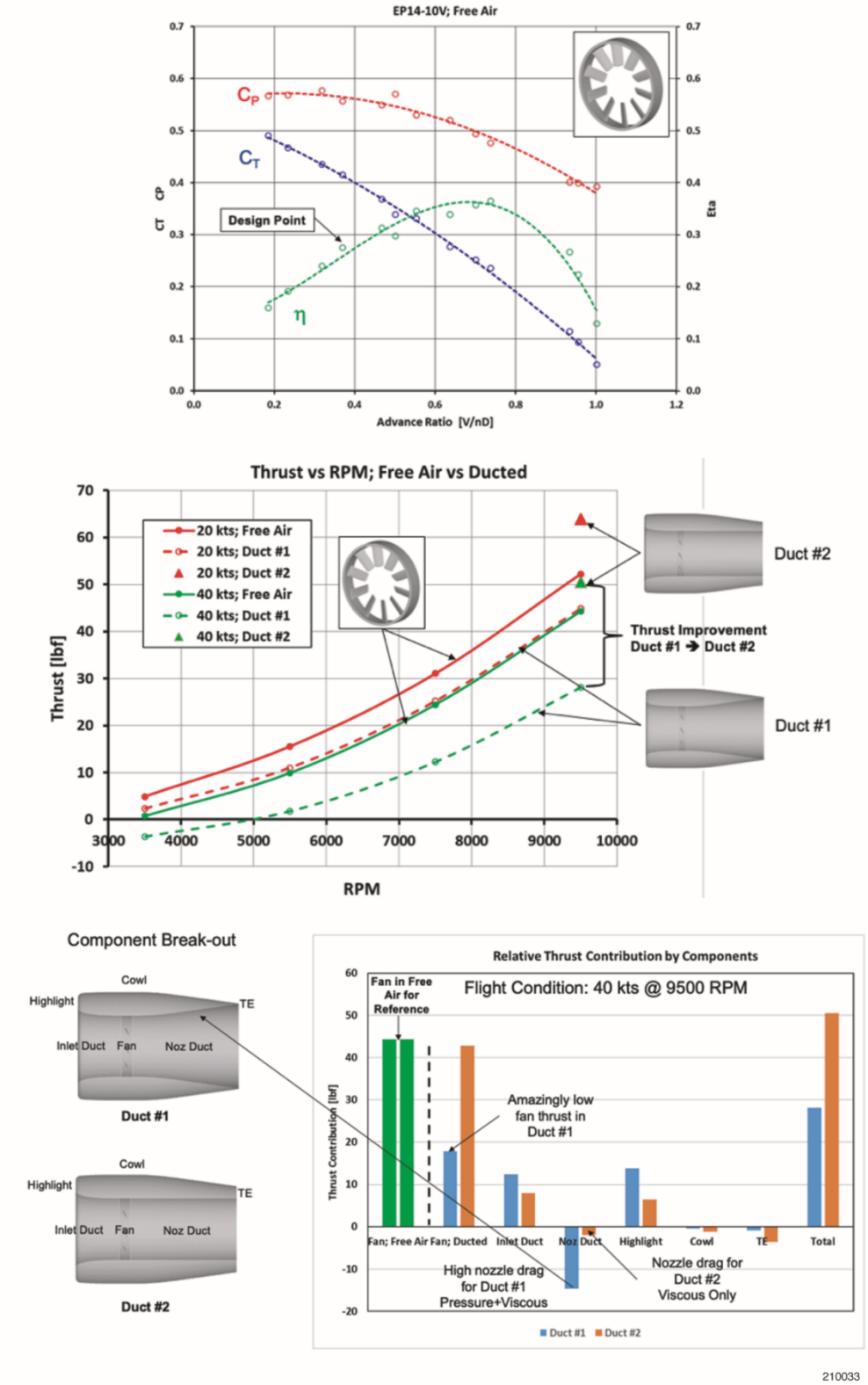

Figure 34. Rim-driven fan design point analysis (top); duct analysis (middle); and thrust contributions by component where green represents idealized fan thrust without installation losses (bottom).

Because existing tools were unavailable or insufficient and to better model the blade geometry, a new geometry scheme was developed: the “pie” sector or single vane geometry. This sector geometry allows for minimal calculations during analysis/optimization and utilizes a re-entrant rotational boundary condition.

The AQUIFER team demonstrated good correlation between the full geometry calculations and the “pie” sector scheme, as shown in figure 35.

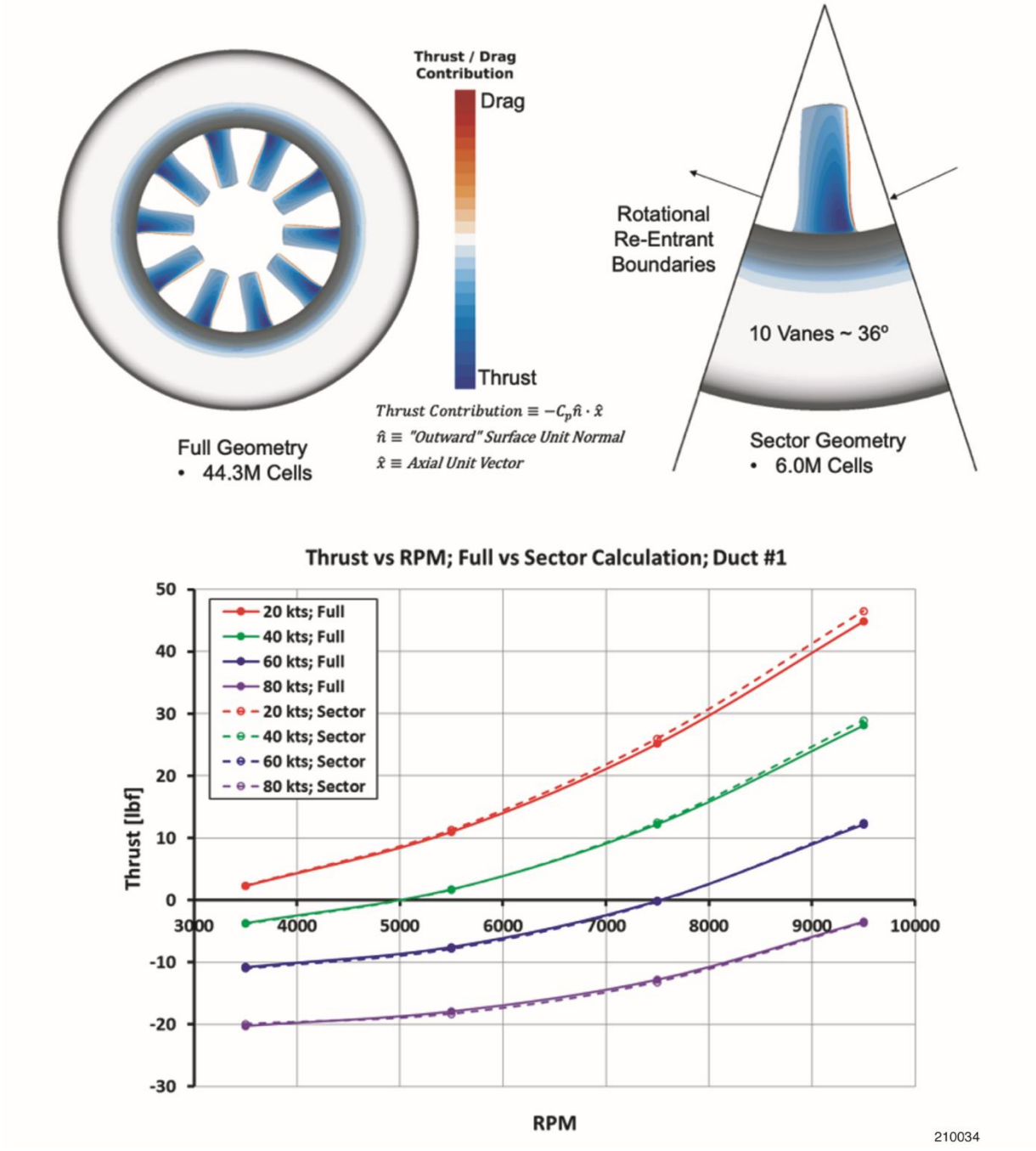

Figure 35. Correlating full fan geometry with "pie" sector.

While the motor manufacturer Engineered Precision, Inc. (Costa Mesa, California) was designing the full-scale 14-in motor, engineers at NASA developed 3-D printed versions of

different sizes to obtain insight into the effectiveness of the concept and understand the technological barriers.

The work completed at the NASA Langley Research Center (LaRC) identified design characteristics and concerns and followed the design path shown in figure 36. Completed work started in October 2019 and ended in February 2020.

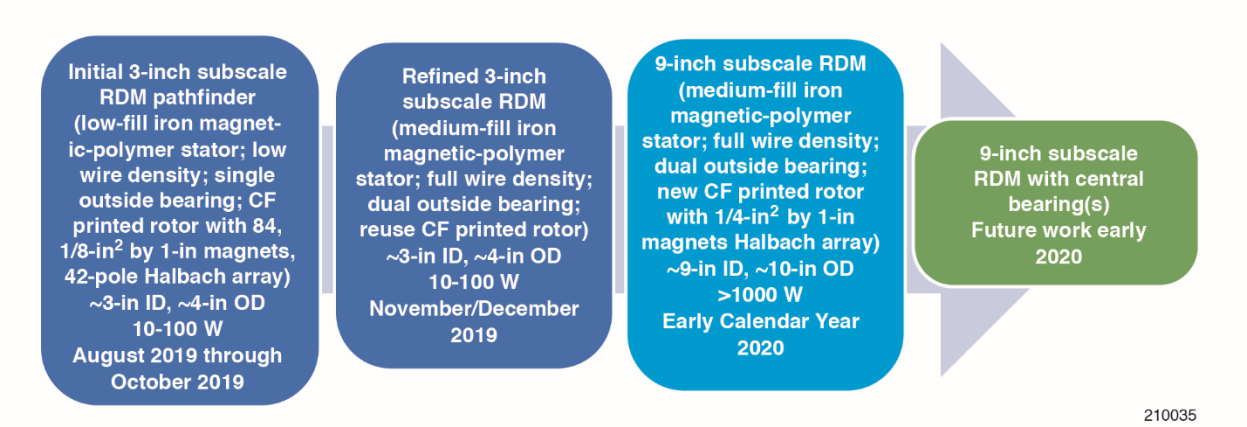

Figure 36. In-house National Aeronautics and Space Administration rim-driven motor buildup pathway and lessons learned.

Figure 37 shows some of the preliminary design considerations and findings for the initial RDM prototype, these are:

- Ball bearings are typically thermally limited in speeds in long-life applications (100,000 hours).
- A rule of thumb in such situations for ball bearings is a speed of about 85 ft/s (26 m/s) for a 3-in by 3.5-in bearing or approximately 6,000 RPM.
- To operate at the rated approximately 6,000 RPM, a factor of 10.9 lower thrust was needed, or about 34 grams. This lower-thrust factor may be too low to measure reliably with a motor that itself weighs hundreds of grams. It is estimated that a motor speed of about 20,000 RPM is required to have a thrust equal to motor weight. At 10,000 RPM, thrust would be about 92.5 grams, which should be enough to reliably measure (even if blades are very suboptimal). To monitor performance of the bearings, thermocouples were added to the bearing as well as the stator coil.
- Single bearing limited speed significantly, causing the motor to shake violently on the test stand when spun up to a few thousand RPMs.
- A second bearing was installed which enabled higher stability and thus higher RPMs while more properly centering the rotor about the stator.
- Based on these considerations, NASA completed an RDM protype which was then inspected and tested to validate the design. The initial NASA in-house RDM prototype inspection verified that 21 active pole pairs were functional. Further operational testing demonstrated that the tested motor matched the following design parameters:
    - 376.2-Hz electrical frequency;
    - 13.15-Hz mechanical frequency (for 21 poles) matched the design, which equates to an estimated internal natural frequency for the motor; therefore, recommended keep out zone for operations were at 789 RPM (13.15 revolutions per second); and
    - 100-W peak power.

The following performance characteristics were also measured:

- Constant velocity constant (Kv) up to 755 RPM, including 95-percent factor.

- Torque constant (Kt) of 0.012 Nm/A.

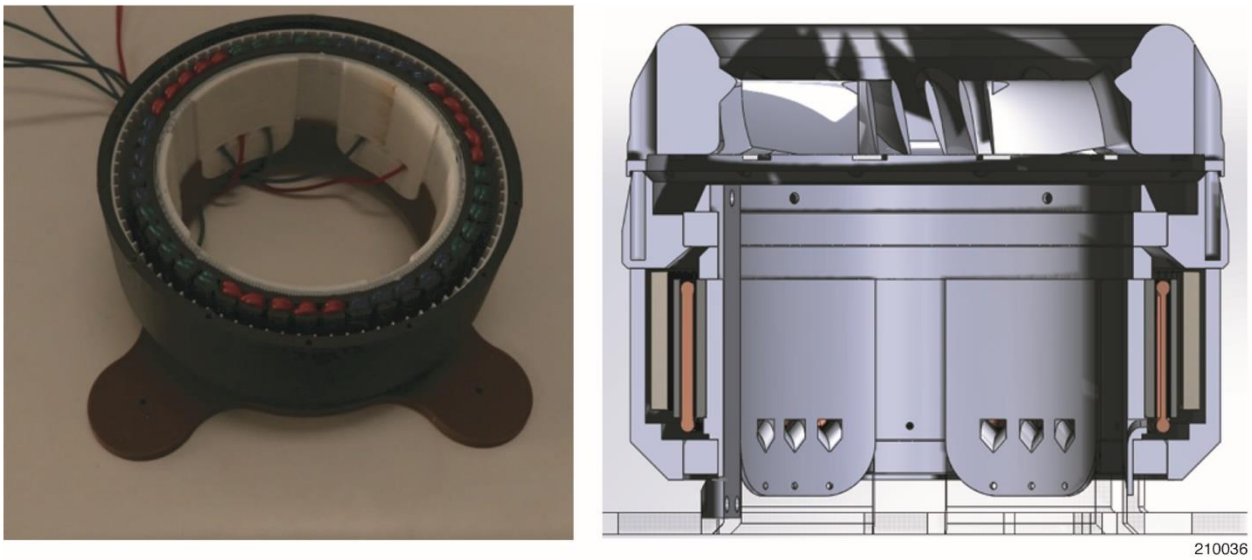

Figure 37. Initial National Aeronautics and Space Administration in-house rim-driven motor prototype build.

Figure 38 shows a second prototype build. Attempts to alleviate some of the measurement and design problems with the first build are shown and include: poor electrical connections between the leads and windings; inability to measure the motor temperature; and potential safety hazards caused by the inability to remotely test the motor. The following mitigations were performed to rectify the identified problems: resoldering the leads to the three-phase motor to improve the connection between the leads and windings; inserting a temperature probe into the motor windings to monitor temperature during operation; and extending the controller cable for increased safety.

Additionally, the motor performance requirements were increased to provide a more capable motor and an improved instrumentation suite, providing thrust measurements. The improved specifications for the second motor, which were not able to be measured with the first prototype, included:

- Approximately 22 to 24 grams-force of thrust at 2,040 RPM and 22 W.
- Thrust efficiency of approximately 1 gram-force/Watt.
- Weight was approximately 11.5 grams or approximately 2 kW/kg if scaled up to full scale.
- Measured about 35 °C after operating a few minutes at high RPM.
- The speed rating for the bearings estimated to approximately 6,000 RPM.
- Thrust measured to approximately 200 grams-force.

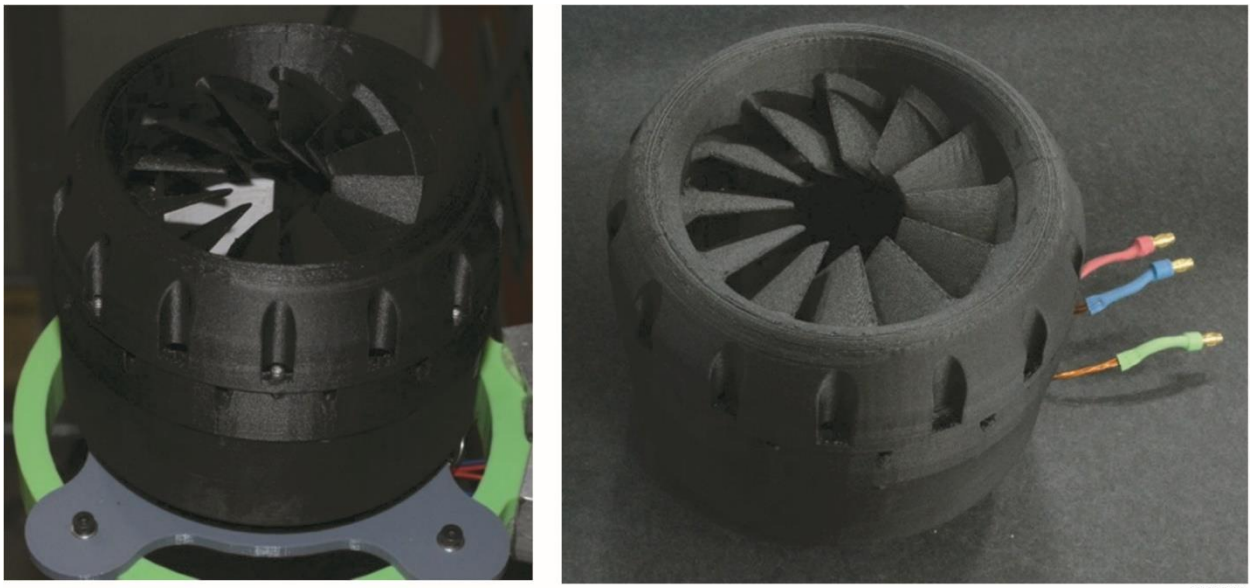

Figure 38. Second National Aeronautics and Space Administration in-house rim-driven motor prototype build.

Figure 39 shows a motor spin-down test that was conducted to better understand the motor design characteristics. The results for the 1,000 RPM spin-down test are as follows:

- Deceleration was largely linear, which is consistent with bearing drag dominating in the regime of speed less than 1,000 RPM.
- Linear decay suggests air drag, eddy currents, and hysteresis were not significant and mechanical bearing drag was dominant.
- Spin-down behavior confirms large diameter ball bearings are inefficient for this motor type.
- Given spinning component mass distribution, it is therefore possible to estimate drag power and more quantitatively assert linearity versus non-linearity, figure 39.

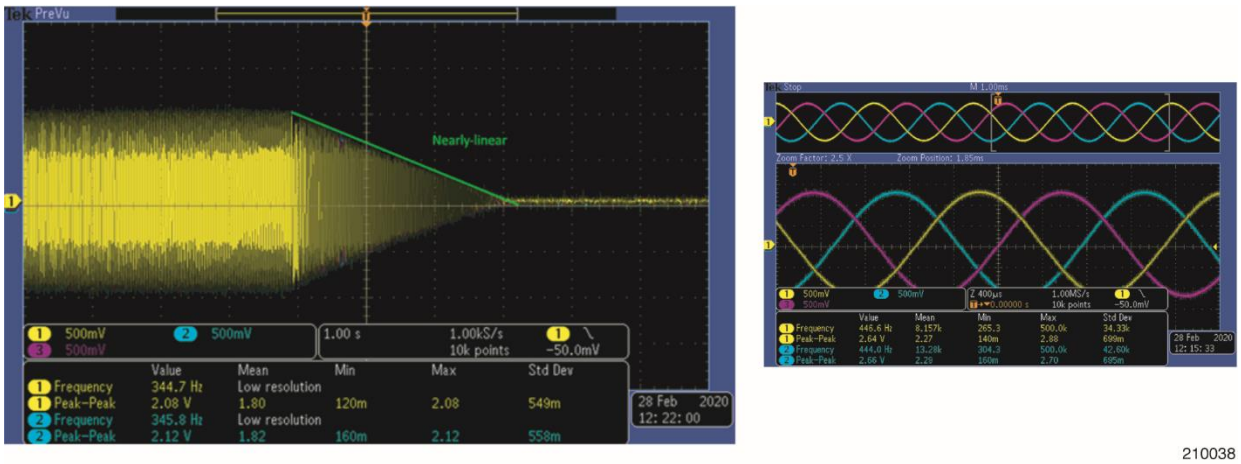

Figure 39. (left) Ramp-down performance; and (right) associated motor steady-state performance.

One of the major shortcomings of the second prototype was the inability of the power supply to provide enough power to test bearings to destruction. Other motor and bearing design lessons learned included:

- Multiple bearings were required for stability and to keep rotor magnets from pulling on the ferromagnetic stator core (even when stationary).
- A 9-in diameter motor would allow a high-power demonstration of the final prototype build (figure 40).
- Stable motor and balancing are important to allow a motor to reach high speed to produce measurable thrust (instability due to the extremely small diameter of the propeller swept area).
- Drag on the rim components as a result of high speeds reduced any efficiency gains from having electrical components on the outside.
- High pole count allows high theoretical-specific energy but limits availability of motor drivers and can limit driver efficiency and reduce per-magnet force, but assembly complexity is increased.
- Annealing can allow polylactic acid components to be used at more useful temperatures, allowing shrink-fitting of components; thus, reducing the number of fasteners needed.
- After the medium-iron-fill stator (including soldering) was reassembled, the rotor and stator stuck together magnetically because of the higher iron fill; these parts were not mechanically stiff enough to resist this increased ferromagnetic attraction.

The final NASA in-house RDM prototype utilized all the lessons learned stated above and is shown in figure 40. Further development was not continued after the AQUIFER project officially closed out at the end of February 2020.

Figure 40. Final National Aeronautics and Space Administration in-house rim-driven motor prototype build.

Wing Demonstrator Structural Layout

One of the driving requirements of the Wing Demonstrator was trying to connect the design with a relevant electrified aircraft concept. By simplifying the structure and removing the skins from the load path, a structurally representative layout was achieved (figure 41). This design integrated a forward and aft spar with integrated ribs - a similar structural layout used on most conventional aircraft. The nacelle mount also ties into the main spar, transitioning the loads from the RDM and NEF into a main structural member. Though the structure was originally designed as a simple welded system, this layout can be transitioned into a more efficient structural design for future NEF and RDM integrations.

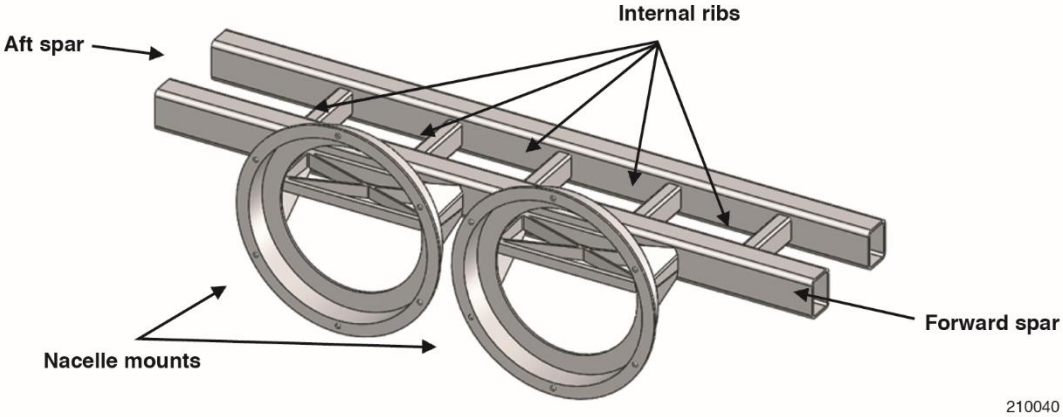

Figure 41. Wing Demonstrator structural layout.

The Wing Demonstrator was required to be capable of supporting the operational loads imposed by the NEF and RDM systems while being powered by the NEF system. In addition to meeting the design structural requirements, the goal was to make the system capable of handling the full operational loads of the RDM system when externally powered. The design driver was the cantilevered load that the NEF system imposed on the design. Because the NEF system cantilevered off the spar, the system had to handle a large bending moment imposed on the nacelle mounts and twist on the spar system when coupled with the thrust loads of the RDM (figure 42).

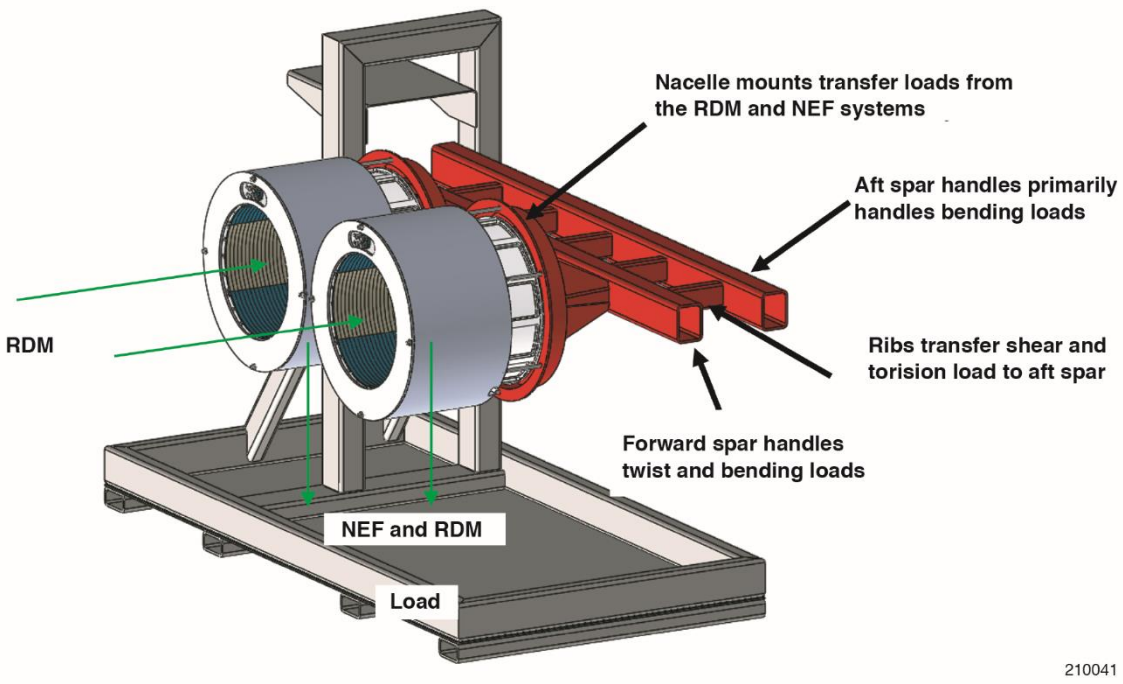

Figure 42. Structural loading diagram.

The structural design challenge for this system was transferring the loads imposed by the cantilevered NEF system while still representing a design for future NEF/RDM wing integration efforts. For this design, the wing spar handled these loads but an increase in thickness to the structural members of the nacelle mounts was required to achieve passing margins. Moving toward the envisioned NEF system, this design can be optimized for future integration because the NEF system was expected to significantly reduce in size and weight.

Nano-electro Fuel System Integration

The NEF system consists of two NEF stacks, fuel pumps, controllers and fuel tanks for the anode and cathode material and is shown in figure 43. Figure 44 shows the updated ZEST design which had the main NEF stack installed in front of the RDM with the pump mounted to the forward spar and the tanks located between the forward and aft spar.

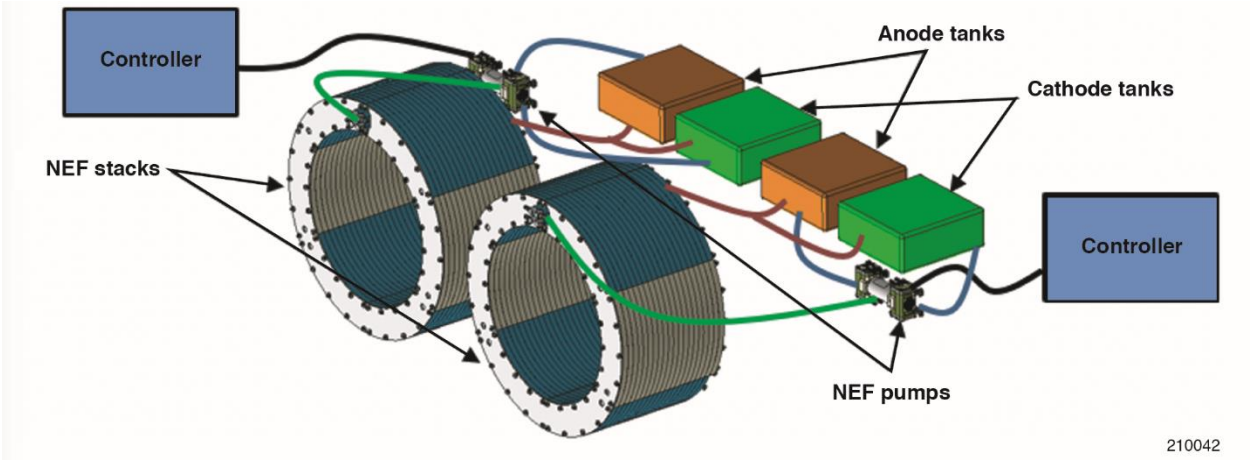

Figure 43. Nano-electro fuel system architecture.

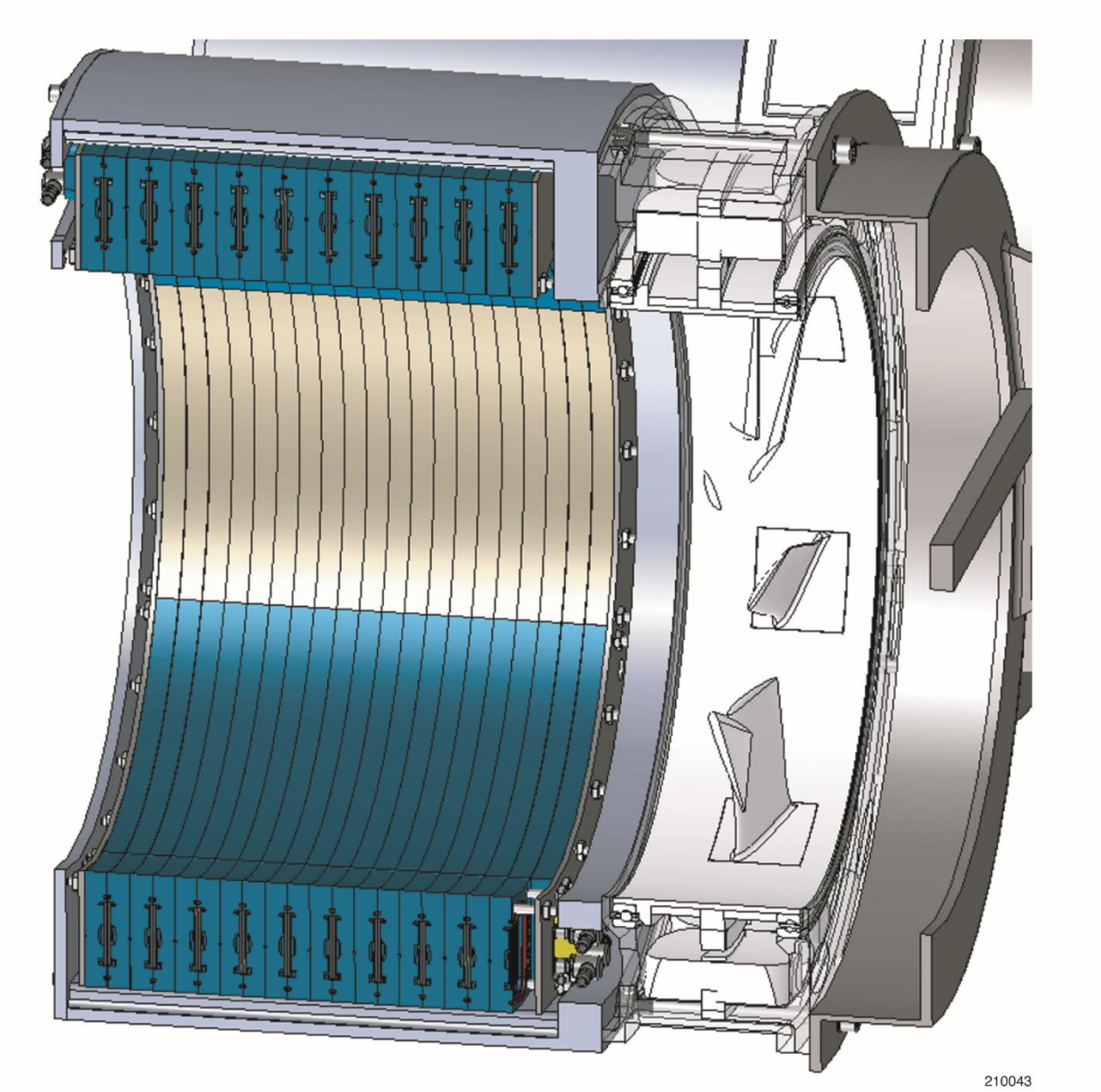

Figure 44. Nano-electro fuel stack integration.

With the overall dimensions of the NEF system locked in, initial integration design was completed (figure 44). The design provided internal pathways to route the fluid lines and electrical wires required to run the NEF system while structurally tying the loads back into the nacelle mount.

The plan was to run the NEF system using an Arduino controller (Arduino LLC, Somerville, Massachusetts). The Arduino would power the pumps used to run the NEF system. The Arduino would be controlled from a workstation that was directly connected to the system, allowing monitoring and control of the NEF system. The instrumentation for the Wing Demonstrator was baselined using the Peripheral Component Interconnect (PCI) eXtension for Instrumentation (PXI) Data Acquisition system, supplied by NASA.

Wing Demonstrator Power Budget

The power budget for the Wing Demonstrator consisted of two different systems: (1) the NEF powered system; and (2) a potential wall-powered system that would allow the RDM units to spin at full speed. The wall-powered system would run all instrumentation including the RDM controller (low power only); the NEF controller; and the NEF fuel pumps (power required by the pumps would have to be tracked to determine efficiency of the full NEF system).

Wing Demonstrator Power Supply System

Although the design would have been capable of structurally handling full power from the RDMs, the NEF system was not capable of providing the power required to spin the motors at full speed. To achieve full speed, an additional power supply Sorensen SGI 600/50C-1CAA (AMETEK Programmable Power, Inc., San Diego, California) or similar would have been required. A potential problem with this design was the motor controllers which were expected to take in 50 VDC and at this voltage the power supply would have to provide over 280 A. This amperage rating was beyond the capability of the original power supply and would have required a second system or a DC-DC converter; the second system setup was not developed because the project was closed out. The breakdown of the power required to run the RDMs at full power can be seen in table 12. Ultimately, the full fabrication and buildup of the Wing Demonstrator did not occur because of an early project closeout.

Table 12. Preliminary instrumentation and sensor list.

	Supply Voltage	Max Current (1x)	Power (1x)	QTY	Max Current (Total)	Max Power (Total)
DC Voltage Sensors						
CR Magnetics CR5310	24.0 VDC	40.0 mA	1.0 W	6	240.0 mA	5.8 W
AC Voltage Sensors						
CR Magnetics CR4550-250	24.0 VDC	60.0 mA	1.4 W	2	120.0 mA	2.9 W
DC Current Sensors						
CR Magnetics CR5210-100	24.0 VDC	40.0 mA	1.0 W	6	240.0 mA	5.8 W
AC Current Sensors						
CR Magnetics CR4110-100	24.0 VDC	25.0 mA	0.6 W	2	50.0 mA	1.2 W
RPM Sensors						
Melexis MLX90217LUA-CAA-000-BU	24.0 VDC	6.0 mA	0.1 W	2	12.0 mA	0.3 W
Temperature Sensors						
Omega SA1-E Surface Thermocouple	TBD	TBD	TBD	6	TBD	TBD
Omega FTP-E-2-SMP-M Flow Temp. Sensor	TBD	TBD	TBD	2	TBD	TBD
Flow Rate Sensors						
Omega FLR1001 Air/Water Flow Sensor	15.0 VDC	30.0 mA	0.5 W	2	60.0 mA	0.9 W
Environmental Sensor (Pressure, Humidity, Temperature)						
Bosch BME280	3.3 VDC	0.01 mA	0.0 W	1	0.008 mA	0.00003 W
PXI						
PXIe-1082 (PXI Chassis)	240.0 Vrms	1.8 Arms	420.0 W	1	1750.0 mArms	420.0 W
PXIe-8840 (PXI Controller)	12.0 VDC	5160.0 mA	61.9 W	1	5160.0 mA	61.9 W
PXIe-6358 (PXI Multifunction I/O Module)	12.0 VDC	1833.3 mA	22.0 W	2	3666.7 mA	44.0 W
PXIe-4353 (PXI Temperature Input Module)	3.3 VDC	570.0 mA	1.9 W	1	570.0 mA	1.9 W
USB-8451 (I2C/SPI Interface Device)	3.3 VDC	500.0 mA	1.7 W	1	500.0 mA	1.7 W
PXI-8513 (PXI CAN Interface Module)	3.3 VDC	940.0 mA	3.1 W	1	940.0 mA	3.1 W
Total					**14.2 A**	**571.3 W**

Note PXI: PCI eXtensions for Instrumentation.

Instrumentation and Wing Demonstration Test Plan

ESAero was tasked with developing the instrumentation and Wing Demonstration test plan. Table 13 shows the requirements for the instrumentation measurements.

Table 13. Wing Demonstrator measurement requirements.

Reqt. No.	Requirement Statement	Child Reqt. No	Child Requirement(s)
Performance Requirements			
PERF-INT-01	Wing Demo shall measure NEF performance during operation.		
		PERF-INT-01.A	Wing Demo shall measure pump(s) flow rates of the NEF in terms of mass of fuel per unit of time, between 0 g/s to 300 g/s, with a 30 g/s accuracy, at 1/20 Hz sample rate.
		PERF-INT-01.B	Wing Demo shall measure voltage output of each NEF stack in voltage, between 0 VDC and 50 VDC, within 0.5 VDC accuracy, at 10 Hz sample rate.
		PERF-INT-01.C	Wing Demo shall measure electrical current output of each NEF stack, between 0 A and 50 A, with a 0.5 A accuracy, at 10 Hz sample rate.
		PERF-INT-01.D	Wing Demo should measure rotational speed of the RDM(s).
		PERF-INT-01.E	Wing Demo shall measure input power to RDM(s), between 0 W and 250 W, with a 5 W accuracy, and sample rate should be 10 Hz.
		PERF-INT-01.F	Wing Demo should measure Motor Controller(s) efficiency.
		PERF-INT-01.G	Wing Demo shall measure temperatures of the RDM(s), Motor Controllers, NEF stacks, and pump(s), between 0º C and 150º C, to within 5º C accuracy, at 1 Hz sample rate.
		PERF-INT-01.H	Wing Demo shall measure power for the Pump(s) and Motor Controller(s) (if applicable), between 0 W and 250 W, with a 5 W accuracy, and sample rate should be 10 Hz.
		PERF-INT-01.I	Wing Demo shall measure Ambient Temperature, between 0º C and 50º C, with a 5º C accuracy; Pressure, between 80 kpa to 120 kpa, with a 5 kpa accuracy; and Humidty, between 0% and 100%, with a 5% accuracy, and sample rate should be 1 Hz.

Using these requirements, a comprehensive list of sensors was derived for the Wing Demonstrator and is summarized in Table 14.

Table 14. The Wing Demonstrator sensor list.

	Reading	Requirement	Item	Units
AMBIENT	Temperature	PERF-INT-01.I	Ambient Air	Celsius
	Pressure	PERF-INT-01.I	Ambient Air	kPa
	Humidity	PERF-INT-01.I	Ambient Air	%
SYSTEM1	Flowrate	PERF-INT-01.A	Pump1/NEF1	kg/s
	Output Voltage	PERF-INT-01.B	NEF Stack 1/Controller1	Volts
	Output Current	PERF-INT-01.C	NEF Stack 1/Controller1	Amps
	Temperature (1,2,3)	PERF-INT-01.G	Pump1	Celsius
	Voltage	PERF-INT-01.H	Pump1	Watts
	Current	PERF-INT-01.H	Pump1	
	Temperature1	PERF-INT-01.G	NEF Stack 1	Celsius
	Temperature2	PERF-INT-01.G	NEF Stack 1	Celsius
	Temperature3	PERF-INT-01.G	NEF Stack 1	Celsius
	Temperature1	PERF-INT-01.G	RDM1	Celsius
	Temperature2	PERF-INT-01.G	RDM1	Celsius
	Temperature3	PERF-INT-01.G	RDM1	Celsius
	Rotational Speed	PERF-INT-01.D	RDM1	RPM
	Temperature (1,2,3)	PERF-INT-01.G	Controller1	Celsius
SYSTEM2	Flowrate	PERF-INT-01.A	Pump2/NEF2	kg/s
	Output Voltage	PERF-INT-01.B	NEF Stack 2/Controller2	Volts
	Output Current	PERF-INT-01.C	NEF Stack 2/Controller2	Amps
	Temperature (1,2,3)	PERF-INT-01.G	Pump2	Celsius
	Voltage	PERF-INT-01.H	Pump2	Watts
	Current	PERF-INT-01.H	Pump2	
	Temperature1	PERF-INT-01.G	NEF Stack 2	Celsius
	Temperature2	PERF-INT-01.G	NEF Stack 2	Celsius
	Temperature3	PERF-INT-01.G	NEF Stack 2	Celsius
	Temperature1	PERF-INT-01.G	RDM2	Celsius
	Temperature2	PERF-INT-01.G	RDM2	Celsius
	Temperature3	PERF-INT-01.G	RDM2	Celsius
	Rotational Speed	PERF-INT-01.D	RDM2	RPM
	Temperature (1,2,3)	PERF-INT-01.G	Controller2	Celsius
E-STOP	E-STOP	OPS-INT-03	NEF1/Controller1	
	E-STOP	OPS-INT-03	NEF2/Controller2	
	E-STOP	OPS-INT-03	Pump1	
	E-STOP	OPS-INT-03	Pump2	

Zero-Emission Super-short Takeoff and Landing Collaboration and Analysis

The original RDM distributed electric wing layout with flap and nacelle cowling is shown in figure 45. Ultimately, the team decided to alter the orientation of the RDMs on the wing with the new design, shifting the motors to be centered in front of the leading edge. This configuration helped reduce wing size, lift requirements at takeoff, and induced drag during cruise. As a result of high drag at cruise conditions, the under-wing design was replaced with a system in front of the leading edge, but the integrations concepts are similar.

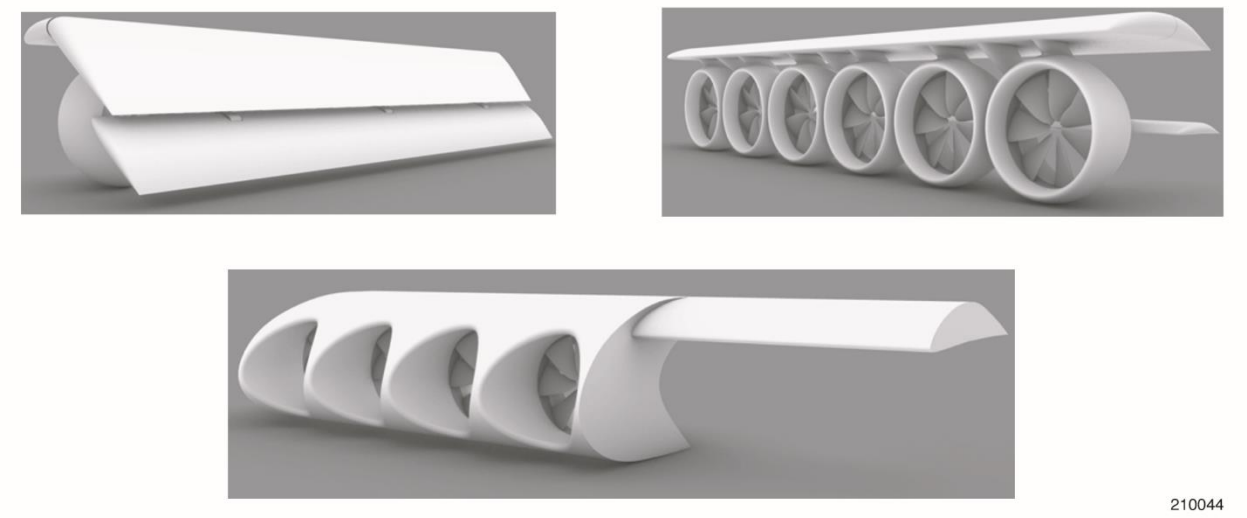

Figure 45. (top-left) Bi-flap; (bottom) with integrated cowling; and (top-right) with rim-driven motor in distributed propulsion configuration.

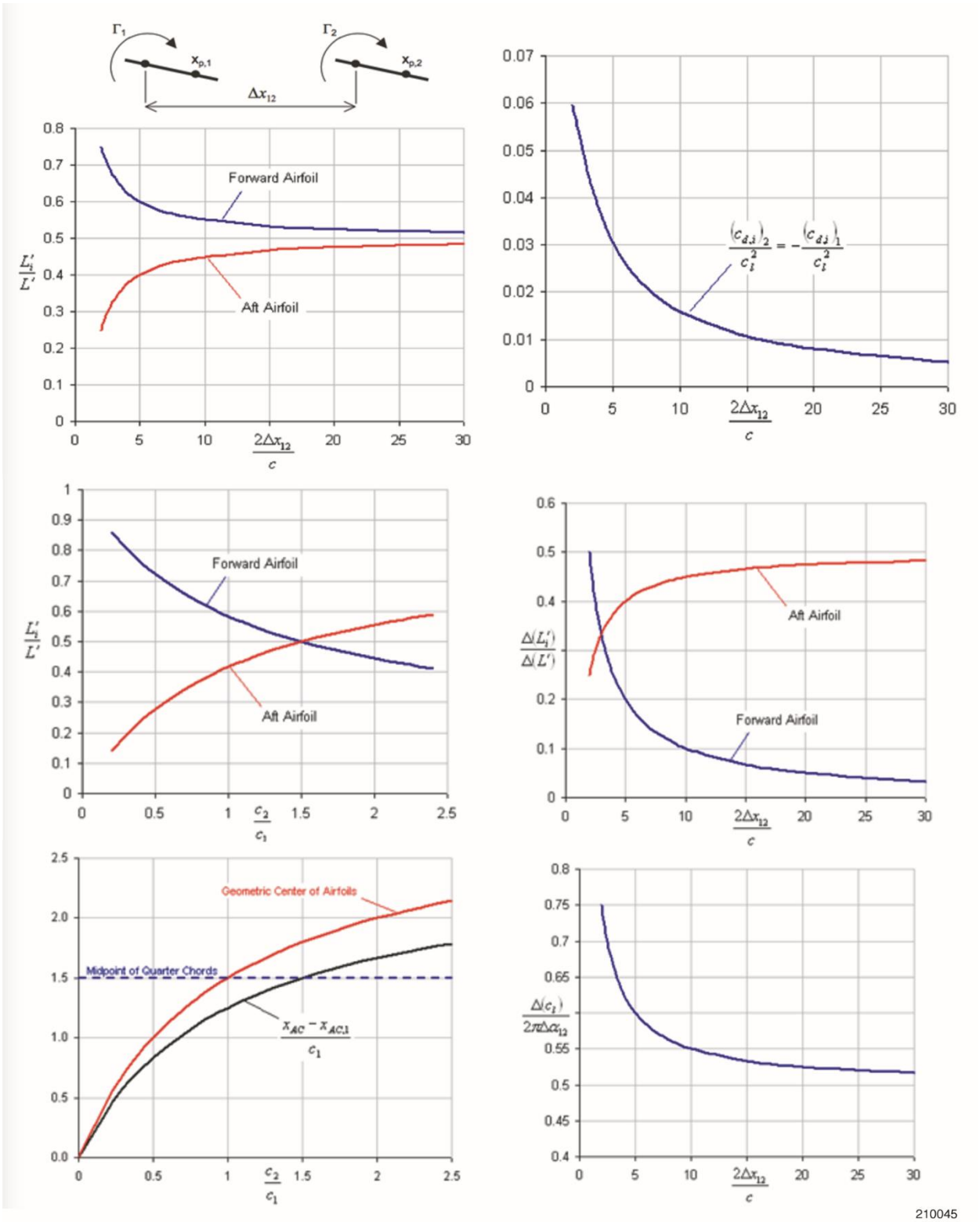

Figure 46. (top-left) Lift effects on horizontal separation; (top-right) induced drag variation for tandem wing; middle- and lower-left) chord effects; and (middle- and lower-right) decalage effects).

The lessons learned associated with this tandem wing design are discussed below.

Stagger or Horizontal Separation

Figure 46 show the effects of stagger on the lift of each airfoil. The lift is shown using the ratio of airfoil lift to total system lift. The forward airfoil experiences upwash from the aft airfoil; thus, increasing forward airfoil lift. The aft airfoil experiences the downwash from the forward airfoil; therefore, decreasing aft airfoil lift. The effects reduce as the airfoils are separated by greater and greater distances, until each airfoil experiences the freestream flow without the effects of the other airfoil (ref. 8).

Induced Drag Variation

Variation of induced drag on each airfoil is normalized by the overall lift coefficient squared. The induced drag on the two airfoils has been shown as a single line, since curve for the other airfoil would be a reflection across the x-axis.

Chord Effects

Figure 46 shows the effects of chord ratio on the lift of each airfoil. The lift is transferred from the forward airfoil to the aft as c_2/c_1 (root-to-tip chord ratio) increases. The transfer is nonlinear because the lift is proportional to the chord and circulation on the airfoil, both grow linearly as c_2/c_1 is increased. The Δx_{12} is the x station between root and tip. The two curves cross at the point shown in equation 1.

$$\frac{c_2}{c_1} = \left(2 - \frac{c_1}{\Delta x_{12}}\right)^{-1} \tag{1}$$

This chord ratio can be used to balance the lift on two airfoils without any décalage (ref. 9).

Multiple computational fluid dynamic (CFD) runs were conducted on the ZEST concept. The coefficient of pressure for different angles and streamlines are shown in figure 47.

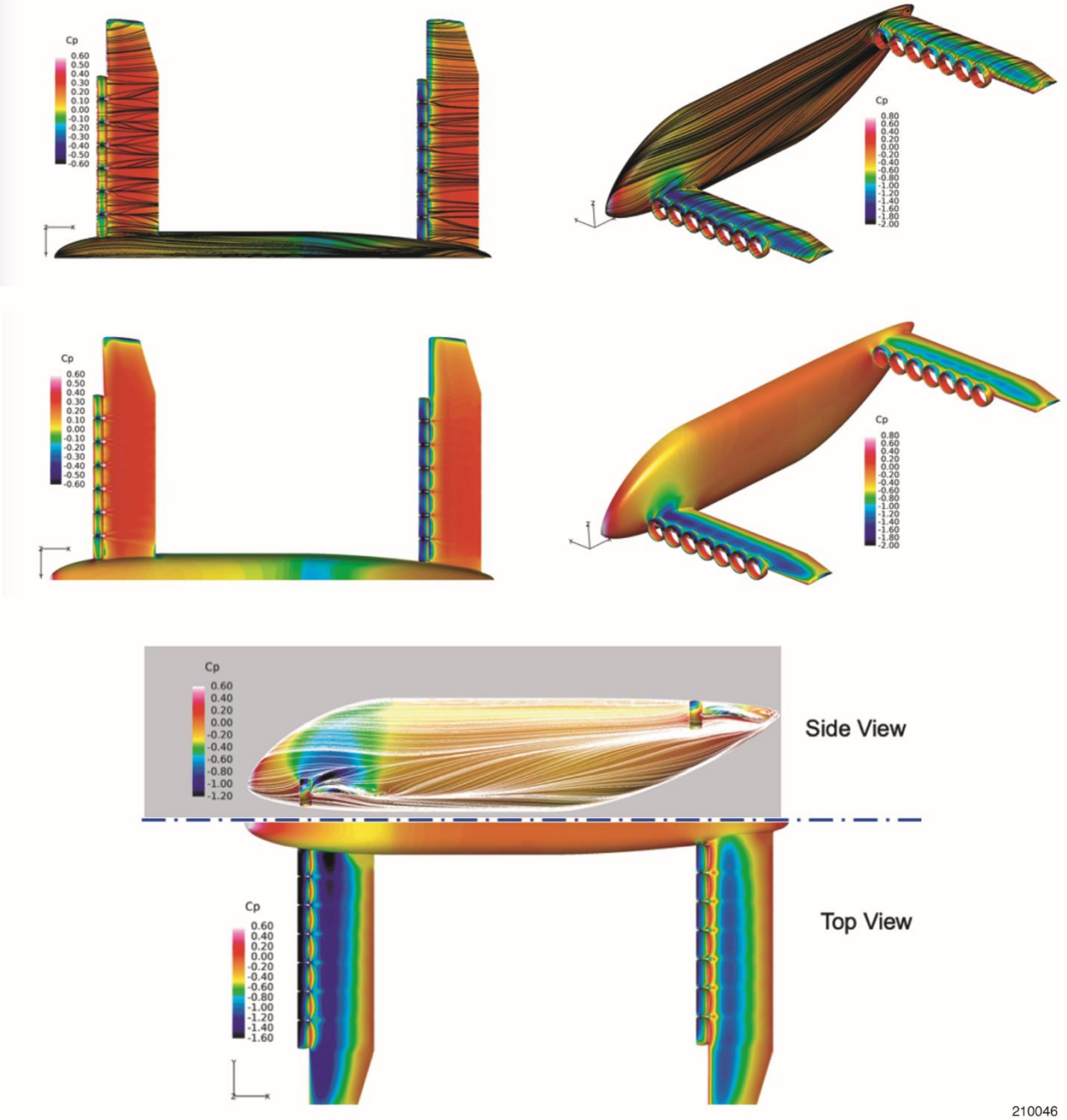

Figure 47. Coefficient of pressure for tandem wing section on The Boeing Company Zero-Emissions Super-short Takeoff and landing 8A and B configurations.

Shown in figure 48 are The Boeing Company final ZEST 8.0 A and B concept with varying views: with panels extended, closed, a walkaround, and a takeoff/landing.

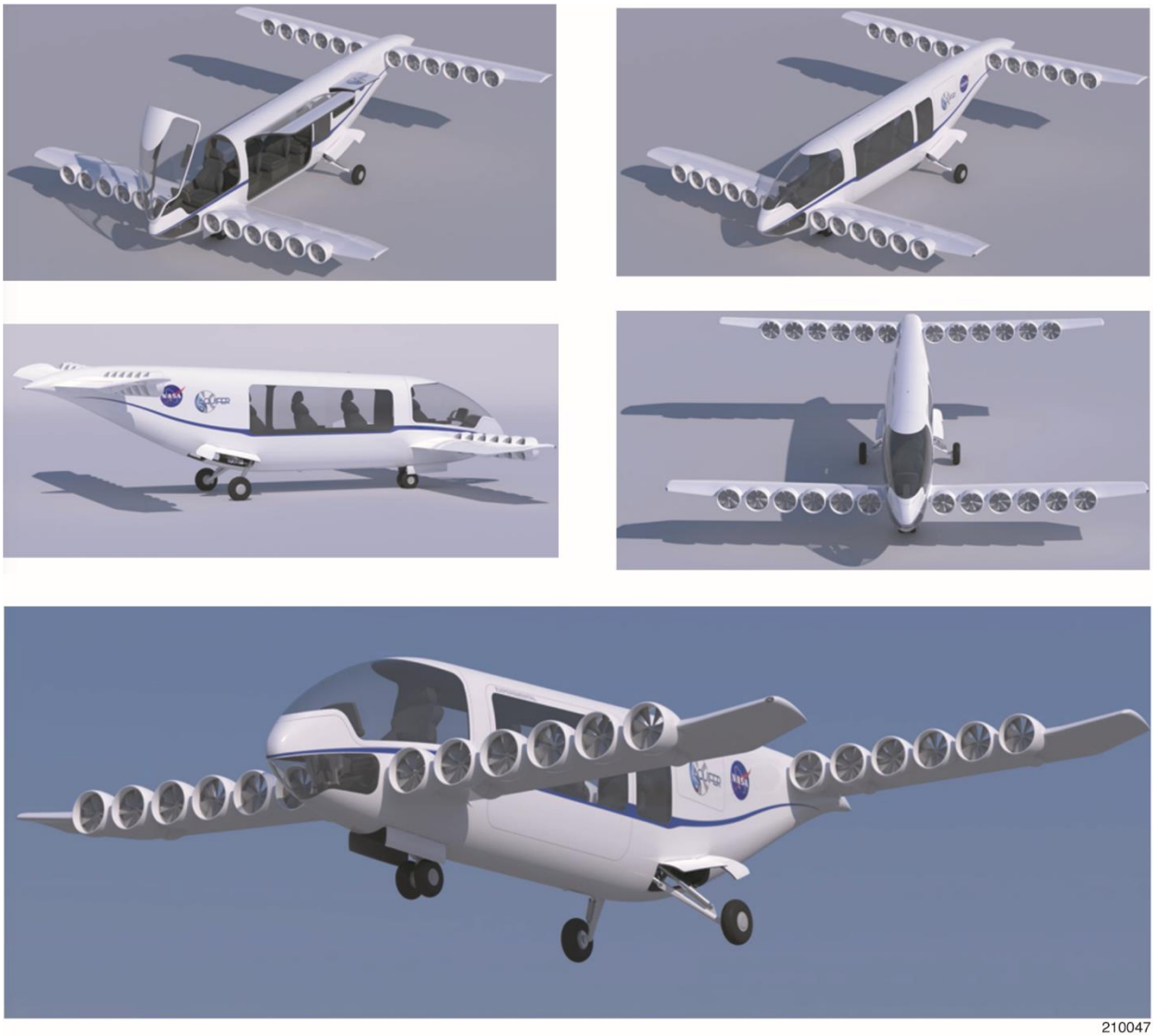

Figure 48. The Boeing Company Zero-Emissions Super-short Takeoff and landing 8A and B with the Aqueous, QUick-charging battery Integration For Electric flight Research and the National Aeronautics and Space Administration livery.

The AQUIFER team also analyzed the operations and utility of the ZEST eSSTOL concept. The Boeing Company ZEST 5.0 is shown in the top two pictures of figure 49; the middle and bottom pictures show the ZEST 8A for operational considerations, including services out of San Diego harbor and Los Angeles Convention Center. As previously shown, figure 14 shows the development of the ZEST concept for reference.

Figure 49. (left- and right-top) The Boeing Company Zero-Emissions Super-short Takeoff and landing with The Boeing Company, the Aqueous, QUick-charging battery Integration For Electric flight Research, and the National Aeronautics and Space Administration livery; (middle-center) approach (yellow) and takeoff (green); (bottom-left) conops for Zero-Emissions Super-short Takeoff and landing 8A for San Diego harbor; and (bottom-right) Los Angeles Convention Center.

Outer Mold Line Requirements for the Wing Demonstrator

The Wing Demonstrator was intended to be used to conduct systems integration of NEF and RDF/RDM together in a subset of a wing that included four nacelles. The shape of the wing was intended to represent a configuration similar to, but not exactly representative of, The Boeing Company ZEST concept. The Wing Demonstrator would demonstrate the technology readiness on completion of the two-year CAS project, whereas the Boeing Company ZEST concept was based on Vision System technologies.

The LaRC personnel completed the Wing Demonstrator sizing task while the Boeing Company ZEST mission parameters were conducted simultaneously and are shown in table 15. These requirements do not directly align with current Federal Aviation Administration regulations, but it is anticipated that changes will be made to accommodate these types of vehicles.

Table 15. The Boeing Company Zero-Emissions Super-short Takeoff and landing mission parameters, dated February 7, 2019.

Sizing mission		Comments/reasoning
Balanced field length (BFL)	300 ft	300 ft: reuse of abandoned football or soccer fields (Based on 1/24 engines inoperative)
Obstacle clearance height	35 ft	14 CFR § 23.2115 currently refers to a 35 ft obstacle clearance height for BFL calculations.
Cruise mission range	250 nmi	Inter-city mission
Cruise speed	250 kt	~1-hour mission; max speed for aircraft flying below 10,000 ft [14 CFR § 91.117]
Cruise mission altitude	5000 ft	
Reserve requirement	20 min	Cruise power
Payload	800 lb	200 lb per person
Runway ambient temperature	15 °C	Sea level standard day (SLSD)
Runway height	0 ft	SLSD

The Wing Demonstrator outer mold line (OML) requirements are listed in table 16 and were based on the AQUIFER system requirements, considerations, mechanical constraints, ZEST mission requirements, and aerodynamic considerations. The requirements did not fully define the shaping between each nacelle; detailed aerodynamic design for nacelle integration was deemed a future research area. For the purposes of the Wing Demonstrator, a low-complexity modular-mechanical design was of higher priority.

Table 16. The Wing Demonstrator outer mold line requirements.

Parameter	Value
Chord length	30 inches
Airfoil	NACA 4415
High-lift device	40-percent chord double slotted flap, similar to that used in NASA TN D-7034. The Wing Demonstrator must demonstrate high lift actuation per AQUIFER requirement SYS-INT-03.A.
Dihedral	0 degrees

Sweep	0 degrees
Twist	0 degrees
Taper ratio	1
Number of nacelles	Minimum of two, up to four nacelles. Accommodate at least two RDM/NEF systems [SYS-INT-01].
Nacelle inner diameter	14 inches
Nacelle outer diameter	22 inches; radial thickness will house 1.5-in acoustic lining in addition to RDM/NEF.
Nacelle axial length	Minimum length sufficient to house NEF + RDM + acoustic liner + streamlining. Not greater than 18 inches.
Nacelle vertical location	Under-wing configuration with top section inset into wing, such that top of nacelle ID is tangent with wing lower surface.
Nacelle lateral location	Inboard nacelle: inboard OD is coincident with fuselage. Remaining nacelles: aligned such that nacelle OD is coincident with OD of neighboring nacelle.
Lower wing	Nacelle bottom surfaces will be merged into lower wing. Lower wing airfoil section to be symmetric NACA 00XX series, where XX is as low as possible to house internal systems. Chord length: greater than or equal to nacelle axial length; not greater than 18 inches.

The Zero-Emissions Super-short Takeoff and landing – Aqueous, Quick-charging Battery Integration For Electric flight Research Vision System Aircraft Conceptual Design

The objective of the ZEST-AQUIFER Vision System aircraft conceptual design was to design a vehicle which utilized the AQUIFER Vision System technologies to achieve The Boeing Company ZEST four-passenger eSSTOL mission and is described in table 3 and table 18. At the start of the AQUIFER Vision System design, The Boeing Company already had a set of mission parameters defined (shown in table 15) and an initial ZEST 1.0 aircraft design completed via spreadsheet analysis. The Boeing Company requested that NASA perform an independent review of their results.

In order to evaluate The Boeing Company ZEST aircraft configuration and associated mission requirements, the NASA LaRC Aeronautics Systems Analysis Branch (ASAB) developed a MATLAB® (The MathWorks Inc., Natick, Massachusetts) aircraft sizing routine using a low-fidelity approach. The routine attempted to obtain the following two mission requirements: (1) achieve takeoff within a specified balanced field length; (2) meet cruise range at cruise velocity and altitude with specified reserve. The steps to verify the aircraft configuration and mission requirements included:

- Making initial guesses of total wing area and takeoff gross weight (TOGW).
- Specifying wing aspect ratio and calculating induced drag in cruise using an Oswald efficiency factor (ref. 9), based on the aspect ratio and required lift coefficient as based on weight and cruise speed.

- Using Open Vehicle Sketch Pad (OpenVSP) (The National Aeronautics and Space Administration, Langley, Virginia) software (ref. 10) to create look-up tables for a variety of wing sizes with 24 representative ducts for RDFs and a fuselage in order to calculate parasite drag at cruise and sea-level altitudes and velocities. One representative wing configuration can be seen in figure 50 and was based on the following:
- Specifying propulsive efficiency (85 percent from battery to airflow) and using cruise total drag (sum of induced and parasitic drag) to calculate energy required for cruise and reserves.
- Adding climb energy as a potential energy (TOGW multiplied by cruise height).
- Specifying NEF battery specific energy (890 Wh/kg) and calculating battery weight.
- Predicting wing weight using an average of the Raymer equation for general aviation wing weight, Roskam equations for United States Air Force light and utility aircraft, Torenbeek equations for light transport airplanes; a composite wing weight fudge factor of 0.95 (ref. 10) was used.
- Specifying fuselage weight (900 lb) and payload weight (800 lb), summed with wing and battery weights to find new TOGW.
- Using new TOGW, calculating the wing area required to meet balanced field-length requirements using the Raymer takeoff model (Ref. 10):
    - Specify maximum lift coefficient and calculate stall velocity.
    - Specify thrust-to-weight ratio at takeoff and lift-to-drag ratio in a high lift configuration and calculate ground roll and climb-out distances for regular and one propulsor inoperative conditions.
    - Specify friction coefficients based upon Raymer (0.03 for rolling conditions and 0.3 for breaking conditions), assume 20-percent thrust reversal capability, and calculate one propulsor inoperative braking distance.
    - Solve for wing area required to meet balanced field length (BFL) requirement.
- Repeating each step and changing aspect ratio at each iteration until wing area and TOGW converge.

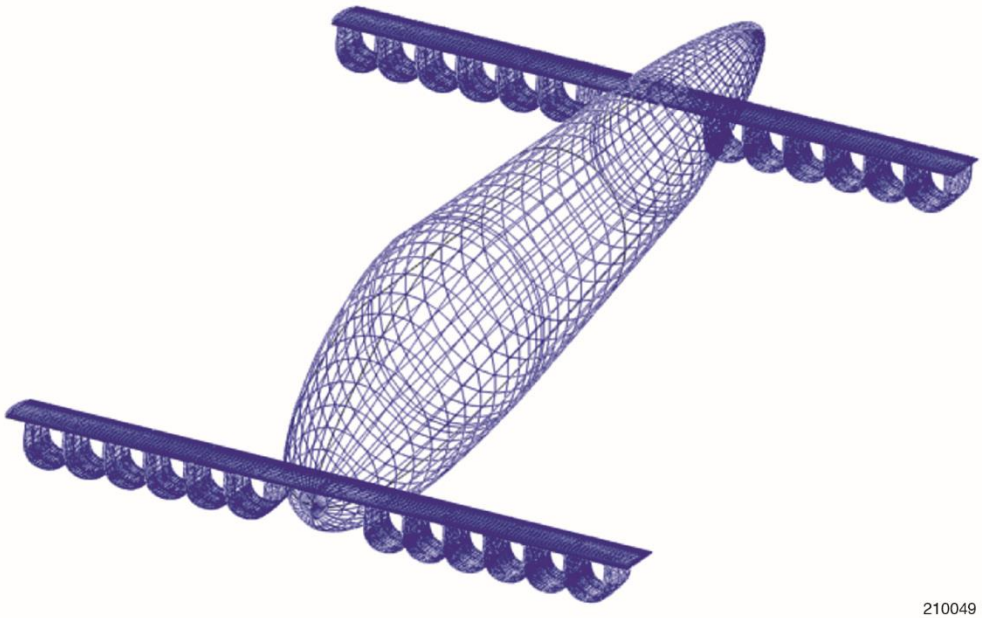

Figure 50. Representative parasite drag model using the National Aeronautics and Space Administration OpenVSP software (ref. 11).

The NASA analysis predicted excessive drag because of the large wetted area of the ducts and suggested that The Boeing Company design was infeasible given their mission requirements. In order to use 24 RDFs and their associated ducts, it was required to either reduce the cruise speed or increase the runway length.

After several cycles of CFD, The Boeing Company concurred that the mission requirements could not be met with the desired ducted fan configuration; therefore, mission parameters were relaxed. Table 17 lists the ZEST-AQUIFER mission requirements at the completion of the AQUIFER project. The values denoted in bold text are those which differ from values in table 15.

It is recommended that a more thorough study be conducted to investigate the sensitivity of the design to runway length and cruise speed; therefore, achieving a better understanding of the associated tradeoffs. Additionally, for improved estimates of mission parameters, further studies into the SSTOL market are desired.

Table 17. The Zero-Emissions Super-short Takeoff and landing mission parameters upon completion of the Aqueous, QUick-charging battery Integration For Electric flight Research project.

Sizing mission		Comments/reasoning
Balanced field length	300 ft	Maintain 300 ft: reuse of abandoned football or soccer fields (Based on 1/24 engines inoperative).
Obstacle clearance height	35 ft	14 CFR § 23.2115 currently refers to a 35-ft obstacle clearance height for BFL calculations.
Cruise mission range	200 nm	Inter-city mission (previously 250 nm)
Cruise speed	200 kt	~1-hour mission (previously 250 kt)
Cruise mission altitude	5000 ft	
Reserve requirement	20 min	Cruise power
Payload	875 lb	Pilot: 200-lb passengers: 3x 225 lb (previously 800 lb.)
Runway ambient temperature	15 °C	Sea level standard day (SLSD)
Runway height	0 ft	SLSD

Vehicle-Level Studies: Application of Nano-electro Fuel to the National Aeronautics and Space Administration X-57

In order to gain an improved understanding of the application of NEF to aircraft, NASA ASAB performed a study of the application of NEF to the NASA X-57 “Maxwell” (Mod II) airplane

(electric retrofit). The X-57 airplane is a twin-engine four-seat Tecnam P2006T (Tecnam, Capua, Italy) modified to use an electric propulsion system (Ref. 11). The Mod II configuration refers to the second stage of development, which maintains the Tecnam wing and nacelles with the internal combustion engines and fuel system removed and replaced with the electric propulsion system. The X-57 airplane was designed to use lithium-ion batteries, and a study has also been conducted to investigate the application of solid oxide fuel cells (SOFC). A study, therefore, of the use of NEF on the X-57 airplane would not only allow the project team to investigate the installation of NEF on a vehicle level but allow a comparison with other battery types.

Nano-electro Fuel Vision System Definition

Projected NEF technology development (assuming sufficient investment and no unexpected technical barriers) is shown in table 18; this table was compiled jointly by ASAB and Influit Energy. GEN 2 and the Vision System technology levels are also provided as an initial look and appear to provide properties of a suitable order of magnitude for use on aircraft.

Table 18. Projected nano-electro fuel technology development.

		GEN 1				GEN 2				Vision
System	Technology parameter	2018	2019	2020	Target	2021	2022	2023	Target	System
Cell	Cell outer thickness, cm	2	0.8	0.6		0.5	0.5	0.4		0.2
	cell active membrane area fraction	80%	80%	85%		85%	85%	85 %		85%
	current density, mA/cm^2	6	50	100		200	500	1000		1700
	cell voltage, VDC	1.2	1.2	1.2		1.28	1.28	1.28		2.25
Stack	Stack average density, kg/L	1.2	1.2	1.2		1.2	1.2	1.2		1.2
Fluid	Cell efficiency	10%	25%	50%		80%	90%	90 %		90%
	Cell parasitic Power losses		8%	5%	2%	2%	2%	2%	2%	2%
	Electroactive Solids specific Energy, Wh/kg	192	192	192		1331	1331	1331		1331
	Electroactive Solids weight fraction	20%	50%	70%	80%	80%	80%	80 %	80%	80%
	NEF discharge efficiency	10%	30%	60%	90%	30%	60%	80 %	90%	90%

	Fluid specific Energy, Wh/kg	4	29	81	319	639	852	958
	Electroactive Solids density, g/cm^3 (kg/L)	5.1	5.1	5.1	7.7	7.7	7.7	7.7
	Aqueous solution density, g/cm^3 (kg/L)	1.5	1.5	1.5	1.5	1.5	1.5	1.5
	Average Fluid Density, g/cm^3 (kg/L)	2.2	3.3	4.0	6.5	6.5	6.5	6.5
Ancillary	Large-scale system: weight fraction of installation materials	15%	15%	15%	15%	15%	15 %	15%

In addition to the specific technology development targets, many other questions about the application of NEF specific to aircraft were discussed. These questions and the responses from Influit Energy are documented in table 19.

Two questions were raised as a result of these conversations, which warranted further investigation: (1) how realistic is the assumption of a 15-percent weight fraction for installation materials, and how sensitive is the battery density to changes in this fraction; and (2) what are the pumping requirements in order to push fluids through the battery?

An attempt to answer these questions was made during the X-57 airplane NEF study which is described below.

Table 19. Influit Energy responses to National Aeronautics and Space Administration questions on nano-electro fuel properties related to aircraft design requirements.

Question/comment	Response
Are there any restrictions on shape/size? Can it be any shape/do cells have to be flat?	In principle, cells can be any shape/size; however, sealing surface on the perimeter of the cells is required; thus, high aspect ratio geometries may be less efficient. Cell voltage is independent of cell size: determined by chemical reactions.
What is the cell efficiency?	Cell efficiency is not used in calculations; instead, NEF discharge efficiency is used in the calculation, which is an equivalent of "cell efficiency" of solid battery cells.

Question/comment	Response
Cell parasitic power losses	An eight-percent estimate comes from the limited power of a Wing Demonstrator NEF battery and fixed maximum pump power of the pump and other Battery Control System components. We don't anticipate running the pump at full power for the demo - this parameter (flow rate and corresponding pump-power requirements) will be optimized during the course of the project. Pump/infrastructure losses are expected to be less than two percent.
Electroactive solids specific Energy	Electroactive solids are the solid nanoparticles which are suspended in aqueous solution to create the fluid. Electroactive solids specific energy is the average specific energy between cathode and anode. GEN 2 and "Vision System" will use an air cathode: this specific energy includes lower density cathode. This calculation for GEN 2 takes the weight of pure oxygen into the account. The ability to use air instead of pure oxygen is not validated yet but could enable the battery to be air breathing.
NEF discharge efficiency	NEF discharge efficiency is the fraction of energy that we can harness from the fluid.
How does efficiency vary with partial throttle (power) settings, altitude, temperature, or other operating parameters?	The question on efficiency can only be answered once the technology is developed. Generally, higher temperature improves kinetics of reactions, i.e. efficiency, lower temperature slows things down. Temperature limits: 70 °C is normally fine; boiled water (100°C) or frozen (-40 °C as a result of solution) is undesirable. Higher power will also reduce efficiency because of over potentials and incomplete reactions. The magnitude of all these effects cannot be evaluated at this stage. Altitude may affect the GEN 2 battery if the cathode is air breathing as a result of depletion of atmospheric oxygen and can be compensated with stored oxygen. That explains why all calculations for energy density are done with assumption of oxygen weight being a part of the system.
Aqueous solution density: why is this solution heavier than water?	An alkaline electrolyte, KOH, is added to water for ionic conductivity between cathode and anode chambers.
Weight fraction of installation materials: where does this weight fraction come from?	This weight fraction is based on 15 percent achievable in regular flow cells.

Question/comment	Response
Does efficiency reduce during flight, given we're recirculating the fluids? Are there any benefits to having four tanks over two tanks?	If the fluids are recirculated (two tanks) the average state of charge (cell voltage) gradually reduces - just like in any battery. The battery packs are engineered with assumption of known voltage decay and battery shut down if the average voltage drops below a certain value. With single pass fluids (four tanks) the voltage will fluctuate within the acceptable device values, as each fraction of NEF passing through the cell will have to go though I-V curves for given materials. A reduction in voltage can be compensated for with increased current draw (higher flow rate) for a constant power.
What are the requirements for fuel tank material?	Ethylene propylene diene monomer/polypropylene, i.e. plastic, no metal to contact fluid. Tank wall thickness dependent on fuel loadings.
What are the costs?	A GEN 1 cost estimate for the 80-L, 36-VDC, 15.5-kWh battery pack (smaller - lead-acid battery replacement for utility electric vehicles) is $130/kWh, with the assumption of cells providing 1.2-VDC and 100-mA/cm^2 current density. The calculations include cost of materials required to produce cathode and anode nanoparticles, nanofluid manufacturing costs as well as stack component costs. For GEN 2, a cost estimate of <$90/kWh was made because the cost of cathode material is reduced by factor of 10 (air cathode) while the rest of stack components are maintained. About 75 percent of the cost of the battery comes from cathode and anode NEF and 25 percent from stack-component costs.
Are there any restrictions as to how fast we can pump the fluid in / out during refueling?	The fluid itself doesn't suffer from pumping and is limited only by flow physics. Mechanical, pressure drop, and pumping power penalties will be the restricting factor on the flow rate; thus, no restriction on the flow rate when refueling tanks. During NEF battery operations, however, electrochemical perspective reaction kinetics is the limiting factor on how fast we should pump the fluids. Ultimately it is envisioned that the flow rate will be optimized for the highest reaction efficiency, with ability to use the flow rate to tune the cell and stack current per power requirements.
Is there cooling required?	No, the NEF liquid can be used as coolant. No cooling loop within stack.

Question/comment	Response
What is the expected life of the NEF system/cells? Cycles/longevity? Does fluid performance degrade over time?	Lifetime estimated to be 1,000 cycles (based on solid battery chemistry). At the end of the 1,000 cycles you can recondition the fluid into its original form. If the fluid sits for three to six months, the particles will settle but can be agitated to redistribute the particles and therefore be useable. It is possible that the fluid gets contaminated with dust, impurities, particle agglomeration, or change in concentration because of moisture/evaporation. These types of degradation can be addressed with routine maintenance, such as filtering the larger particulates, check/adjustments of water/particle concentration, etc. After 1000 cycles refer to degradation of the NEF liquids. Cell degradation, although possible, can be engineered for stability under NEF cycling conditions. With proper choice of materials and design of the cell seals/interconnects there should not be any degradation, as only liquid will be participating in redox transformation. If charging and discharging of the fluids is done in a separate facility (i.e., recharging in a separate ground facility rather than plugging in the battery), one can expect that cells will last longer, as they are exposed to less corrosive conditions. The anode will discharge when in contact with oxygen; this discharge needs to be prevented as much as possible but does not degrade the fluid - it will just need to be recharged. No effect of oxygen on the cathode.
How is the system recharged?	To recharge, switch polarity of the battery and keep the pumps running, so electrons flow the other direction. The charger system will control the charging current and will shut-off charging when desired state of charge is achieved to prevent/eliminate degradation of electrolyte.
Is the NEF system susceptible to changes in acceleration, e.g. +/- G-limits? Could it work upside down? What about turbulence/hard landings?	Continuous acceleration in one direction: particles will settle eventually. Aircraft, however, will act as an agitator. Battery can be designed to work upside-down. Hard landings: should be fine.
Are GEN 2 and “Vision System” flammable, toxic, magnetic?	Aqueous solutions are inflammable, environmentally friendly, non-toxic materials, but nanoparticles may be an inhalation hazard if they become airborne. Follow general handling guidelines for nanoparticles in fluid. GEN 1 anode and cathode are nonmagnetic; GEN 2 anode nanoparticles are magnetic in charged state and nonmagnetic in discharged state.

Application of NEF to the X-57 airplane

The feasibility of incorporating the NEF power system into the X-57 Mod II airplane configuration was investigated using the parameters identified from Influit Energy in table 18 and table 19. Scaling studies and conceptual estimates conducted by the NASA ASAB team indicated that such a system could be used for primary power pending some assumptions; however, a more detailed analysis was needed to increase confidence that the complete power system incorporation was feasible and to clarify the assumptions on weights and fluid dynamics associated with pumping NEF during flight.

An initial layout of the NEF power system in the X-57 Mod II airplane can be seen in figure 51. This configuration shows two storage tanks located in the fuselage for the NEF. The NEF is pumped from two these tanks to the NEF flow cells, which are located just aft of the motors in the wing. Additionally, traditional lithium-ion batteries are included in the system to start the NEF pumps, and these batteries were placed in the fuselage ahead of the NEF pumps.

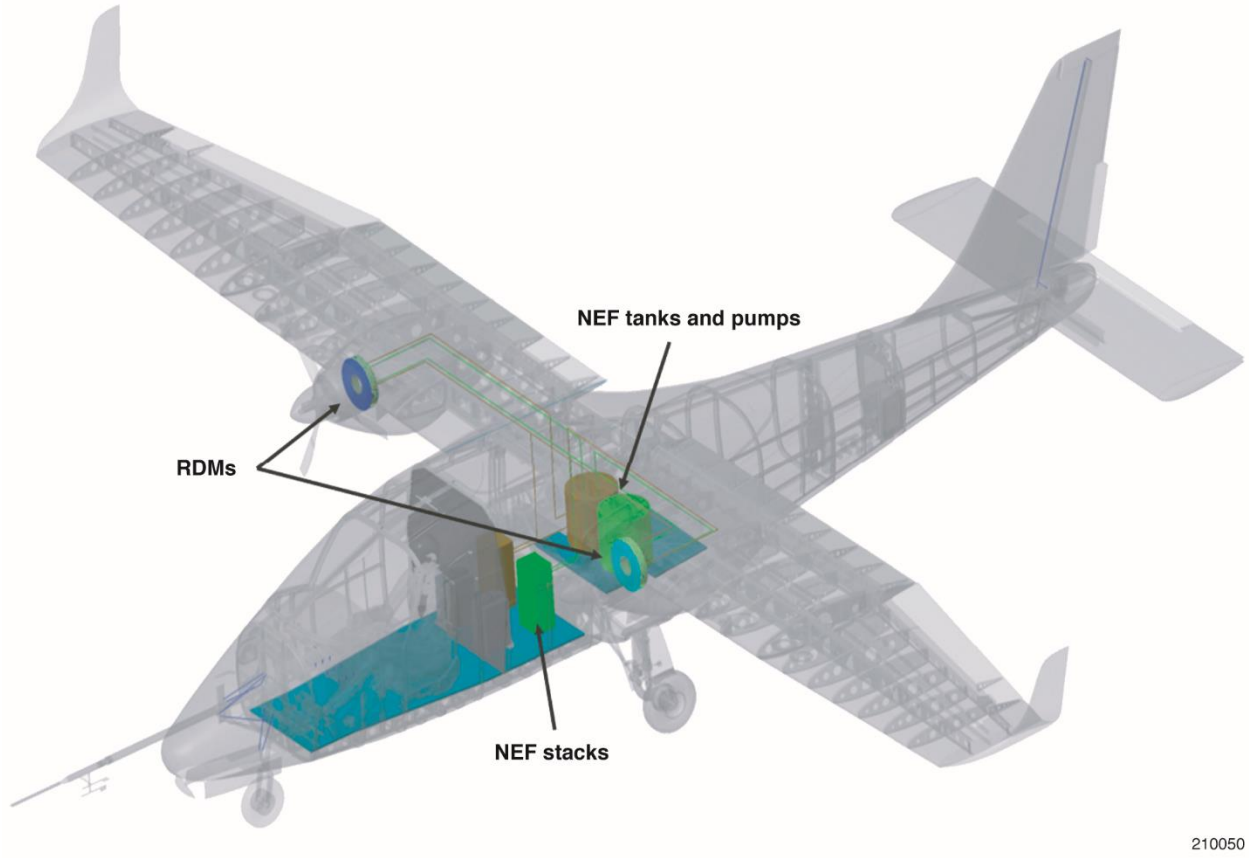

Figure 51. The X-57 Mod II airplane with initial integration of nano-electro fuel power system.

The maximum power requirement during takeoff was 145 kW (ref. 12), and the NEF cell system was designed as annular disks with an outer diameter equal to the motor diameter (14 inches). The inner diameter of the NEF cell system was estimated to be large enough (five inches) to allow a motor shaft to run through, if needed.

Throughout the study there were assumptions made concerning mounting structure, fuel lines, safety structure, tanks, and pumps. A base assumption of weight from a similar mounting structure used in the X-57 airplane for the lithium-ion batteries was used to hold the pumps and tanks. A fuel line diameter of 0.25 inches was estimated from the information on the NEF cell flow diameter of approximately 0.2 inches. A mass per length of the fuel lines (0.051 lb/ft) was

determined based on polypropylene - a material that would not interfere with the chemical composition of the anode or cathode fluid, and diameter assumption. Associated weights were created by using polypropylene with fuel line lengths going from the tanks in the fuselage to the nacelles where the NEF cells reside. Return lines were also incorporated into the same tank with the assumption that the used NEF would return to the same storage tank, as suggested by Influit Energy. Finally, there were short-length fuel lines that were incorporated into the system loop for the pumps.

A 0.25-in thick steel firewall was placed between the NEF system and the pilot; however, future design iterations may not require this firewall because NEF fluids are not expected to be flammable. In order to meet the mission requirements, two tanks (one for anode fluid and one for cathode fluid) were placed in the fuselage at approximately the quarter-chord point of the wing with the size of the tanks dependent on the available fuel weight to be carried by the X-57 Mod II airplane and the maximum required fuel. Positioning of these tanks was preliminary and would be modified during the balance of the vehicle in future iterations. Weights of these tanks were based upon recommended material properties from Influit Energy and an empirical equation for tank size and weight.

The pump weight and selection were the primary unknown. Based upon the NEF composition and properties, the pump would be required to pump a viscous fluid (similar to that of heavy motor oil) through narrow friction-inducing channels with many 90- and 180-degree turns at a sufficient flow rate to produce the required power of the X-57 airplane during takeoff (ref. 12). Calculations of the turning pressure losses in the NEF cell with the fluid flow required to meet the power requirements of a light aircraft, indicated that the pumps for the fluid would be significant in weight. There was also a pressure loss from the tanks to the motors that was not taken into consideration, although this loss could be reduced in the future by placing the tanks in the wings. Because pumping pressure losses could not be estimated until a NEF cell was designed, two placeholder pumps were used and assumed a very optimistic pump weight of 2 kg per pump, each drawing 8-A current at 12 VDC. Pressure losses in the system were ignored and it was assumed that the pumps could provide the needed fluid flow to achieve the power requirements at each phase. As a result of this study, this optimistic assumption provided a basis for an initial calculation but needs to be amended at later stages if the NEF version of the X-57 airplane is found to be worth investigating further.

Because pump weights were not known, a check of the center of gravity location of this light aircraft was not performed, but it is known that there is flexibility in positioning of the tanks in the aft part of the X-57 Mod II airplane; therefore, a center of gravity location could most likely be met. The NEF system requires minimal equipment, which is an advantage for packaging and volume constraints.

For the current configuration, it was assumed that there would be a startup battery for each pump. These batteries take the assumption of 300 Wh/kg for the Vision System timeframe and 250 Wh/kg for near-term technology. Each battery would be recharged in 30 minutes during cruise flight phase. These batteries were sized to provide power to the pumps for a 1-hour time frame. Future iterations could eliminate these batteries and provide an alternative solution to start the NEF battery under its own power.

A payload-range graph was created to compare the NEF technology to other potential solutions. Figure 52 shows payload-range results for a conventional fuel-based P2006T airplane; a traditional battery-electric X-57 Mod II airplane; a solid oxide fuel cell SOFC hybrid-electric version of the X-57 Mod II airplane; and the NEF power system version of the X-57 Mod II airplane. The P2006T refers to the fuel-based Tecnam P2006T light airplane, the X-57 Mod II refers to a current lithium-ion battery-electric airplane, and two technology levels for the hybrid-electric SOFC are labeled as: (1) the X-57-F airplane power system Design / Analysis Cycle (DAC) 2 (current technology); and (2) DAC 1 (near term future). For this study, only the NEF Vision System (2025) and near-term technology (2023) were investigated. Because the

current 2020 NEF technology has significantly lower-specific energy, the NEF technology was not considered. Additionally, the present results do not include any energy requirements for pumping the NEF, so the results shown in the figure for the NEF configurations are optimistic. In comparison with other solutions for the X-57 Mod II airplane, the projected NEF technology shows the ability to carry more payload, and NEF may have an advantage over current battery technology in range capability (bearing in mind the assumption of optimistic pump weights). The NEF, however, does not reach the range capability of the hybrid-electric SOFC X-57 Mod II airplane or the conventional fuel-based P2006T airplane (ref. 13).

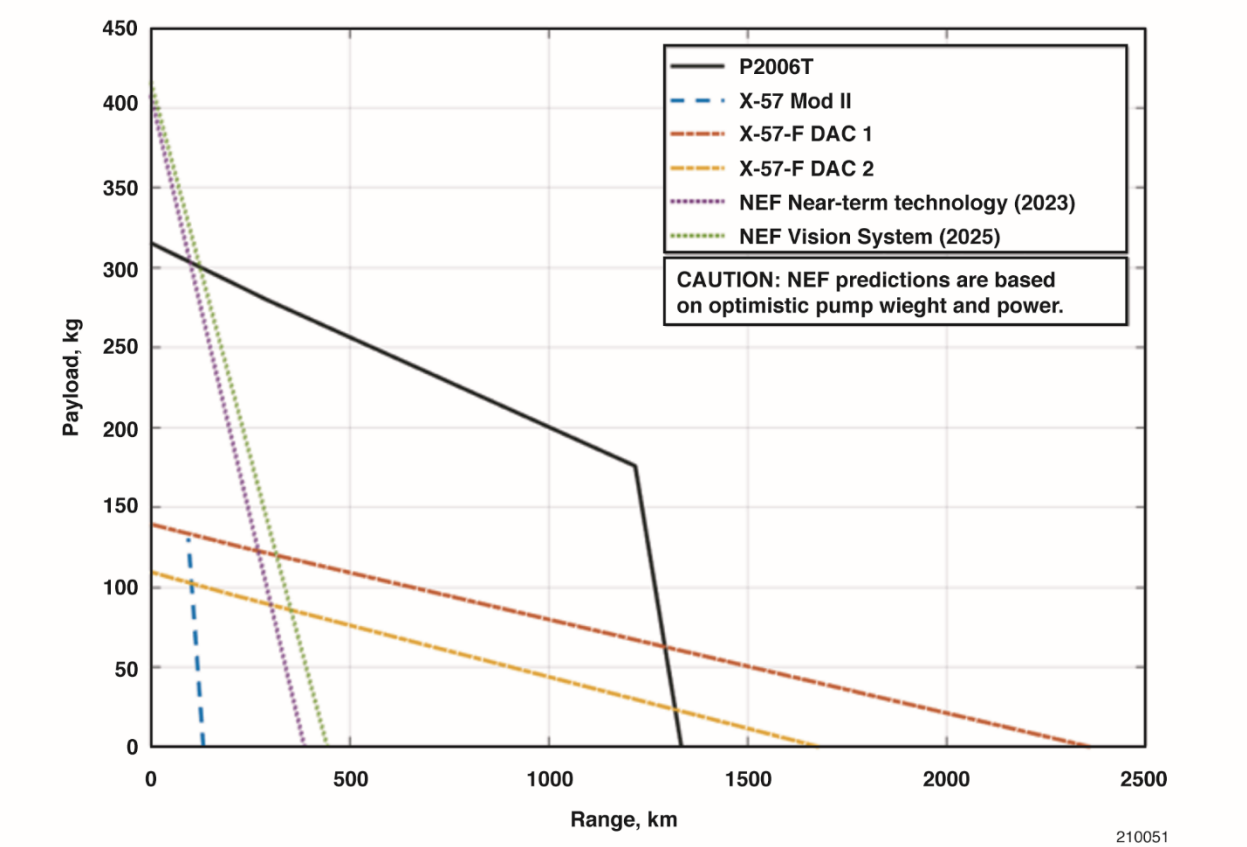

Figure 52. Payload-range plot results showing comparisons between different power technologies with nano-electro fuel, based on an optimistic pump weight and power assumption.

These initial results show that NEF may provide a competitive solution to existing battery technologies for aircraft, only if NEF pumping can be achieved without excessive power. Influit Energy did not optimize for those parasitic loses during their CAS efforts for GEN 1 development.

Rim-driven Motor / Rim-driven Fan Collaboration and Analysis

Design of the RDF blades were formulated as a multi-objective optimization problem of the fan performance at two thrust conditions: The first being 140 N at 50 kn and at sea-level for takeoff conditions; the second being 60 N at 200 kn and 5,000 ft for cruise conditions. A non-dominated sorting genetic algorithm (NSGA-II) (ref. 15), optimized with 3,000 population and 200 generations was used to find Pareto optimal solutions that minimized the power required at each thrust condition.

Design variables included: the blade chord and twist distributions; number of blades; inner-tip radius; and the RPM at each thrust condition. Outer-tip radius was already constrained by the 13.75-in inner diameter of the RDM. Chord and twist distributions were parameterized as non-uniform rational basis spline curves clamped at both ends. Each curve was controlled by three control points where (x_1, y_1) is the position of the i^{th} control point. Of the six coordinate values required to define the three control points for each distribution, two were fixed where x_1 was set to zero and x_3 was set to one. The remaining four values were design variables. The distributions were then scaled to lie between the inner-tip radius fraction r_{in}/R and one. Scaling to the inner radius separately allowed the bounds on the abscissae of the middle control points to remain independent of the other design variables: between zero and one instead of between r_{in}/R and one. Figure 53 shows an example of the chord- and twist-distribution parameterizations after scaling where the superscripts c and β differentiates between control points for chord and twist, respectively. The design variable bounds are given in table 20. Bounding values were chosen to give the optimization algorithm a wide design space to explore but were trimmed down in some cases to prevent unnecessary searching in fruitless regions. For example, the lower bound on y_3^c was increased to 0.25 because blades with narrow outer tips would likely fail in compression. Additionally, an odd number of blades n_{blades} were used due to acoustic considerations and in case the use of stators might be needed in the future. A constant Wortmann FX 60-126 airfoil cross-section was used (ref. 14 and 15); this airfoil was selected for its low-drag coefficient over the wide range of lift coefficients and was observed at local blade section points between the two thrust conditions.

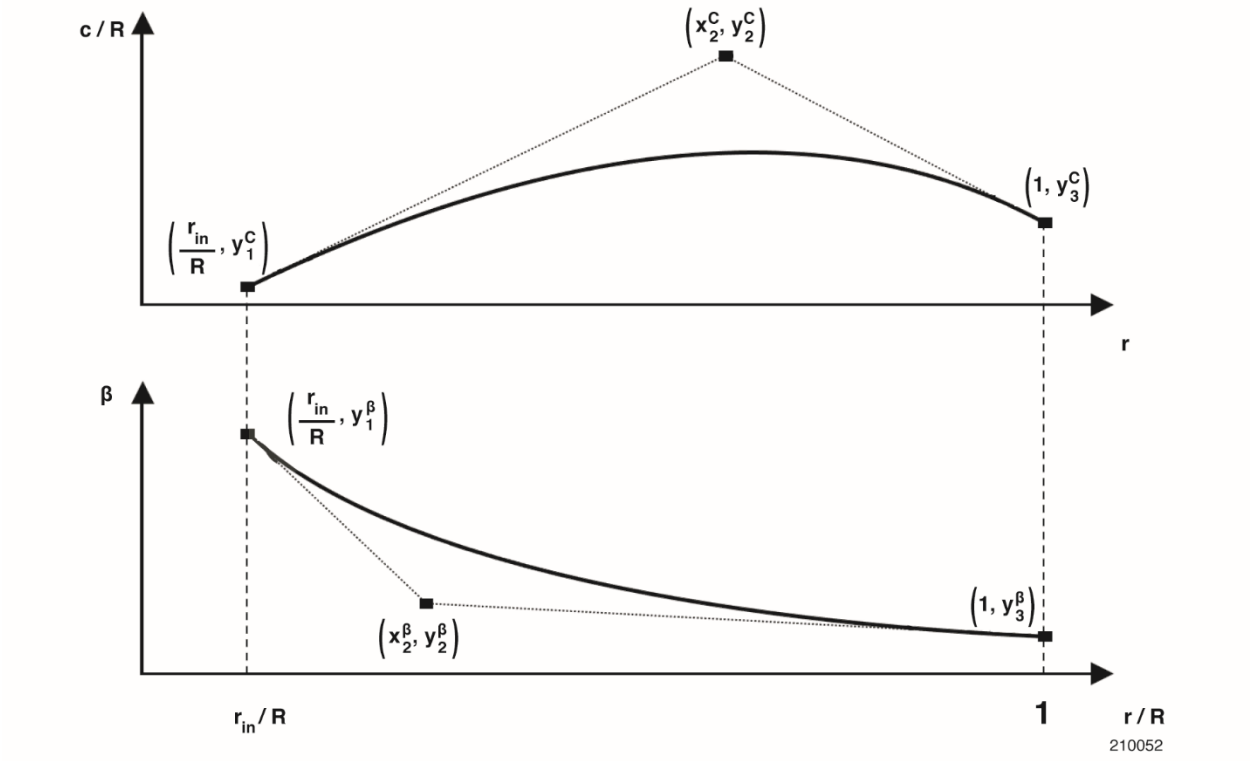

Figure 53. Notional chord and twist distributions.

Table 20. List of design variable bounds.

Design variable	Lower bound	Upper bound
r_{in}/R	.05	.75
x_2^c	0	1
y_1^c	.01	.4
y_2^c	.05	.6
y_3^c	.25	.6
x_2^β	0	1
y_1^β	20°	90°
y_2^β	0°	85°
y_3^β	0°	60°
n_{blades}	3	9
rpm_{cruise}	4000	15000
$rpm_{takeoff}$	2000	10000

Because of acoustic considerations, the design was constrained to have a maximum Mach number of 0.5 at takeoff; for structural considerations, the chord at the outer blade tip was not allowed to be the shortest from tip to root. Because preliminary studies showed that the optimization algorithm would occasionally find geometric designs containing a sudden flare in twist at the outer blade tip, twist distribution was constrained to monotonically decrease toward the outer tip. While it is possible that this family of exotic “flared” geometries could actually provide for aerodynamic improvements, it was thought to likely be an exploitation of the assumptions within the aerodynamic analysis that are not representative of the true physics. The investigation of these exotic geometries was considered beyond the scope of the project, hence twist constraints to more conventional distributions were accepted.

Aerodynamic analysis for the fan blade design was provided by open-source software XROTOR (ref. 16). It was believed that XROTOR would provide reasonable low-order performance predictions of a hubless ducted fan by enabling the ducted mode and setting the wake displacement radius to zero. The ducted mode, by default, outputs the thrust of the fan-duct system, but the thrust conditions described earlier applied only to the fan blades (any thrust from the duct was to be bookkept as airframe drag). The fan-only thrust was extracted by subtracting the duct thrust (Tnacel in the XROTOR output) from the total thrust. The XROTOR ducted mode precluded the use of vortex formulations. Of the two remaining solution formulations, graded momentum and potential, potential was selected for its wider range of valid operating conditions and blade geometries.

Figure 54 illustrates the general progression of the NSGA-II optimization algorithm in the output space with the 200 generations progressing from blue to orange (results shown are representative of the AQUIFER design). The black points represent the final generation of designs. The final blade design was chosen in the final design region on the Pareto front, visualized in figure 55. Because of the sharpness of the knee point, very little consideration was taken into account regarding the tradeoff between takeoff and cruise power.

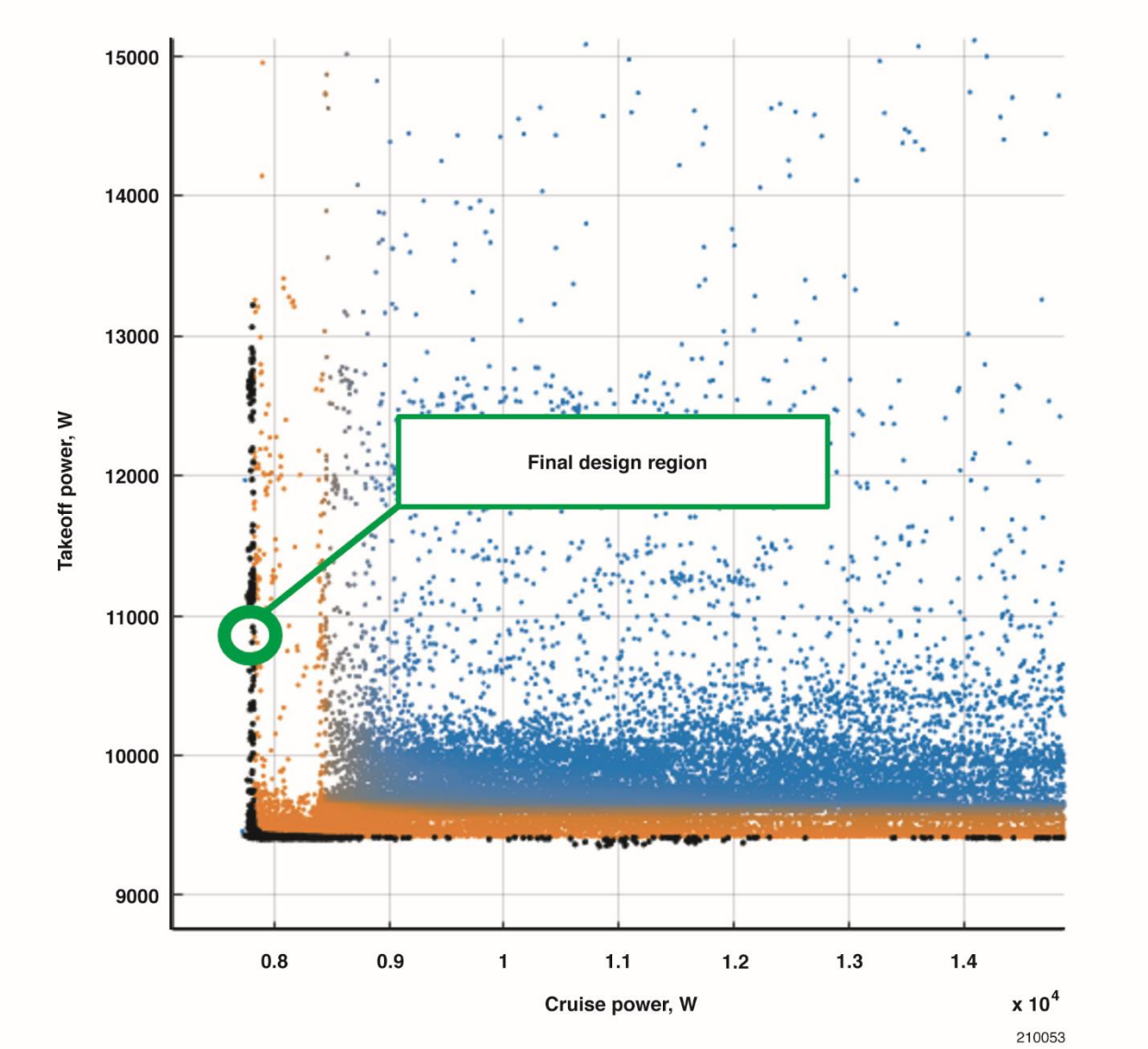

Figure 54. Example of NSGA-II optimization history for the Aqueous, QUick-charging battery Integration For Electric flight Research rim-driven motor / rim-driven fan takeoff and cruise requirements.

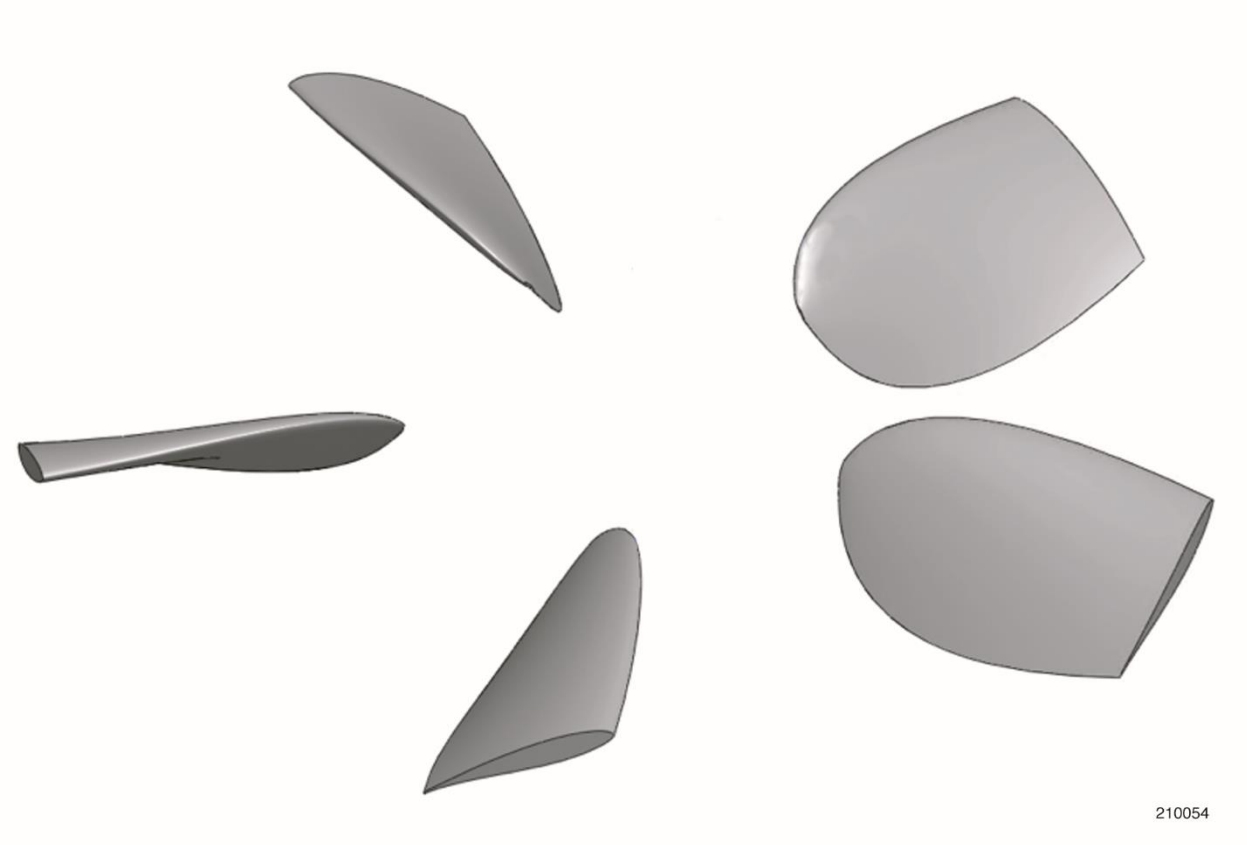

Figure 55. Visualization of the final fan blade design.

An RDF blade analysis was performed and included weight studies and strength analysis. The stress analysis was performed using the FEA software analysis tool Pro/ENGINEER (Pro/E) Mechanica (PTC Inc., Boston, Massachusetts). The analysis performed for load cases utilized 9,000 RPM and seven to 11 lb of thrust as input conditions. The materials considered were nylon/carbon, aluminum, and titanium. The nylon/carbon and aluminum model studies used a solid design. The titanium model used a hollowed blade with an isogrid footprint mount for weight savings. A brief representation of the work is shown in figure 56.

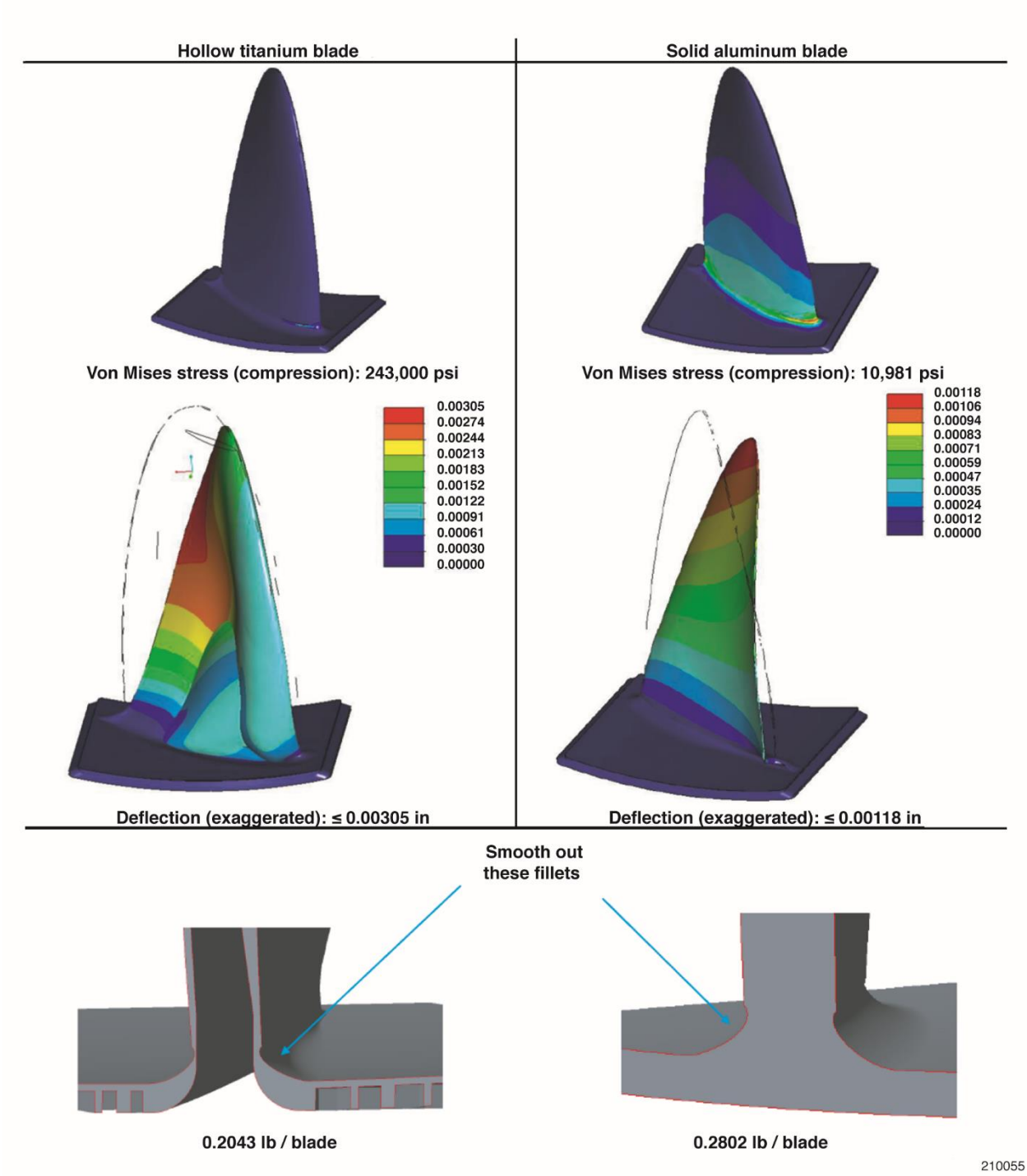

Figure 56. Rim-driven fan blade material and blade root design trade study.

Aqueous, Quick-charging battery Integration For Electric flight Research Rim-driven Motor / Rim-driven Fan Acoustics Predictions, Tools, and Testing Strategies

The AQUIFER project was planning a wind tunnel test using the NASA Langley Low Speed Aeroacoustic Wind Tunnel (LSAWT). The test was designed to capture the fan noise and motor noise so that the AQUIFER researchers could effectively isolate the fan acoustics in order to

properly assess the feasibility of the secondary objective relating to the RDM/RDF acoustics. Figure 57 shows various test fixtures and designs for the planned LSAWT test.

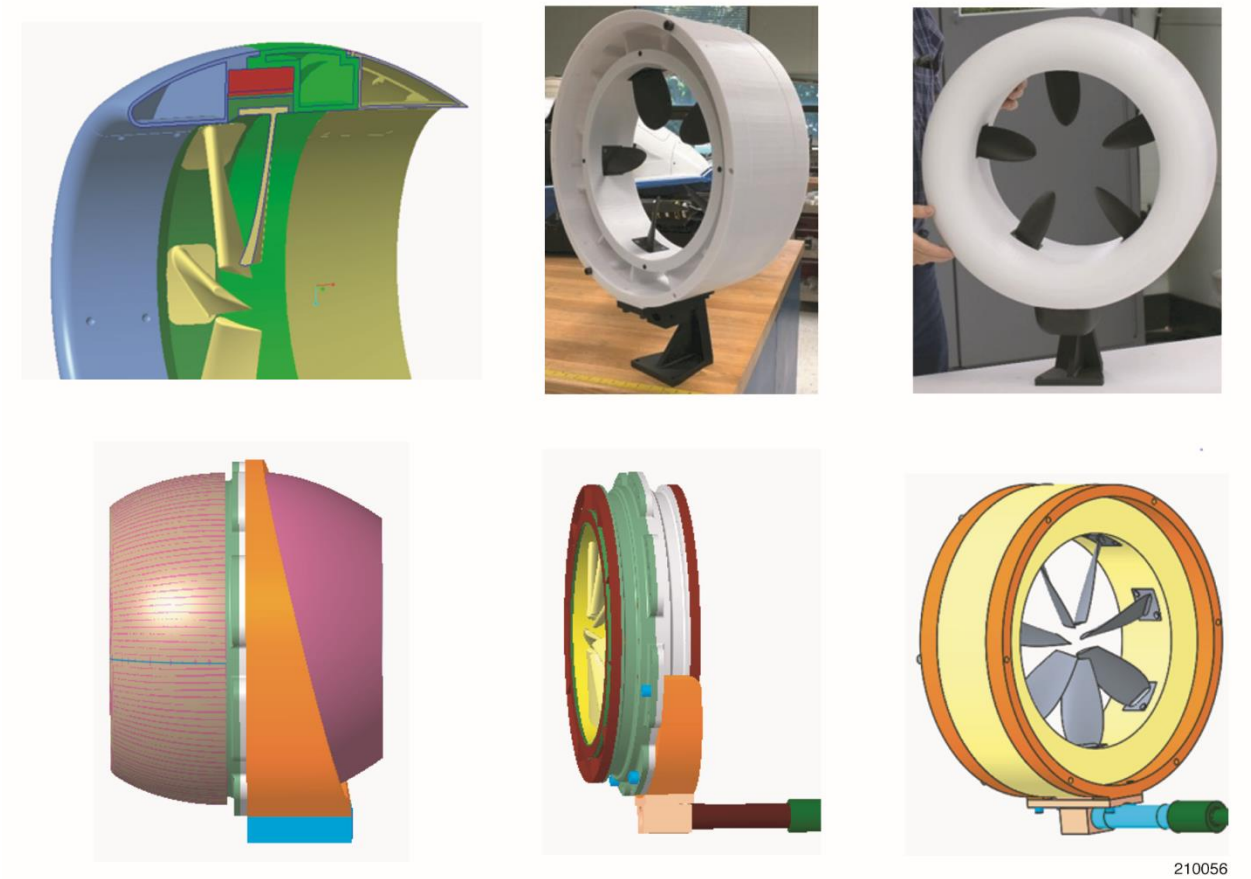

Figure 57. The Aqueous, QUick-charging battery Integration For Electric flight Research rim-driven motor / rim-driven fan design for Low Speed Aeroacoustic Wind Tunnel testing.

When the final motor frame and mounting points geometry was received, a mockup motor was developed along with mounting- and tunnel-support hardware. The motor and mounting hardware dimensions were provided to the duct designer so the baseline ducts could be completed. A minimal-sized duct was designed for initial tests in the tunnel. Several blade designs were received for seven- and five-blade configurations. The final design that was chosen was a five-blade configuration. The final design allowed the ability to replace a fan ring with another using a different blade count if needed. All mockup motor parts were 3-D printed along with mockup motor mounts and the balance adapter. The “minimum” duct design was also 3-D printed and fit to the motor assembly. The final blade geometry was received, and a complete set of spare blades were 3-D printed using carbon-infused nylon material. Work began on designing a 3-D printed metal version of the blade using titanium, but because of the early closeout of the AQUIFER study, the final motor and fans were not produced, and wind tunnel testing was not conducted.

Acoustic Assessment of Aqueous, Quick-charging battery Integration For Electric flight Research Rim-driven Fan Concept

Acoustic assessment of the AQUIFER RDF was divided into three primary phases: (1) acoustic prediction of a fan concept using low-fidelity aerodynamic and acoustic tools; (2) preliminary assessment of potential acoustic benefits offered by ducted liners on the RDF

assembly; and (3) Acoustic wind tunnel testing of the RDF and associated duct liner concepts for determination of validity or shortcomings of acoustic prediction methodologies.

Prediction Tools Utilized

Three acoustic prediction tools have been utilized in the assessment study. The first prediction tool is part of the NASA Aircraft Noise Prediction Program and is titled the Propeller Analysis System (PAS) (ref. 17). The PAS is a blade-element code for predicting the aerodynamic performance and noise of propellers. The PAS has been found to perform very well at predicting the periodic noise of propellers and rotors across a wide range of propeller sizes and operating conditions. It is important to note, however, that the applicability of PAS for modeling a bounded rotor (or fan) is unknown; therefore, the predictions conducted on the AQUIFER RDF are considered preliminary.

The second prediction tool is the Broadband Acoustic Rotor Codes (BARC) suite (ref. 18 and 19). These codes predict the self-noise generated by the fan blades via a blade-element analysis technique using rotor/propeller inflow conditions computed from a separate flow solver (PAS in the current case). The BARC specifically incorporates correlated airfoil boundary layer and noise data (ref. 20) into a rotational reference frame. The resulting outputs of the BARC are acoustic spectra in one-third octave bands, which can be added to the tonal levels predicted by PAS to yield a total blade noise prediction.

The third prediction tool considered is the CDUCT-LaRC (CDL) code (ref. 21). This code calculates the propagation of a given acoustic source ahead of the fan face or aft of the exhaust guide vanes (if present) in the inlet or exhaust ducts, respectively. In addition to the propagation calculations, the code can compute the noise radiation field outside the duct.

Performance and Acoustic Outputs

As mentioned in the previous section, PAS is a multifunctional set of codes that computes the pertinent propeller aerodynamic characteristics as well as the periodic acoustic content for a defined flight condition. The inflow conditions seen by the different blade sections are then input into BARC for a broadband noise prediction. The following section lists the prediction results of these tools in the form of propeller performance (thrust, power, efficiency) coefficients; characteristic blade passage frequency (BPF) acoustic directivities (in terms of SPL); and broadband noise content (SPL in one-third octave bands) for takeoff and cruise flight conditions.

Rim-driven Fan Aerodynamic and Acoustic Prediction Results

Table 21 documents the predicted aerodynamic forces of the five-bladed RDF using PAS; the calculations shown are for takeoff and cruise flight conditions.

Table 21. Aerodynamic performance of rim-driven fan at prescribed takeoff and cruise conditions.

Flight Condition	U_∞ (m/s)	Ω (RPM)	J	Thrust (N)	Power (kW)	C_T	C_P	η
Takeoff	25.72	6251	0.71	145.02	7.87	0.73	1.09	0.47
Cruise	102.90	9402	1.88	70.17	8.78	0.18	0.42	0.82

Note that comparison of these values with those predicted in figure 58 show some discrepancies in predicted thrust and power, particularly for the takeoff condition. These discrepancies are believed to be a result of the relatively high angles of attack experienced by the blade at this flight condition, compared to those for cruise. As a result, the computed aerodynamics can vary considerably between different low-fidelity codes (in this case, XROTOR

versus PAS). An illustration is provided in figure 59 which displays a comparison of the blade-element angles of attack computed by PAS for the different flight conditions and the zero-lift angle of attack ($\alpha_{C_l=0}$) of the Wortmann FX 60-126 airfoil (computed in PAS), of which the RDF blade is composed.

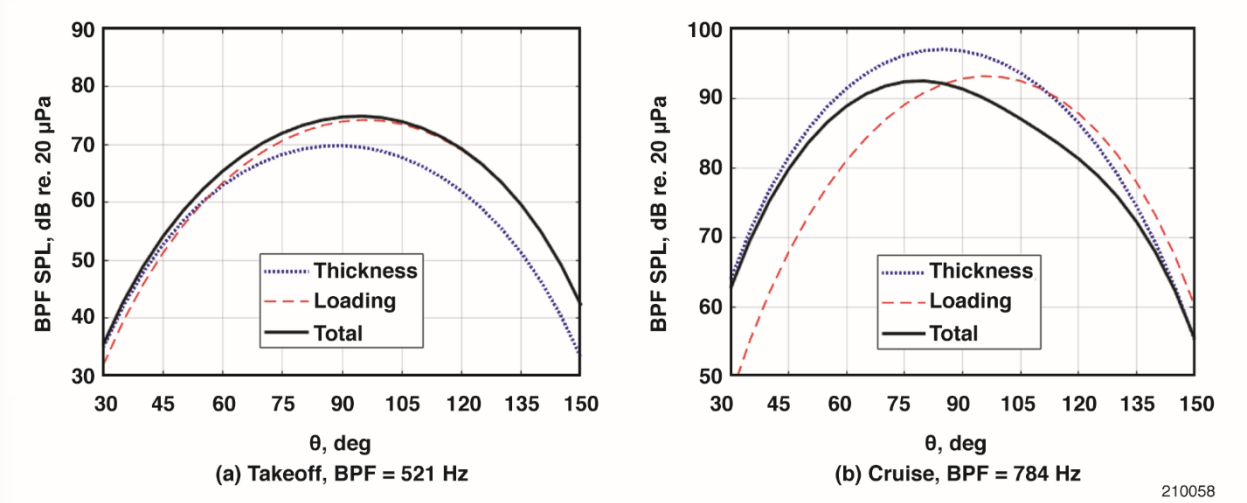

Figure 58. (a) Predicted blade passage frequency acoustic directivities of five-bladed rim-driven fan for takeoff; and (b) cruise flight conditions.

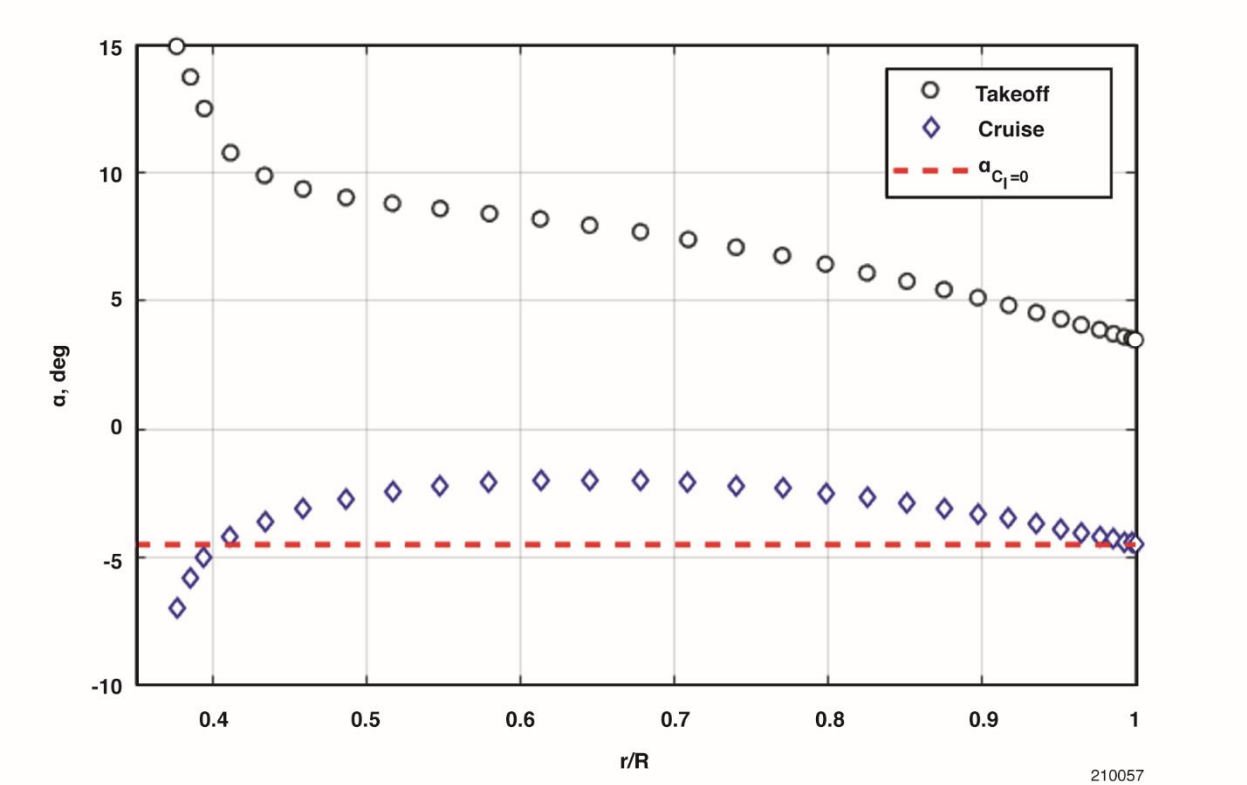

Figure 59. Blade element angles of attack computed in the Propeller Analysis System for rim-driven fan at takeoff and cruise flight conditions.

Rim-driven Fan Acoustics

Tonal-acoustic predictions are performed on the RDF for a line of observers oriented in the direction of flow, distanced 11.6 ft (3.54 m) from the fan axis of rotation. This line of observers is intended to represent the microphone positions within the NASA LSAWT. Figure 59 shows the PAS predictions of the BPF acoustic directivities for takeoff and cruise flight conditions. Note that $\theta = 90°$ represents the plane of the fan (in-plane measurement), with increasing observation angles in the downstream direction. The directivity plots are sub-divided into the thickness (monopole source term) and loading (dipole source term) noise components, the sum of which yield the total noise.

As seen previously in figure 58(a), the aft range of observer angles is dominated by loading noise and is attributed to the high thrust generated by the RDF for takeoff operation; conversely, figure 58(b) shows comparable levels of thickness and loading noise in this aft observer region for the cruise condition, resulting in a total noise directivity pattern that is less than the thickness and loading noise components in the respective forward and aft range of observer angles. Results are believed to be attributed to a combination of the relatively high blade count and twist angles of the RDF. It is worth noting that the noise at cruise conditions is considerably higher than that at takeoff because of the much higher fan tip speed ($M_{tip} = 0.51$ for cruise, $M_{tip} = 0.34$ for takeoff) required for the target thrust generation.

Blade self-noise predictions are computed using BARC at an in-plane location coinciding with the $\theta = 90°$ observer location; these codes are then summed with a one-third octave-band representation of the tonal noise components (shown previously in figure 58) yielding an overall RDF noise prediction. The results are shown in figure 60.

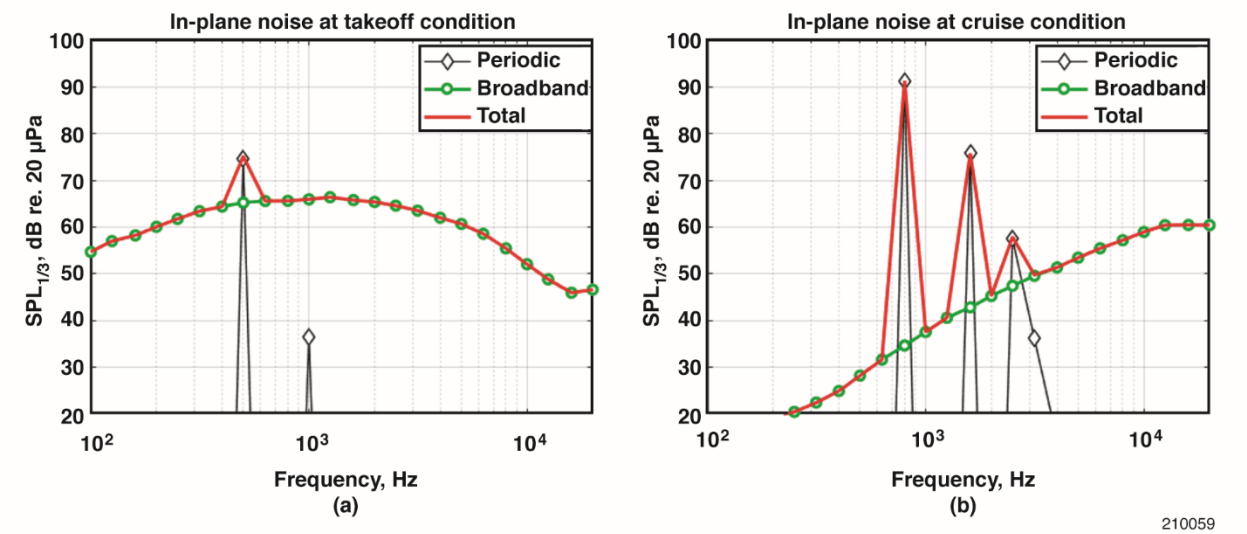

Figure 60(a) shows a primarily broadband spectrum with the BPF appearing at the 500-Hz band approximately 10 dB above the broadband level. The secondary BPF harmonic (1,042 Hz) is considerably lower than both the BPF itself and the broadband spectral levels. Figure 58 shows this broadband-dominant spectrum is a result of the high angles of attack experienced by the RDF blades during takeoff, resulting in thicker trailing-edge boundary layers and higher levels of self-noise as a result of trailing-edge boundary layer separation; meanwhile, figure 60(b) reveals a primarily tonal spectrum composed of the BPF second and third harmonics with broadband levels only becoming prominent at higher frequencies. Again, the increased tonal content is a result of the higher fan tip speed at cruise conditions as compared to that at takeoff; while the reduced broadband noise is a result of the more moderate angles of attack encountered by the blade.

RDF Duct Liner Concepts

Possible candidates for implementation of acoustic liner concepts include the internal flow surfaces of the inlet and outlet portions of the duct. Figure 61 provides an illustration of a preliminary RDF duct concept with inlet and outlet flow regions appropriately annotated. Note that the pertinent geometric parameters are indicated as the fan diameter D, as well as the inlet and outlet duct lengths, L_{inlet} and L_{outlet}.

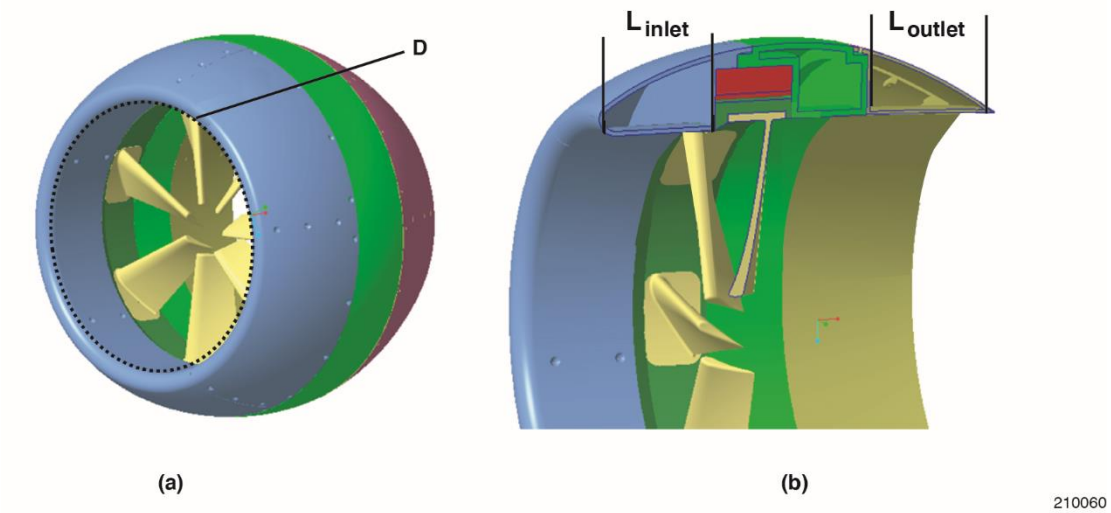

Figure 61. (a) Illustrations of preliminary rim-driven fan duct concept: overall assembly; and (b) cut-away view of interior duct areas.

Initial Acoustic Treatment Estimates

Initial estimates of acoustic treatment benefits were obtained based on a constant area duct with a fan diameter D of 14 inches. For acoustic treatment of axial extent (L), predicted attenuation of the least attenuated radial mode at various circumferential mode numbers (m) as a function of length over diameter $\left({}^{L}/_{D}\right)$ are shown in figure 62.

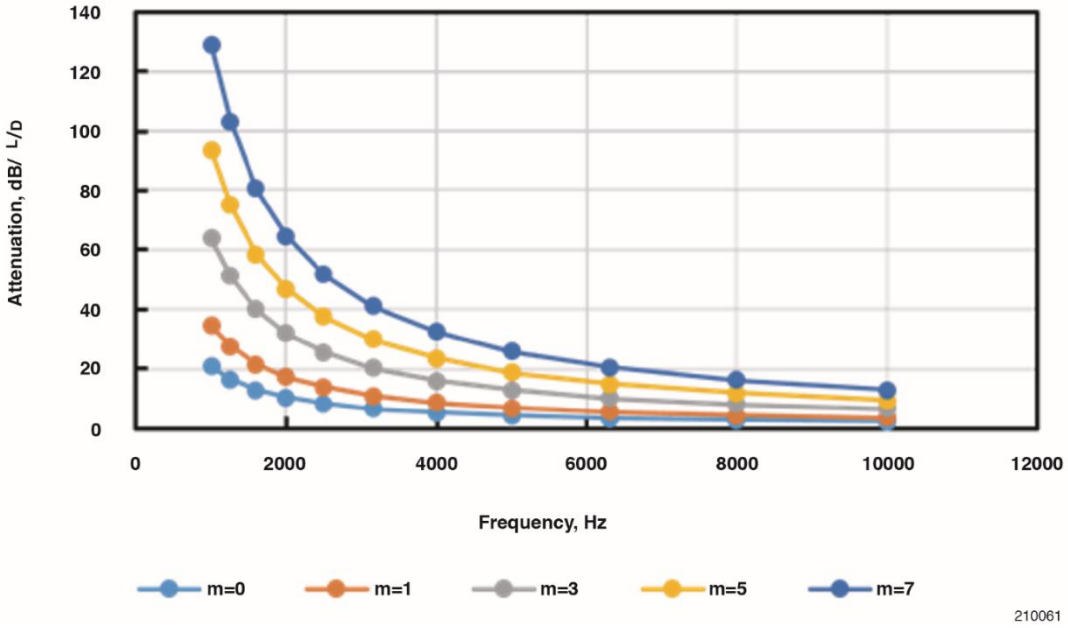

Figure 62. In-duct attenuation for various circumferential modes (m) at a nominal takeoff condition.

The predicted optimum impedances associated with the aforementioned attenuation predictions at the takeoff and cruise conditions are provided and shown in figure 63 and figure 64.

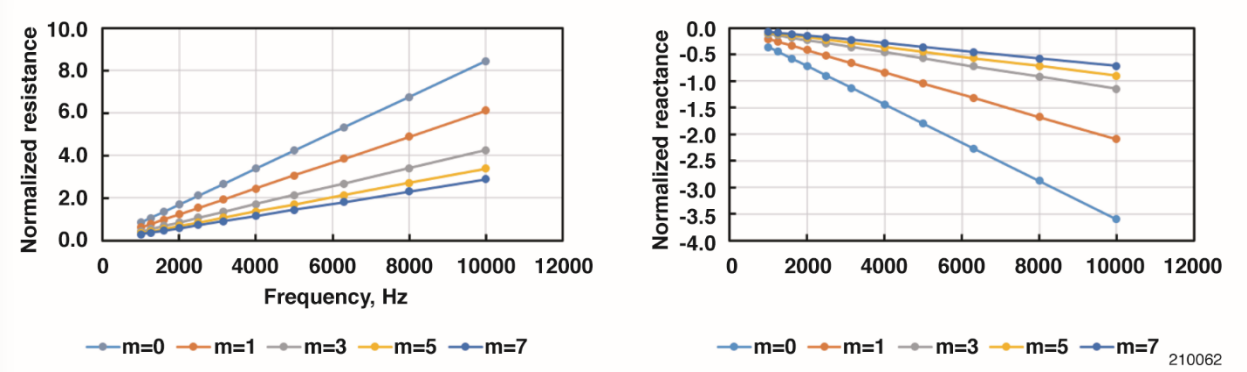

Figure 63. Predicted optimum impedance for various circumferential mode numbers (takeoff conditions).

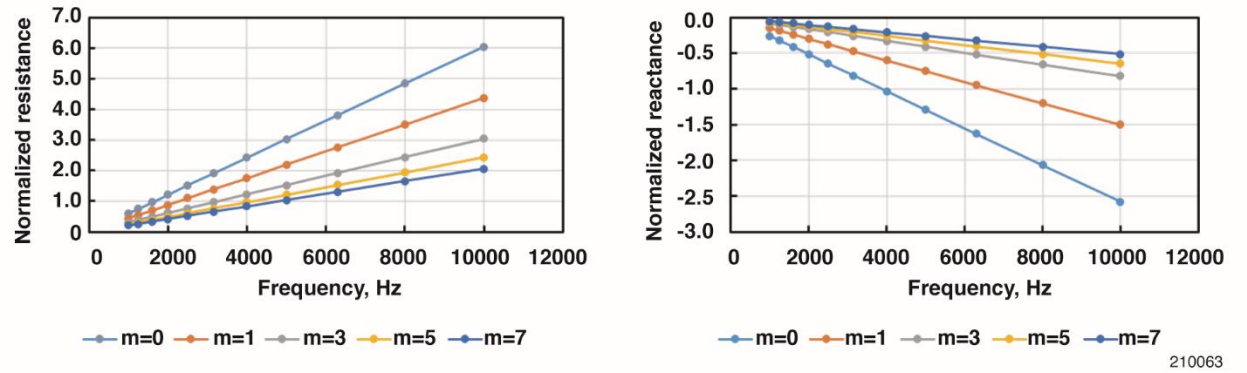

Figure 64. Predicted optimum impedance for various circumferential mode numbers (cruise conditions).

Predicted optimum impedances are generally difficult to achieve over a full frequency range. A number of novel liner configurations, however, have recently been developed that provide greater design flexibility and increased broadband attenuation. Examples of two degrees of freedom (2 DOF) and multiple degrees of freedom (MDOF) designs are shown in figure 65 where h1 represents the height of the treatment above the cowling.

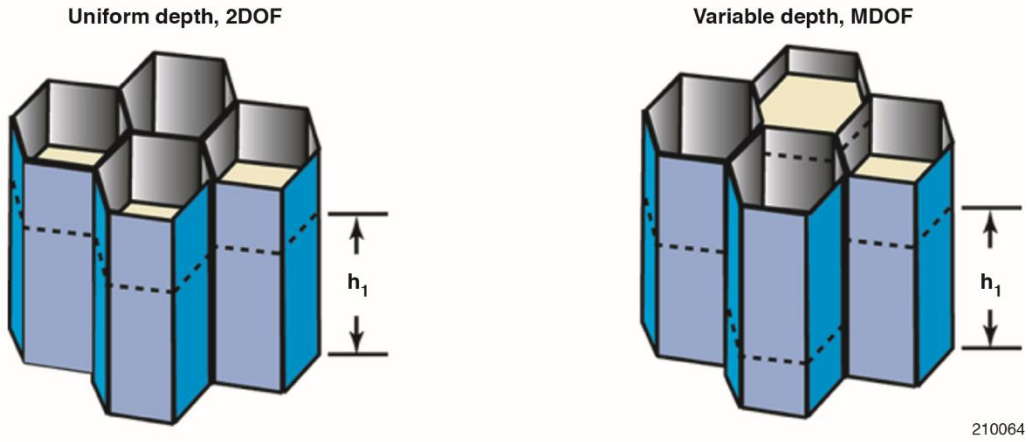

Figure 65. Example liner core designs to achieve broadband attenuation.

Given a nacelle design, higher fidelity in-duct and far-field predictions may be performed using the CDL code (ref. 22). This code calculates the propagation of a given acoustic source ahead of the fan face or aft of the exhaust guide vanes (if present) in the inlet or exhaust ducts, respectively. Subsequent to the propagation calculations, the code can compute the noise radiation field outside the duct. The 3-D duct, modeled using CDL, may include acoustic treatment (possibly circumferentially and radially segmented) and incorporate struts/bifurcations.

If nacelle geometry was available, predictions could be performed to optimize linear treatment based on physical constraints. For example, in-duct attenuation is used in determining the objective function (M, f) for optimization where M and f are the Mach number and frequency, respectively. The in-duct attenuation A_{in} at a given flow condition and frequency is computed in equation (2);

$$A_{in} = SPL_s - SPL_t \tag{2}$$

where SPL_s and SPL_t refer to the sound pressure level (dB) at the source and termination, respectively. Propagation predictions are performed across the frequency range and flow conditions of interest from which in-duct attenuation values are determined. Each of these levels are converted to a corresponding root mean square pressure, as shown in equation (3):

$$\Delta P = (20 \text{ x } 10^{-6}) 10^{A_{in}/20} \tag{3}$$

Finally, the sum of the squares of these values is used as the objective function to be minimized, as shown in equation (4):

$$F(M, f) = \left\{ \sum_{i=1}^{m} \sum_{j=1}^{n} W_{i,j} \Delta P\left(M_i, f_j\right)^2 \right\} \tag{4}$$

The double summation is used to allow consideration of multiple flight conditions over a range of frequencies. For example, $m = 3$ would be used to account for the three certification conditions (approach, cutback, and takeoff) and $n = 7$ would be used to cover the one-third octave band center frequencies from 1,000 to 4,000 Hz. Various flight conditions and frequencies may require increased weighting as well by using variable weighting values $(W_{i,j})$. These predictions could subsequently be radiated to the far-field region to estimate community noise impacts. A nacelle design was not finalized, and necessary input was not available to perform such calculations.

Aqueous, Quick-charging battery Integration For Electric flight Research Concept Feasibility Assessment

The following tables show the assessment of the feasibility study, pertinent details, and pathways forward. Table 22 shows the primary objectives of the feasibility assessment, per the AQUIFER MCR. The first objective was to demonstrate inflammability / non-explosivity. For feasibility, this design benefit was determined using the NASA system safety analysis process. The second objective was related to the NEF current density performance. Throughout the duration of the project, the NEF current density has steadily improved, starting with 2 mA/cm^2 in a NEF cell and attaining an 85 mA/cm^2 of the 100-mA/cm^2 goal in a NEF cell within two years. The third and final primary objective was the integration of the NEF/RDM performance, which was designed but not constructed or tested.

Table 22. The Aqueous, QUick-charging battery Integration For Electric flight Research primary objectives and feasibility assessment.

Primary Objectives (per MCR)	Details	Path Forward
Demonstrate no spark/fire/explosion when mixing anode/cathode	• NEF has overcharging gas evolution concerns associated with charging (likelihood: improbable) • NEF anode/cathode have been mixed in small quantities	• No future work planned
Demonstrate competitive battery performance (100 mA/cm^2)	• NEF demonstrated discharge: 85 mA/cm^2 for 1 min (NEF flow cell). 200 mA/cm^2 for 1 min (rotating current collector) • NEF demonstrated charge: 30-41 mA/cm^2 for 120 min	• NEF flow cell development, designing and building electrified aircraft charging station demonstrator
Demonstrate integrated NEF and RDM system	• NEF stacks for the Wing Demonstrator need 50- to 70-mA/cm^2 cell-level and approximately 20-mA/cm^2 stack-level discharge for motor operation • Maximum motor speed approximately 400 RPM	• No future work planned

The secondary objectives of the AQUIFER feasibility assessment are shown in table 23; these objectives related to the RDM performance, acoustic predictions, fan blade development, buildup of the Wing Demonstrator, and project transition beyond CAS.

Table 23. The Aqueous, QUick-charging battery Integration For Electric flight Research secondary objectives and feasibility assessment.

Secondary Objectives (per MCR)	Details	Path Forward
Demonstrate RDM capable of eSSTOL operation	• Current state-of-the-art 14-in bearings cannot be certified over 1,000 RPM, seeking 9,000-RPM operation • Air bearings are envisioned to have 9,000+ RPM capability and improved acoustics	• RDM concept has no future unless integration of air bearings or magnetic bearings
Characterize RDM/ RDF acoustics performance	• Current bearing capability substantially limits usefulness of acoustics test at LaRC • Acoustics testing being planned and ready to accept test article (pending survivability)	• Dynamometer and wind tunnel testing will need to be conducted
Complete RDF blade development	• NASA design delivered to motor manufacturer and is being fabricated • Fan ring design allows for different blades	• Acoustics testing will need to be conducted
Complete aircraft mock Wing Demonstrator with two NEF-powered RDMs	• Wing Demonstrator design progressing • NEF stacks for Wing Demonstrator need approximately 20-mA/cm^2 stack-level discharge for motor operation • Maximum motor speed approximately 400 RPM	• No future work planned

Design Considerations for Nano-electro Fuel-Powered Aircraft Operations

The target configurations of the AQUIFER project are SSTOL and conventional takeoff and landing (CTOL). These configurations support near-term support of Urban Air Mobility (UAM), providing an urban range service at a lower cost without addressing the many hurdles of the full UAM concept. These technologies are currently being developed and the topics in this section are related to general aircraft technology in the AQUIFER project.

In general, powered aircraft operations identify instructions, procedures, guidance, and references to clarify the way in which an aircraft is to be maintained, modified, and inspected (ref. 22). Some topics that have been identified require iterative evaluation and will be mission- or configuration-dependent. Powered aircraft operations that require specific consideration as a result of NEF technology include the following: weight and balance, emergency procedures, accident-incident procedures, maintenance, aircraft servicing procedures, hazardous materials, and the flight-safety program. Early subsystem design and system integration with respect to maintenance are also identified as part of component failure rates that could affect reliability.

Weight and Balance

Weight and balance - a basic aircraft operation constraint - was addressed in a NEF aircraft and evaluated because of the expected movement of NEF from one tank to another (from “used” to “depleted” NEF tanks). Nano-electro fuel fluids are not consumable, thus it was assumed that each of the anode and cathode fluids would need to be moved from an energy-rich tank to a depleted-energy tank, using at least two, and potentially four, separate fuel tanks or a pair of two-compartment tanks separated by a flexible piston or bladder. The design is expected to have two separate tanks (one for the anode and one for the cathode) that will recirculate each NEF fluid separately or two tanks with moveable bladders, separating the new and used fluid. The current design eliminates the NEF-driven weight and balance considerations and, if implemented in the final design, is expected to improve weight and balance considerations over the entire flight envelope.

Emergency Egress

Egress procedures would likely be complex given a vehicle configuration with many motors in various quadrants (or zones) of the passenger compartment. Similarly, in the event of an emergency, emergency response considerations for first responders could be problematic given the large number of small motors. If significant noise reduction for the propulsors is realized, the motors would be more difficult to hear during an emergency situation. Other considerations would be canopy or door removal, ground procedures, and in-flight procedures for the crew and passengers, but these considerations apply to any ZEST vehicle, whether powered by a NEF system or by conventional batteries.

Accident, Incident, and Mishap Response

A mishap response plan describes procedures to minimize risk to emergency responders, presents crew and passenger rescue procedures, and sets forth relevant material or chemical handling considerations to be applied in the event of a mishap. The expected AQUIFER configuration will have twelve or more low-powered ducted fans that surround the entire vehicle and are expected to have their own integrated power sources. Once the final aircraft configuration is identified, processes will need to be defined toward crew and passenger rescue in the event of a mishap; these processes should include: instructions regarding safing all of the power sources; restrictions regarding contact with the fuel sources; and procedures for extracting anyone onboard the aircraft who is unable to move or is otherwise incapacitated. If the fuel is considered hazardous to the environment, liquid spill clean-up procedures will need to be developed.

Maintenance: Early Subsystem Design and Integration

Early subsystem design and integration often reveals many components that increase the possibility of subsystem failures. These subsystem failure rates complicate the support of future operations. Some of the NEF stack components that are likely to fail are the pumps and the

membrane between the anode and cathode. Additionally, there are many O-rings between chambers of the NEF stack. Any of these components could be sources for NEF fluid leaks. As a potential noise source, bearings are of critical concern for the RDM and are a focus of critical development. It is anticipated that several iterations will simplify the design and greatly reduce the number of components or eliminate areas where these potential failures have been identified during early development.

Aircraft Servicing

Aircraft servicing procedures in this section include fueling, defueling, and recharging methods. The processes for these topics would need to be modified or altered as compared to current processes.

Fueling and defueling

Current processes for fueling addresses efficiency, safety, and reduction of contamination or static electricity. The fueling process for NEF will need to be evaluated carefully. Consistent use of NEF would normalize the NEF defueling process, as compared to conventional aircraft configurations, currently available today. Jet fuels and petroleum-based fuels are consumable and generally defueled for specific reasons such as maintenance or storage, whereas NEF would be removed as a matter of course for recharging.

Two types of fueling are typical for aircraft. The first type uses a single-point method (large aircraft generally use a single-point method), most small aircraft use an over-the-wing method. The single-point fueling method is straightforward, but infrastructure alterations would need to be made. Precautions would need to be put in place to ensure neither jet nor aviation fuel could be put into a NEF-configured aircraft. Additionally, if two GEN 1 separated fuels were used, precautions would need to be in place to ensure these fuels were neither mixed nor added to the wrong tank. The effects of mixing NEFs are currently unknown and mixing fuels could result in any number of adverse consequences. Defueling processes are generally accomplished using either gravity- or pump-fed systems; these processes for NEF would, of course, need to be performed safely. GEN 2 is planned to use one fluid and would be much simpler to implement logistically.

Another consideration that was not addressed during this study is the concept of mixed NEF fluids, based on estimated number of cycles the fluid has undergone. Mixing new NEF fluid with NEF fluid that has undergone several hundred charges might have deleterious effects on NEF performance.

Recharging

The NEFs are expected to have significantly different characteristics than those of jet or aviation fuels. Special considerations will need to be understood for the NEFs regarding ratios, pressurization, vaporization, contamination, freezing, and evaporation.

Because NEF batteries are fundamentally different from most batteries and other fuel cell technologies, there are entirely new concerns regarding the recharging of the NEF. It is envisioned that most of the recharging would be accomplished through green energy resources such as wind turbines, solar panels, or hydroelectric generation. The recharging infrastructure could be onsite, or the NEF could be transported “trucked” to and from offsite recharging facilities. In the early development phase it is expected that there will be one recharging facility to service the demonstration aircraft; specialized recharging equipment will need to be incrementally developed into a production-type process and facility. Overall, recharging is expected to be a simple process that is software-controlled to avoid electrolysis (hydrogen production).

Movement of the anode and cathode for recharging could be logistically challenging, depending on the requirements of the system at hand. It is expected that the transportation vehicle traveling to and from the aircraft and the recharging stations could be a fuel truck, similar to aviation fuel trucks in use today. The GEN 1 NEF trucks would need two tanks: one tank to be used for defueling the aircraft and one for refueling; one truck with two separate tanks, or one truck for each anode or cathode, could be utilized. The same expectations apply to the GEN 2 NEF trucks; the GEN 2 NEF trucks would need to have either one truck with two tanks or one truck for each process of fueling and defueling.

Recharging methods

The project has not yet addressed some of the topics that must be investigated further, such as electrical connection requirements for electrified aircraft (standards or certification) and charging keep-out zones. Both project topics would be critical to the design and operation of the aircraft.

An important concern regarding NEF will be reducing the degradation of the battery anode and cathode fluid and chemistry components. There are several factors that accelerate degradation of Li-ion batteries such as high current rate, over-voltage (overcharge), and under-voltage; thus, it is important to consider the charging methods that will be utilized for NEF. Internal resistance is one of the most important indicators of degradation of a battery, but the particulars of this aspect will remain unknown until flight-ready batteries have been developed. Additionally, specialized storage tanks and procedures would be required and would likely influence the degradation of these fluid compounds.

Another potential obstacle concerns the amount of available green-source energy and NEF recharging time versus use time. The available energy from green sources is not expected to be a factor early in demonstration, but if the technology becomes viable, the energy production and charge-use-recharge support infrastructure could be primary limitations. Recharging power could also be capped by the power limitations to charging cables, charging stations, and vehicles. The total charge capacity of all the utilized batteries is another important parameter to be investigated. Similar to the fuel capacity, it is important to choose the battery capacity relative to the mission. Technology limitations associated with battery capacity, however, will most likely be the limiting factor for mission capability.

Hazardous Materials Handling and Training

It is possible that the NEF solid particles would be regarded as hazardous chemicals and would be required to be handled and stored in compliance with specific hazardous materials rules and procedures.

Generally, nanomaterials are known to potentially pose health risks (ref. 23); thus, during development and testing great care should be taken to reduce or eliminate human exposure to experimental nanomaterials. Once the pertinent parameters have been established, studies should be conducted to evaluate and fully understand any potential health hazards.

Flight Safety and Hazards

The topic of flight safety is a very broad one, covering a wide range of material and operations. The topics discussed in this section are safety and hazard elimination and are restricted to NEF RDM technologies. Additionally, these transportation systems might be piloted, autonomous, or remotely piloted, further complicating an already labyrinthine topic. A NEF-specific hazard analysis is shown in both figure 66 and figure 67. Figure 66 shows the AQUIFER hazard report (HR) for hazardous release of NEF fuel (HR-01); figure 67 shows the AQUIFER hazard report for gaseous H_2 and/or O_2 release as a result of exceeding the nominal operating conditions of the NEF battery (HR-12).

Nano-electro fuel is expected to have a relatively-high energy density. Some regulations restrict electrical power and battery charging near general aircraft and hangars, requiring charging stations to be attended at all times with charging activities restricted without waivers or strict oversight in place. In addition, some regulations specify that electrical connections must be a distance of at least 18 inches above the floor when other flammable-fueled aircraft are in the vicinity. Special consideration must be implemented with subsystem integration of the motor and the NEF so that each unit is de-energized prior to (location of motors) maintenance.

An Airbus Zephyr (Airbus SE, Leiden, Netherlands) battery (ref. 24) with silicon nanowire anode and an energy density of 435 Wh/kg was identified as a similar technology. Although NEF is not considered at this time to be a fire danger, the Zephyr program found that the energy density at the cell level creates the challenge of how to prevent a fire if a short-circuit releases that energy. The NEF manufacturers will need to understand whether the higher energy density of the NEF has the same or similar characteristics.

The thermal dissipation behavior of the NEF batteries must be understood in order to ensure a safe operational environment. Knowledge of the effective dissipation of the generated heat during operation of batteries as well as storage temperatures, is critical to ensuring the life, performance, and the avoidance of catastrophic failures of the batteries. Thermal management of battery packs for high-power applications has received significant attention over the past decade in both academia and the industry. Studies (ref. 22) have investigated different battery heat acquisition system (BHAS) approaches at different levels, from individual cells to packaged-battery power systems. During initial testing, fully charged anode and cathode fluid were mixed and the thermal behavior was monitored. The results were minimal increases in temperature, in the order of single-digit degree Celsius. Confidence is high that a NEF mixing event would not lead to an explosive hazard, but further testing would be needed to validate that claim.

The mixing of the cathode and the anode in discharged and charged form is a possibility. In discharged form it is expected that if the cathode and anode nanofluids were mixed there would be very little or no reaction between the nanoparticles. In charged form, if cathode and anode nanofluids were in contact but not mixed, a redox reaction (a transfer of electrons) between nanoparticles is possible. For an electron and ion exchange to occur, the redox reaction requires physical contact of the separate nanoparticles with the electrolyte. This fluid-contact redox reaction would be expected to release stored electrochemical energy in the form of heat. In an instance where mixing occurs in a spill, the release of stored electrochemical energy in the form of heat would be amplified and expected. Nevertheless, once all the water from the electrolyte had evaporated, the redox reaction would be expected to end. In nanofluids having a higher concentration of nanoparticles the electrolyte will evaporate faster, limiting the redox reaction between the nanoparticles; therefore, limiting thermal effects in case of a spill. Hazards inherent to the presence of nanoparticles and alkaline electrolyte, of course, exist.

Hazard Analysis Process

Safety is a primary concern in all aspects of a program. This section specifies some of the hazards that have been identified. Each hazard is built from a scenario-based hazard description. This description is then used to identify causes, effects, and mitigations. Although not included in the examples below, the nominal process would be to construct a hazard action matrix for associated risk to human, asset, or mission which would then be evaluated; a final hazard category justification could then be composed to complete the analysis. The NASA system safety analysis process was used for both technology hazards shown in figure 66 and figure 67. These items together are used to make decisions about the risk and mitigation of the risk. Early identifications of these hazards are intended to inform project members. The project members can then use these informationally identified hazards to proactively implement actions or changes to reduce or eliminate causes, effects, or the overall hazard itself.

Preliminary hazard analysis of the AQUIFER identified the annular NEF battery stacks and the RDMs as possible hazards. Some of the hazards along with a summary of these hazards are identified and provided below and include the hazardous release of NEF as well as gaseous hydrogen H_2 or oxygen O_2 release as a result of exceeding nominal operating conditions of the NEF battery. Additionally, the NEF hazard analysis, relating to charging and discharging operations, are shown below (see HR-01 in figure 66 and HR-12 in figure 67). This analysis was the primary rationale for the statements regarding inflammability and non-explosivity and the general safety posture for the NEF technology.

Hazard 1: Hazardous Release of Nano-electro Fuel

The AQUIFER system contains two annular NEF battery stacks. The NEF fluids (anode and cathode) are to be delivered to the NEF stack by a network of tanks, tubing, manifolds, and pumps. During operation, a failure of NEF system components or seals, system interface components, NEF refueling, or transportation operation anomalies could result in leakage of NEF onto surrounding components, resulting in material degradation or corrosion, or injury to personnel. The causes and effects are listed in table 24.

Table 24. Hazardous release of nano-electro fuel.

Causes	Effects
System leaks (NEF)	Contamination of test area
Refueling operation anomaly (NEF spill) Note: includes transportation of NEF	Thermal reaction as a result of the mixing of the NEF fluids
Component failure (NEF spray)	Hazardous gas evolution
System design deficiency	Material degradation or corrosion
Improper assembly (mechanical or electrical)	Damage to “Center” assets; injury to personnel

Some mitigations include a drip tray, refueling procedures, briefing personnel on all associated hazards, utilizing required personal protective equipment, protective shielding, emergency stops, and subsystem leak tests. Furthermore, complications with the NEF stack such as leakage could compromise the performance of the RDM, possibly causing a structural failure to any of the motor components or the interface mounting structure.

HR-01: Hazardous Release of NEF Fuel

Scenario Based Hazard Description:

The AQUIFER Wing Demonstrator (Wing Demo) contains two annular Nano-Electro Fuel (NEF) battery stacks. The NEF fluids (anode and cathode) are delivered to the NEF stack by a network of tanks, tubing, manifolds, and pumps. During operation, a failure of NEF system components or seals, system interface components, or NEF fuel refueling/transportation operation anomalies could result in leakage of NEF fuel onto surrounding Wing Demo components, resulting in material degradation or corrosion and/or injury to personnel.

Causes	Effects	Mitigations
A. System leaks (NEF dripping/seepage) B. Refueling operation anomaly (NEF spill) Note: Includes transportation of NEF fuel. C. Component failure (NEF spray) D. System design deficiency E. Improper assembly (mechanical/electrical)	E1. Contamination of test area E2. Thermal reaction due to mixing of the NEF fluids E3. Hazardous gas evolution E4. Material degradation/corrosion E5. Damage to Center Assets E6. Injury to personnel	1. Drip tray (Capable of total fuel volume containment) (E1, E4, E6) 2. Refueling procedure (B) 3. Procedure review (A, B, C, E) 4. Test personnel shall be briefed on all associated hazards, and required PPE before testing (E6) 5. Protective shielding (E1, E4, E6) 6. Ensure all test personnel and/or non-projects assets are outside of the established keep out zone prior to system startup until power has been removed (E1, E4, E6) 7. Design review (Wing demo ICD review) (D) 8. E-stop (E1, E2, E4, E6) 9. Subsystem leak testing to be performed (A, C, D, E) 10. Assembly procedure (E) 11. NEF spill kit (E1, E4, E5, E6)

AFRC Hazard Action Matrices

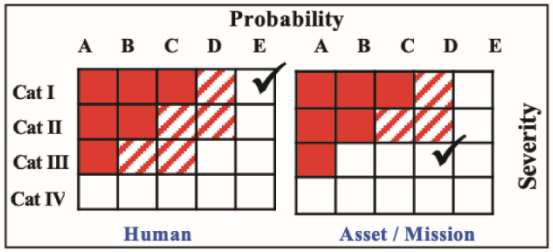

Final Hazard Category Justification Statements

Final Severity Justification

Personnel: In the event of a release of NEF fuel that breaches the physical barriers and comes in contact with personnel, catastrophic injury is credible.

Asset: In the event of a release of NEF fuel that breaches the physical barriers and comes in contact with Center assets, repair and/or clean-up costs could exceed 50K.

Final Probability Justification

Personnel:

Asset:

Rev. 07-30-2019

210065

Figure 66. The Aqueous, QUick-charging battery Integration For Electric flight Research hazard report for hazardous release of nano-electro fuel (HR-01).

Hazard 2: Gaseous H_2 or O_2 release as a result of exceeding nominal operating conditions of the NEF battery

The AQUIFER wing will contain annular NEF battery stacks. During operation, the NEF fluid will be pumped through the stacks. During normal operation, the NEF system will be operated within a nominal voltage window. Exceeding the window voltages can result in the evolution of hydrogen (during charge) or oxygen gas. Over time, sufficient hydrogen could evolve and could lead to fire or explosion, resulting in damage to or loss of project assets, injury, or death of personnel. The causes and effects are listed in table 25.

Table 25. Gaseous H_2 or O_2 release as a result of exceeding nominal operating conditions of the nano-electro fuel battery.

Causes	Effects
Overcharging	Fire or explosion
Overdischarging	Damage or loss of project assets
External short circuit	Damage to “Center” assets; injury to or death of personnel

Some mitigations include: the use of non-conductive battery terminal caps; physically separating the battery controller system; insulating the positive and negative terminals; utilizing a charging checklist; requirements to charging activities monitored and performed by qualified personnel only; use of a hydrogen sensor with inputs to the BCS; observable warning beacons; and operating the system in a well-ventilated area.

These hazards can be routinely mitigated as the project advances. Early identification of these elements can inform the project team of potential system hazards. The project members can then proactively implement actions or changes to reduce or eliminate causes, effects, or the overall hazard (see figure 67).

HR-12: Gaseous H2 and/or O2 Release due to Exceeding the Nominal Operating Conditions of the NEF Battery

Scenario Based Hazard Description:

The AQUIFER Wing Demonstrator (Wing Demo) contains two annular Nano-Electro Fuel (NEF) battery stacks. During operation, the NEF fluid is pumped through the stacks to be either charged or discharged. During normal operation, the NEF system will be operated within a nominal voltage window. Exceeding those voltages can result in the evolution of hydrogen (during charge) or oxygen. Over time, sufficient hydrogen can be evolved that could lead to fire or explosion, resulting in damage/loss of project assets, damage to Center assets, and/or injury/death to personnel.

Causes	Effects	Mitigations
A. Over-charging B. Over-discharging C. External short circuit	E1. Fire and/or explosion E2. Damage or loss of project assets E3. Damage to Center assets E4. Injury or death to personnel	1. Non-conductive battery terminal caps (C) 2. Battery Controller System (BCS) provides upper and lower control for voltage, current, and temperature (A,B) 3. Physical separation and electrical insulation of positive and negative terminals (C) 4. Charging checklist (to include review) (A) 5. Charging activities shall be monitored and performed by qualified personnel only (A) 6. Hydrogen sensor with inputs to BCS and observable warning beacon (E1, E2, E3, E4) 7. Operation in well ventilated area (E1, E2, E3, E4) 8. Ensure all test personnel and/or non-projects assets are outside of the established keep out zone prior to system startup until power has been removed (E2, E3, E4) 9. Restricted access zone (only essential personnel permitted) (E2, E3, E4) 10. Manual E-Stop capable of system power shutdown (E1, E2, E3, E4) 11. Test personnel shall be briefed on all associated hazards, and required PPE before testing (E3, E4)

AFRC Hazard Action Matrices

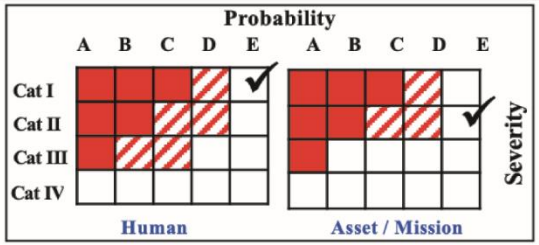

Final Hazard Category Justification Statements

Final Severity Justification

Personnel: In the event of a hydrogen fire/explosion, personnel could sustain catastrophic injuries.

Asset: In the event of a hydrogen fire/explosion, damage/loss of project assets, and damage to Center assets could exceed 500K.

Final Probability Justification

Personnel/Asset: The design includes a physical separation of battery terminals to prevent shorting, and a BCS to control voltage, current, and temperature to prevent gas evolution. Procedural mitigations include operational checklists, personnel requirements, established keep out zones, and required PPE. Hazardous gas sensors, and a manual E-stop are also incorporated. Though theoretically possible for gaseous evolution to occur that would result in a fire/explosion, necessary steps to reduce the risk to an improbable state have been implemented.

Rev. 07-30-2019

210066

Figure 67. The Aqueous, QUick-charging battery Integration For Electric flight Research hazard report for gaseous H_2 and/or O_2 release as a result of exceeding the nominal operating conditions of the nano-electro fuel battery (HR-12).

Technology Application and Future Work Considerations

Energy economy in the context of this application is defined as human utilization of energy resources and energy commodities and the consequences of that utilization. The energy economy for the AQUIFER supply and demand could be based on energy converted from classical energy sources, renewable or green sources, or a combination of both. To introduce the clean energy concepts associated with this work and provide a consistent point of reference, only renewable or green sources are discussed. The energy economy for the AQUIFER supply and demand of electrical power could largely utilize in-place infrastructure. Nano-electro fuel (NEF) technology provides the opportunity to leverage existing infrastructure integration, including fuel transport, gasoline stations, and storage facilities. Energy production - independent from usage - could be accomplished across the nation, leveraging regions with a high supply of green production resources. The utilization of green energy production could be located anywhere in the nation, synergistically where electric aviation is in demand. Additionally, NEF technology provides a storage solution utilizing excess energy produced during high-energy capture times (for example, midday for solar power or high-wind days for wind power) making this energy accessible any time. Collectively, the green resources could have a high impact on the aviation energy economy and could be beneficial to non-aerospace industries.

The general NEF energy charge-use-recharge cycle is shown in figure 68. Conceptually, the NEF production center receives renewable energy input from solar, wind, hydroelectricity, or a combination of any of these. The energy is used to create new or recharged NEF that has previously been discharged. In addition to renewable energy, the NEF production center receives a small portion of non-green energy needed for efficient manufacture. The charged fluid is transported to a NEF fueling station for accessibility to everyday consumers; the NEF could then be used to power trucks, cars, busses, and electric super-short takeoff and landing (eSSTOL) aircraft for safe, emission-free transportation. Once the NEF is discharged, it is brought back to the NEF processing center to repeat the cycle.

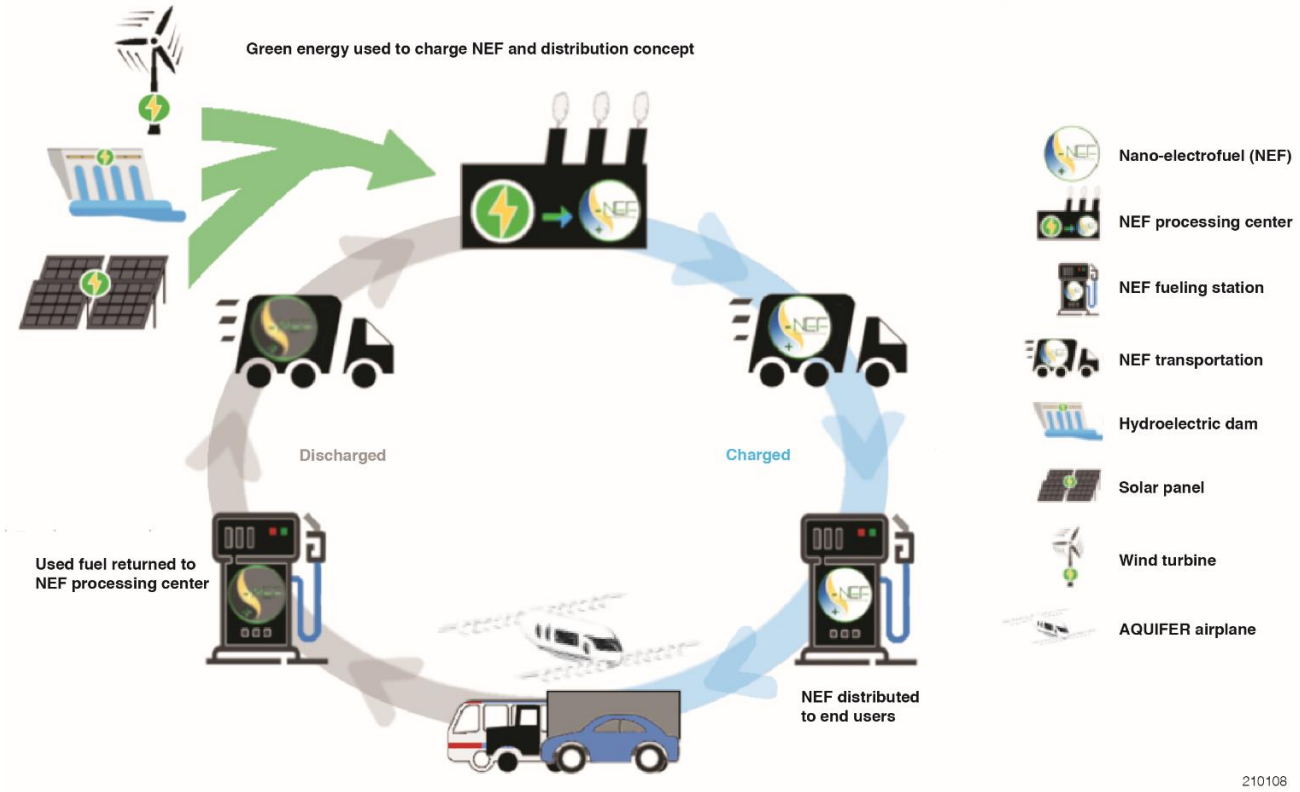

Figure 68. Energy charge-use-recharge concept.

Data provided by the National Renewable Energy Laboratory (NREL) (Golden, Colorado) (ref. 25) on solar and wind intensity were used to create the “Energy Potential” map shown in figure 69. The Energy Potential map shows the amount of energy that is expected to be produced each day in the 48 contiguous United States. This plot uses the projected average amount of wind and sun that each area is expected to see each day of the year for the year 2022. The energy production for both wind and solar is based on wind turbines that are 30-m tall, solar panel energy generation during daylight hours, and rates of efficiency for each source. The results indicate that a sufficient amount of electricity could be produced using wind energy and solar energy, providing power to be used throughout the contiguous United States. Current estimates for NEF cycle life are above 1000 charge/discharge cycles.

The data provided by the Energy Information Administration (ref. 26) on energy distribution was used to create the “Energy Used” map also shown in figure 69. The data shows that the majority of the electricity currently being used are in heavily-populated areas or in industry-heavy areas; additionally, the majority of the electricity is not necessarily being used in areas where it could be most efficiently produced using clean energy.

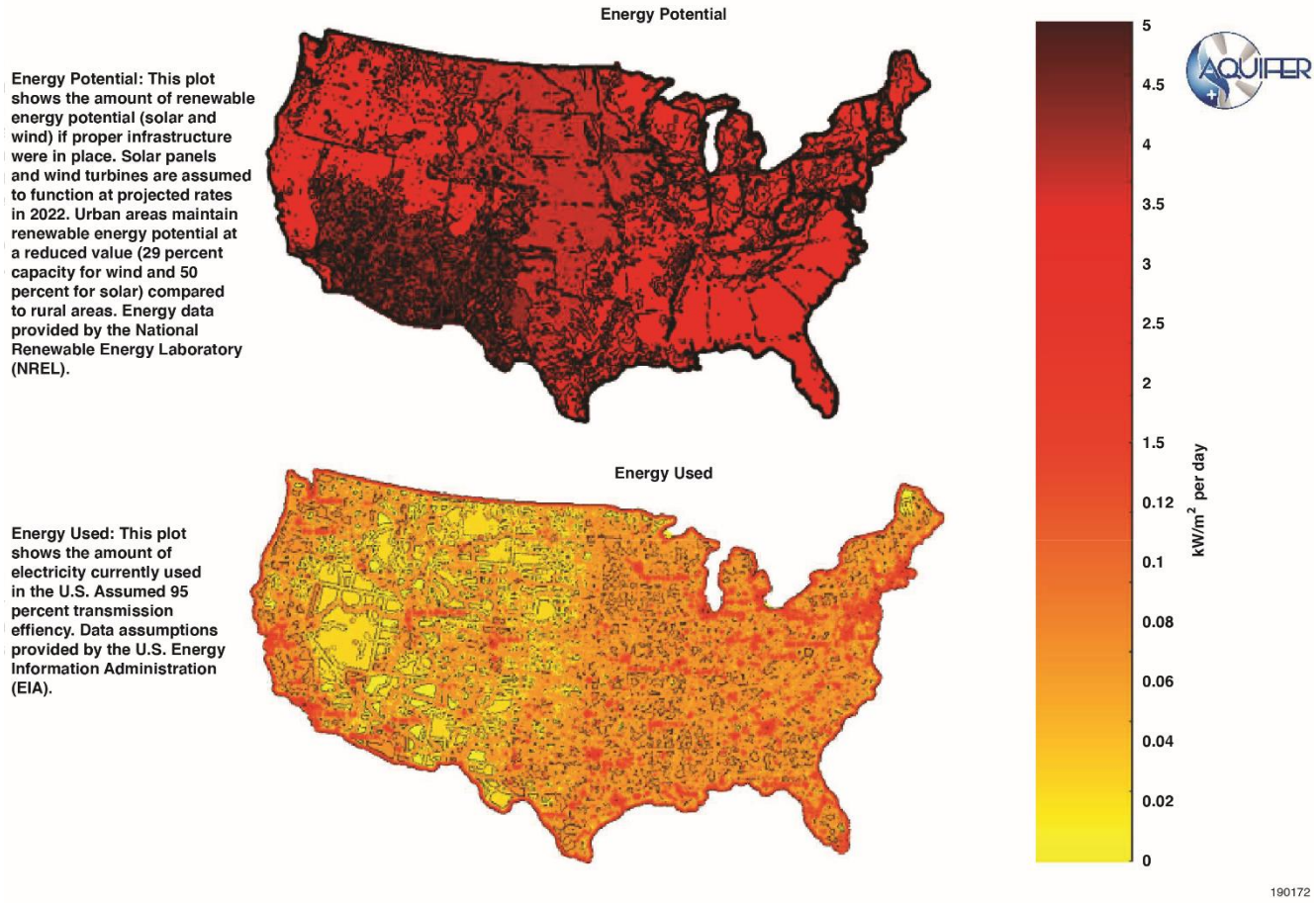

Figure 69. Energy economy: USA energy potential and energy used.

The energy produced in high-potential areas can be transferred to NEF processing plants where it can be converted to fuel and then be transported to high-usage areas. Storing the electricity in the NEF allows energy to be transported more easily while minimizing the loss that is experienced with typical electrical transmission lines.

Once NEF technology is fully operational, distribution to various high-population cities could take place using tankers. Further analysis could identify a vehicle distribution radius versus high-voltage power distribution. Access to NEF at regional airports could easily provide a way to fuel eSSTOL

aircraft. The discharged NEF (after use) could be returned to the storage location, replaced with fully charged NEF, and transported back to the NEF processing center to be recharged from harvested green energy. The charge-use-recharge concept is projected to be a continuous, emission-free cycle. More projections include regional airports that house eSSTOL aircraft in hangars that are equipped with solar panels that could enable recharging of discharged NEF onsite. A 200-nmi eSSTOL flight would require an energy capacity of approximately 220 kWh. Early estimations suggest that renewable energy sources could support these types of flight operations using NEF. A projected long-term large-scale plan includes the use of pipelines to transport NEF. Upon arrival of the NEF to each city, the fuel could be off-loaded and stored at localized energy stations and regional airports where it would be accessible to the everyday consumer.

NASA Technology Readiness Level

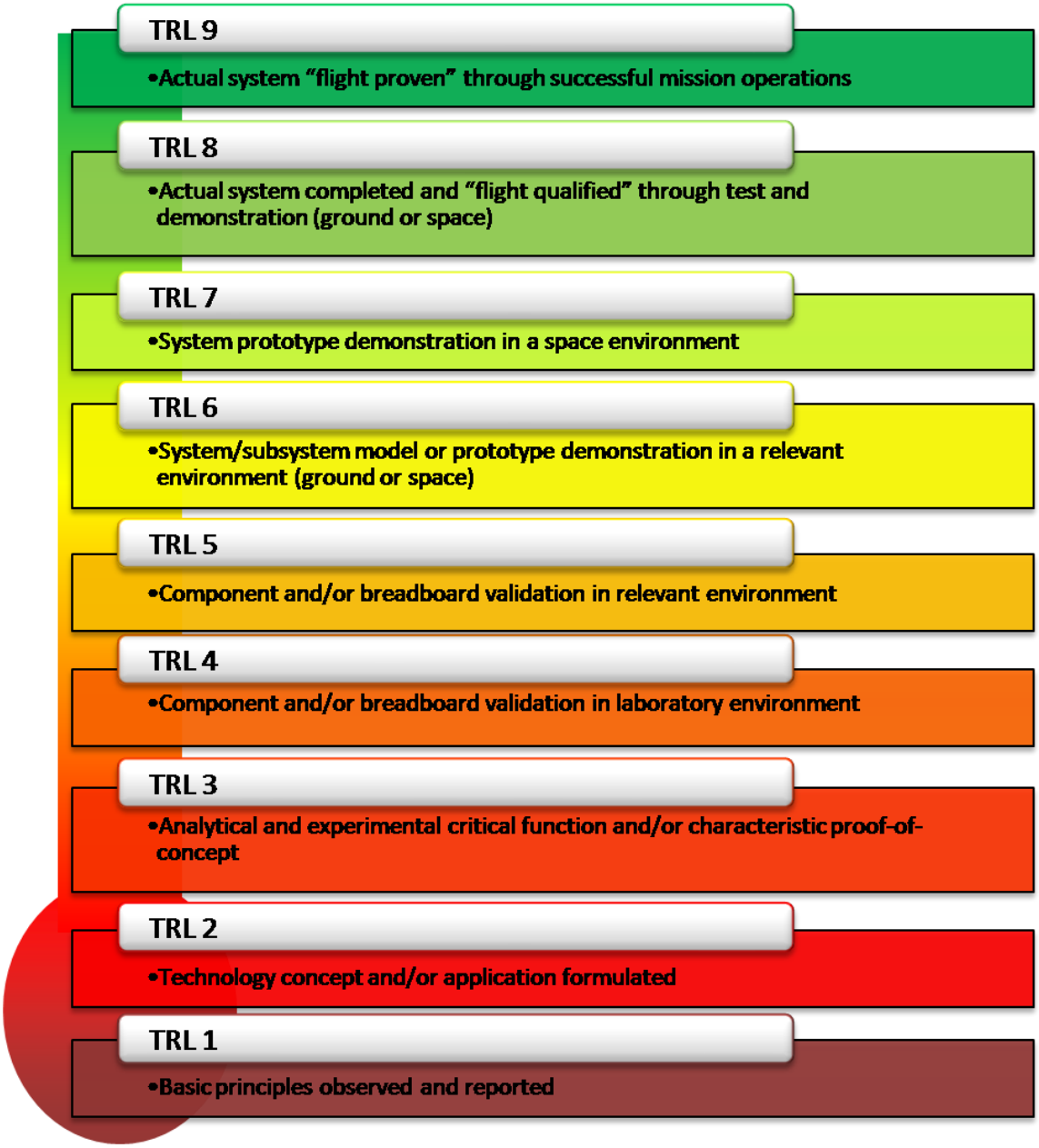

Source: https://www.nasa.gov/directorates/heo/scan/engineering/technology/txt_accordion1.html

References

1. Tallerico, T. F., Chin, J. C. Cameron, Z. A., “Optimization of an Air Optimization of an Air Core Dual Halbach Array Axial Flux Rim Drive for Electric Aircraft,” AIAA Paper 2018-3207, 2018.

2. Zaretsky, Erwin V., Eric N. Bamberger, and Hans Signer, *Operating characteristics of 120-millimeter-bore ball bearings at 3X10^6 DN,* NASA TN D-7837, 1974.

3. Clark, Daniel J., Mark J. Jansen, and G. T. Montague, *An Overview of Magnetic Bearing Technology for Gas Turbine Engines*, NASA/TM-2004-213177, 2004.

4. Dellacorte, Christopher, Kevin C. Radil, Robert J. Bruckner, and S. Adam Howard, *A Preliminary Foil Gas Bearing Performance Map*, NASA/TM-214343, 2006.

5. Xie, Xiaofan, “Comparison of Bearings --- For the Bearing Choosing of High-speed Spindle Design,” Dept. of Mechanical Engineering, University of Utah, 2003.

6. Montage, Gerald, Mark Jansen, Ben Ebihara, Ralph Jansen, Alan Palazzalo, , Randy Tucker, Jason Preuss, Andrew Hunt, Jeff Trudell, and Andrew Provenza, *Design and Fabrication of High-Temperature, Radial Magnetic Bearing for Turbomachinery*, NASA/TM-2003-212300, 2003.

7. Chapman, Stephen J., *Electric Machinery Fundamentals,* 4th edition, McGraw Hill, New York, 2005, Chapter 5.

8. Roskam, Jan, *Airplane Design Part V: Component Weight Estimation*, Roskam Aviation and Engineering Corporation, 1985.

9. Raymer, Daniel P., *Aircraft Design: A Conceptual Approach,* Sixth Edition, AIAA Education Series American Institute of Aeronautics and Astronautics, Inc., 2018.

10. *OpenVSP Parasite Drag Tool*, Software Reference Number LAR-17491-1.

11. Moore, Mark D., Ken Goodrich, Jeff Viken, Jeremy Smith, Bill Fredericks, Toni Trani, et al., “High-Speed Mobility through On-Demand Aviation,” AIAA Paper 2013-4373, 2013.

12. Interagency Committee for Aviation Policy, *Federal Agency Aircraft Operations Manual Guide,* July 10, 1992.

13. Papathakis, Kurt. V., Otto C. Shnarr, Thomas M. Lavelle, Nicholas. K. Borer, Tina Stoia, and Shailesh Atreya, “Integration Concept for Hybrid-Electric Solid-Oxide Fuel Cell Power System into the X-57 “Maxwell,” AIAA-2018-3359, 2018.

14. Kalyanmoy, Deb, Amrit Pratap, Sameer Agarwal, and T. Meyarivan, “A Fast and Elitist Multiobjective Genetic Algorithm: NSGA-II,” *IEEE Transactions on Evolutionary Computation,* Vol. 6, No. 2, 2002, pp. 182–197.

15. Burley, Casey L., Brooks, Thomas F., “Rotor Broadband Noise Prediction with Comparison to Model Data,” *Journal of the American Helicopter Society,* Vol. 49, No. 1, 2004, pp. 28–42.

16. Drela, Mark, and Harold Youngren, *XROTOR* software, web.mit.edu/drela/Public/web/xrotor/, Accessed March 18, 2021.

17. Nguyen, Cathy L., and Jeffrey J. Kelly, *A Users Guide for the NASA ANOPP Propeller Analysis System*. Hampton, Virginia, NASA-CR-4768, 1997.

18. Pettingill, Nicole A., and Nikolas S. Zawodny, "Identification and Prediction of Broadband Noise for a Small Quadcopter," *Vertical Flight Society 75th Annual Forum & Technology Display,* Vol. 1, Philadelphia, Pennsylvania, 2019.

19. Thipphavong, David P., Rafael D. Apaza, Bryan E. Barmore, Vernol Battiste, Christine M. Belcastro, Barbara K. Burian, et al.,"Urban Air Mobility Airspace Integration Concepts and Considerations," AIAA-2018-3676, June, 2018.

20. Nark, Douglas M., F. Farassat, D. Stuart Pope, and Veer Vatsa, "The Development of the Ducted Fan Noise Propagation and Radiation Code CDUCT-LARC," AIAA-2003-3242, May, 2003.

21. Kopardekar, Parimal., Joseph Rios, Thomas Prevot, Marcus Johnson, Jaewoo Jung, and John E. Robinson III, "Unmanned Aircraft System Traffic Management (UTM) Concept of Operations," AIAA-2016-3292, June, 2016.

22. An, Zhoujian, Li, Jia., Yong Ding, Chao Dang, and Xuejiao, "A review on lithium-ion power battery thermal management technologies and thermal safety," *Journal of Thermal Science*, Vol. 26, No. 5, pp. 391-412, September, 2017.

23. Occupational Safety and Health Administration, OSHA® Fact Sheet: "Working Safely with Nanomaterials," osha.gov/sites/default/files/publications/OSHA_FS-3634.pdf, Accessed March 18, 2021.

24. Warwick, Graham, "Record-breaking Zephyr's battery holds eVTOL potential: Amprius cells helped power Zephyr stratospheric UAV; company's current focus is on the aerospace market and high-performance *UAVs," Aviation Week & Space Technology,* pp. 52, January, 2019.

25. National Renewable Energy Laboratory (NREL), *Solar Resource Maps.* nrel.gov/gis/solar.html, Accessed March18, 2021.

26. U. S. Energy Information Administration (EIA), *Consumption and Efficiency.* eia.gov/consumption/, Accessed March 18, 2021.

Related Documents

Year	Presentation / paper title	Author(s)	Report / patent ID	Event conference, etc.
2018	AQUIFER: Integration of Nano-Electrofuel (NEF) flow cell batteries with Rim-Driven Motors (RDM) for Improved Safety, Noise, Charging Time, and Range of Aircraft Electric Propulsion	Kurt Papathakis Linda Taylor	AFRC-E-DAA-TN60723	2018 CAS Showcase
2019	AQUIFER	Kurt Papathakis, Linda Taylor, Robert McSwain, Patricia Loyselle,	NP-2019-04-020-LaRC	2019 AUVSI

		Brianne Demattia, Xiaofan Fei, Jeff Chin, Siena Whiteside, Jason Lechniak, Nikolas Zawodny		
2019	AQUIFER: Determining technology feasibility of non-flammable / non-explosive Nano-Electrofuel (NEF) batteries and acoustically superior Rim-Driven Motors (RDMs) with air bearings for electric flight	Kurt Papathakis Pat Loyselle Robert McSwain	AFRC-E-DAA-TN74576	2019 CAS Showcase
2019	AQUIFER Transformative Concepts and Feasibility Assessments: Overcoming Several Barriers to Electric Flight	Robert McSwain Jason Lechniak	AFRC-E-DAA-TN73729	2019 Sustainable Aviation Symposium
2020	AQUIFER Nano-Electrofuel Energy Economy and Powered Aircraft Operations	Jason A. Lechniak, Michael Salazar, Joseph Morello, Abbigail Waddel, and Kurt Papathakis	AIAA-2020-0117	2020 AIAA SciTech Conference